THE EFFECTS OF NITROGEN AND NICKEL ON THE MICROSTRUCTURE AND MECHANICAL PROPERTIES OF 16 WT.% CHROMIUM STAINLESS STEELS

By

Ross Hutchison

A thesis submitted to the Faculty of Engineering, University of Cape Town, for the degree of Master of Science in Engineering

Department of Materials Engineering
University of Cape Town

May 1990

ACKNOWLEDGEMENTS

I would like to thank the following people for their assistance during the course of this project:

Dr R D Knutsen, my supervisor, for his invaluable guidance and support;

Mr B Greeves and Mr J Petersen for their photographic work;

Mr N Dreze and Mr. G Newins for their Technical Assistance;

Miss K Botha for her assistance in producing this manuscript.

The staff and students in the department of Materials Engineering for their friendly encouragement and Support.

Finally I would like to thank Middleburg Steel and Alloys for the financial support for this project.

ABSTRACT

An investigation has been carried out on the effects of heat treatment on the microstructures and mechanical properties of a number of experimental 16 wt.% chromium dual-phase ferritic-martensitic stainless steels. A comparison was made between an alloy containing 2.5 wt.% nickel (low interstitial content [C + N = 0.03 wt%]), and three alloys possessing low nickel (0 - 1 wt.%) and high nitrogen contents (0.06 - 0.12 wt.%). Samples of AISI 304, 430 and 431 were included in the investigation for comparison with the experimental alloys.

The microstructural response of the alloys to heat treatment was examined using light and scanning electron microscopy techniques. Tensile and Charpy V-notch impact tests were carried out on the alloys in their various heat treated conditions. Fracture surfaces, and deformation markings on the tensile gauge surface, were examined in the scanning electron microscope, while cross-sections of fracture surfaces were examined using light microscopy. Dilatometric traces were obtained for the experimental alloys in order to determine the effects of variations in composition on the inter-critical temperature range.

The combination of good toughness and tensile strength that can be achieved in the low interstitial, nickel alloyed steel suggests that it could be a favourable alternative to both AISI 430 and 431 in many engineering applications. Toughness values superior to those of AISI 430 and 431 can be achieved in the high nitrogen stainless steels by tempering at 700 °C, although the heat treatment results in a substantial loss in strength, and the low toughness exhibited by these alloys in the solution treated condition suggests that their weldability is no better than that of AISI 430 and 431. It is also shown that the formation of a lamellar ferrite/martensite composite phase through intercritical annealing can provide attractive combinations of tensile strength, toughness and ductility in certain of the alloys. However, the ductility of alloys containing a lamellar composite phase is dependent on the δ-ferrite content, and the toughness of the composite phase is adversely affected by a high nitrogen content.

The yielding characteristics of ferritic-martensitic stainless steels are dependent on the hardness difference between the ferrite and martensite phases, and on the volume fraction of martensite. In addition, the morphology of the martensite phase exerts a strong influence on the ductility of dual phase steels. Microvoid initiation in the experimental alloys in the solution treated condition (1000 °C/ 1hour/air cool) occurs primarily by fracture within the martensite phase. In the 700 °C tempered condition alloys having a high nitrogen content may be susceptible to intergranular fracture.

CONTENTS

CHAPTER ONE

GENERAL INTRODUCTION

1.1 INTRODUCTION

Stainless steels play an important role in industry in view of their high resistance to oxidation and corrosion. However, the level of mechanical properties that can be achieved in stainless steels is more often than not equalled or bettered by low alloy steels at considerably less expense. Chromium has an embrittling effect on ferrite as its concentration in solution is increased above 12 wt.% , and the susceptibility of both ferritic and martensitic stainless steels to the adverse effects of interstitial alloying elements in solution is increased as the chromium content is increased. While the ductility and toughness of commercial grade ferritic and martensitic stainless steels (such as AISI 430 and 431) can be improved through heat treatment, the heat treatments employed generally result in a loss in strength, and the properties developed by the heat treatments are destroyed by welding. Stabilising the austenite phase in 16 to 18 wt.% chromium steels through additions of between 8 and 12 wt.% nickel (such as in AISI 304) results in vast improvements in the toughness and weldability of stainless steels, although the yield strength of austenitic stainless steels is generally low, and the production costs of austenitic stainless steels are high as a consequence of the high nickel content.

In view of the vast reserves of chromium in South Africa, there is an ongoing programme of research into improving the mechanical properties and weldability of stainless steels while maintaining low production costs through controlled alloying element additions. The successful introduction of 3CR12 into the stainless steels market within the past decade is a consequence of the high toughness achieved by the alloy through a carefully balanced chemical composition. The presence of martensite in ferritic alloys improves the toughness of the alloys by refining the grain size. Extensive research into low alloy dual phase ferritic-martensitic steels has revealed that attractive combinations of tensile strength, formability and ductility can be achieved in dual phase steels.

In view of the poor weldability of both AISI 430 and 431, and the high cost of AISI 304, there is potential for the development of a 16 wt.% chromium high strength stainless steel which has a good weldability and which is less costly than AISI 304. The prospects of such a steel possibly lie with the development of a dual phase ferritic-martensitic microstructure. While it is most likely that such an alloy would require a low interstitial content, little research has been directed at the properties of high nitrogen, low carbon stainless steels, and the possible benefits that an alloy with such a composition would gain from a dual phase microstructure.

1.2 AIM OF THE RESEARCH

The aim of the work presented in this dissertation was to:

(1) examine the potential of a nickel alloyed ferritic-martensitic 16 wt.% chromium stainless steel, which has a low interstitial content, as a possible substitute for the standard stainless steel grades AISI 304, 430 and 431;

(2) consider the effects of reducing the nickel content, whilst increasing the nitrogen content to maintain a ferrite-martensite phase balance, on the tensile and impact properties of dual phase 16 wt.% chromium stainless steels.

CHAPTER 2

LITERATURE REVIEW

2.1 MICROSTRUCTURAL EVOLUTION IN STAINLESS STEELS

Iron alloys containing in excess of 11% chromium are classified in a class of steels called stainless steels. The stable oxide film, formed by the presence of chromium, imparts a considerable measure of oxidation resistance to this class of alloys[1]. The wide variety of microstuctural conditions and properties that can be achieved in this class of steels can be broadly related to three rudimentary microstructural states that have different crystal structures; namely body centered cubic ferrite, face centered cubic austenite and body centred tetragonal martensite[2].

From the Fe-Cr diagram in Fig. (2.1), it is seen that the addition of 12.7 wt.% chromium to an iron base suffices to close the austenite (γ iron) phase field, rendering the alloy fully ferritic (δ or α iron) over the whole temperature range below the solid/liquid interface.

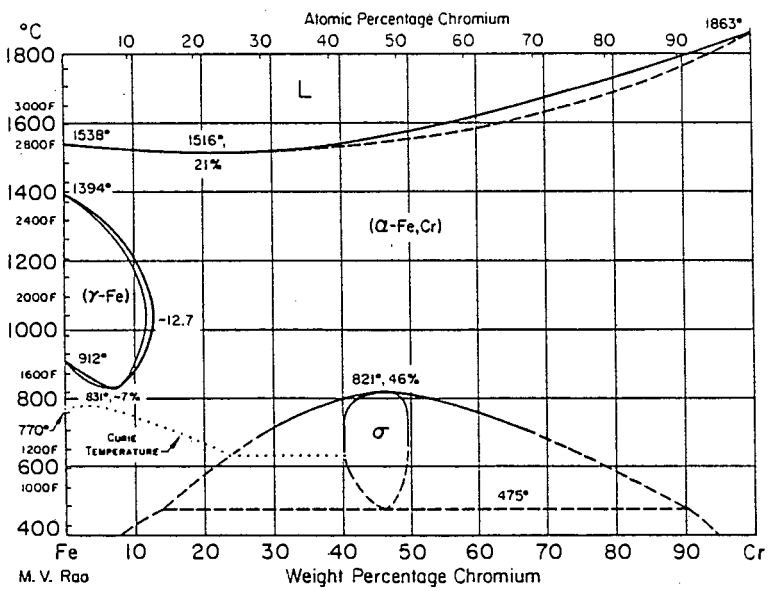

Figure (2.1): Fe-Cr binary phase diagram [3].

The addition of alloying elements which promote the formation of austenite (γ) cause the γ and $\delta + \gamma$ (the narrow transition band between the δ and γ phase fields in Fig. (2.1)) phase fields to extend to higher chromium contents. In effect, while chromium tends to close the γ-loop, austenite forming elements such as nickel, carbon, and manganese show the reverse effect in expanding the temperature and composition ranges for austenite stability[4,5]. By balancing the ferrite and austenite forming elements in solution, the microstructures of stainless steels have been manipulated to produce particular phase constitutions[6,7].

Due to the strong austenitising potential of nickel, and its suitability as a substitutional alloying element in Fe-Cr alloys, the Fe-Cr-Ni ternary phase diagram has been comprehensively studied[8,9]. With the use of isothermal sections of the Fe rich corner of this system, the microstructural developments leading to observed room temperature microstructures can be traced[10].

From Fig. (2.2a) it is evident that a 16% Cr alloy which has cooled through the liquid/solid interface to 1400 °C is composed entirely of δ-Fe, even with additions of up to 8 wt% nickel. As cooling progresses further, the boundaries for the γ and $\delta + \gamma$ phase fields broaden in the direction of a higher chromium, lower nickel content, at the expense of the high temperature δ-iron.

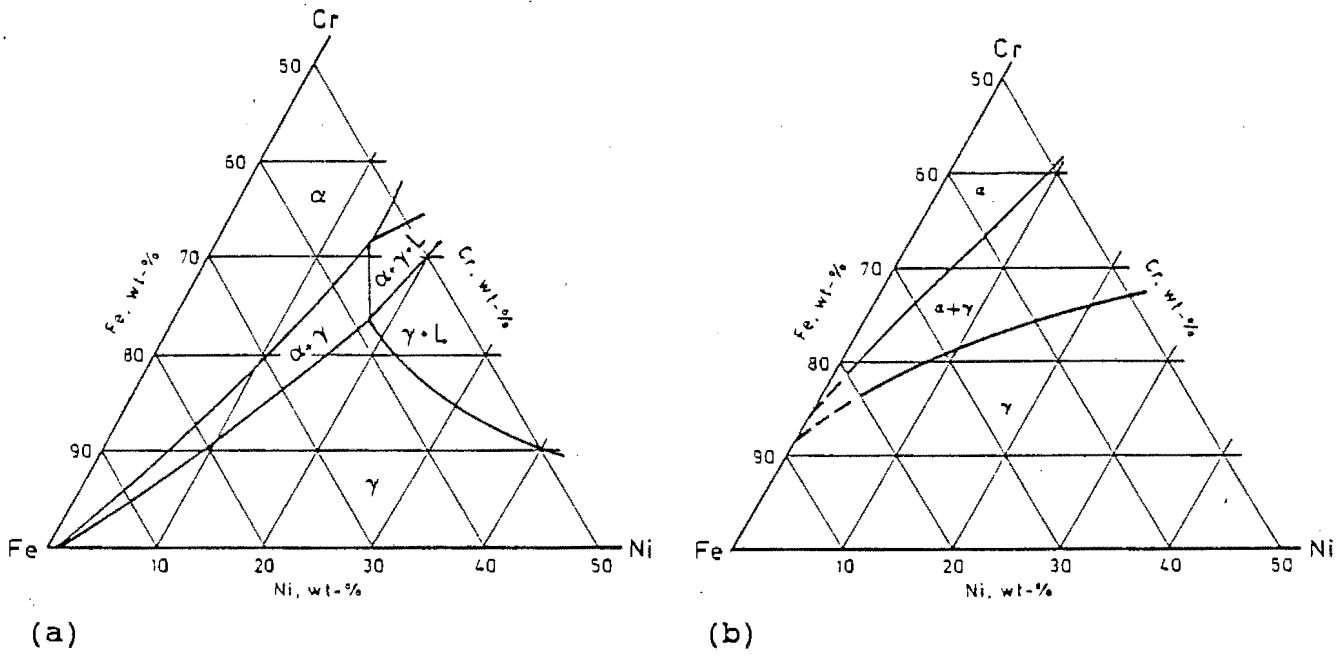

Figure (2.2): (a) 1400 °C and (b) 1000 °C isothermal sections of the iron rich corner of the Fe-Cr-Ni ternary phase diagram[8].

Thus at 1000 °C (Fig. (2.2b)), under equilibrium conditions, an addition of 4 wt.% nickel to a 16 wt% chromium steel would appear sufficient to produce a fully austenitic microstructure. While equilibrium isothermal sections between 1000 and 650 °C indicate a gradual retraction of the γ field, as austenite begins to transform to α-ferrite (α-Fe being a product of the decomposition of austenite, as opposed to δ-Fe which is a product of solidification), equilibrium is not reached in circumstances other than under extremely slow cooling conditions due to the thermodynamic constraints on diffusion of substitutional alloying elements. The phase balance formed in the region of 1000 - 1100 °C, as determined by the Cr and Ni contents, is maintained to room temperature with quenching or air cooling[10]. The austenite may undergo a martensitic transformation during cooling.

As previously mentioned, the δ ferrite microstructure formed in a 16 wt% Cr, 4 wt% Ni alloy at 1400 °C decomposes on cooling to 1000 °C to form austenite (γ). Such a transformation, in accordance with the Lever Rule[11], requires partitioning of austenite and ferrite forming elements as the new austenite is formed. Brown et al[12] proposed that this solid state transformation, a nucleation and growth process, is achieved by the formation of faceted nuclei of austenite at the ferrite grain boundaries, and the growth of these nuclei by the migration of curved , incoherent segments of δ/γ interface into the ferrite grains. This is a form of Widmanstatten growth. In alloys rapidly cooled from the δ-ferrite temperature range, as observed close to the welds in heat affected zones, austenite has been observed to form at ferrite grain boundaries as a Widmanstatten structure[10].

While the above description relates to the effects of nickel additions on the phase stability in Fe-Cr alloys, similar effects can be achieved using other alloying elements. A convenient method of weighting the potentials of the more commonly encountered alloying elements as ferrite and austenite formers is found in the use of chromium and nickel equivalents[10,13].

$$\text{Cr equivalent} = \%Cr + 2\%Si + 1.5\%Mo + 5\%V + 5.5\%Al + 1.75\%Nb + 1.5\%Ti + .75\%W \text{ ------- } 1$$

$$\text{Ni equivalent} = \%Ni + \%Co + 0.5\%Mn + 0.3\%Cu + 25\%N + 30\%C \text{ ----- } 2$$

Used in conjunction with the 1000 °C isothermal section of the Fe-Cr-Ni phase diagram, these equations can be used to predict the effects of combinations of alloying elements on phase constitution.

2.1.1 MARTENSITIC TRANSFORMATION

The martensitic transformation temperature (Ms) is characteristic to individual chemical compositions. Most alloying elements which enter into solution in austenite lower the Ms temperature[14]. However the martensitic transformation occurring in the alloys discussed in this work will be completed above room temperature[13], although the possibility exists of small amounts of retained austenite.

2.2 CLASSIFICATION OF STAINLESS STEELS

While stainless steels fall into three broad classifications based on crystal structure, in many cases an alloy may contain one or more secondary phases in addition to the major phase[15]. This is dependent on the chemical balance and processing conditions. In the following sections a brief outline of the characteristics of the three major classes of stainless steels is given, along with a typical example found in each class.

2.2.1 FERRITIC STAINLESS STEELS

Ferritic stainless steels may contain between 12 and 27 wt.% Cr, and occasionally contain small additions of molybdenum[2]. While being moderate in cost, the alloys are easily converted into sheet and bar products, and are resistant to stress corrosion cracking in chloride environments[16]. However these alloys are generally brittle after welding and only have a moderate degree of corrosion resistance[2]. A typical example is AISI 430 (Table (2.1)). Common applications of ferritic stainless steels include kitchen ware, automobile trim and transportation containers.

2.2.2 MARTENSITIC STAINLESS STEELS

This grade of steel may contain between 12 and 18 wt.% Cr, and is rendered hardenable by the addition of controlled amounts of austenite stabilizing elements, most commonly carbon and nickel[2]. The utilisation of these steels relies on their strength along with a

moderate corrosion resistance, and common applications lie in the chemical and petrochemical industries, airplane parts, tools and bearings[10]. A typical example is AISI 431 (Table (2.1)).

AISI No.	C [Max]	Mn [Max]	Si [Max]	Cr [Range]	Ni [Range]	P [Max]	S [Max]
430	.12	1.0	1.0	14 - 18	-	.04	.03
431	.20	1.0	1.0	15 - 17	1.25 -2.3	.04	.03
304	.08	2.0	1.0	18 - 20	8.0 -12.0	.045	.03

Table (2.1): Composition limits for three standard stainless steels (Based an SAE J405B, SAE Handbook, 1969).

2.2.3 AUSTENITIC STAINLESS STEELS

Standard austenitic stainless steels most often contain approximately 18 wt.% Cr, but additions of up to 26 wt.% Cr may be used[2,17]. While Ni is most commonly used to obtain austenite stability, carbon, nitrogen and manganese have also been used for this purpose. The popularity of austenitic stainless steels stems from their high corrosion resistance, and good weldability and toughness, but they are significantly more expensive than the ferritic and martensitic grades due to the high nickel content, and are susceptible to stress corrosion cracking in chloride environments[16]. Their uses are numerous in corrosion and high temperature applications, and a common example is AISI 304 (Table (2.1)).

2.3 GENERAL CHARACTERISTICS 0F FERRITE-MARTENSITE DUAL PHASE STEELS

The term Dual Phase Steel was originally used to describe a class of high strength low alloy (HSLA) steels containing a dispersion of approximately 20% martensite in a soft ductile ferrite matrix[18]. Interest in this grade of steels escalated in the mid seventies when it was discovered that intercritical annealing of manganese-silicon[19] and vanadium-nitrogen[20] HSLA steels resulted in a product with superior ductility and formability to the conventionally heat treated HSLA steels. Subsequent research has highlighted a number of properties that are characteristic of this class of steel, often termed dual phase properties[18]:

(1) Continuous yielding
(2) Low 0.2% yield strength
(3) High tensile strength
(4) High initial work hardening rate
(5) High total elongation

The combination of high strength, good ductility and formability shown by this group of steels has made them an attractive option for weight saving applications in the automobile industry.

The mechanical properties of dual phase steels are sensitive to a large number of microstructural characteristics, some of which are[26]: (1) shape and distribution of martensite, (2) properties of the martensite, (3) properties of the ferrite, (4) volume fraction of martensite, and (5) microstructural features such as the presence of coarse carbide precipitates.

By utilizing the law of mixtures[18,21], it is apparent that during the deformation of two phase structures both stresses and strains are partitioned between the two phases, as shown in equations 3 and 4 [22]. Increasing the volume and hardness of the martensite increases the tensile and yield strengths of dual phase steels, while the ductility is decreased[23,24,25]. However, in reality the linearity of equations 3 and 4 is offset because the values of σ_f and σ_m are dependent on the back stress developed by plastic incompatibility between the two phases, and because strain is concentrated in the softer more ductile ferrite phase[18].

$$\sigma = \sigma_m V_m + \sigma_f V_f \quad \text{..... EQUATION 3}$$

$$\epsilon = \epsilon_m V_m + \epsilon_f V_f \quad \text{..... EQUATION 4}$$

(σ - stress, ϵ - strain, V - volume fraction, f - ferrite phase, m - martensite phase)

The degree of plastic incompatibility between the ferrite and martensite phases varies with the contiguity of the martensite phase[24], and the hardness and volume fraction of the martensite phase[27]. While attempts have been made to modify equations 1 and 2 in order

to accommodate such factors in the estimation of tensile strengths[27,28] (Fig.(2.3)), no universally applicable equations have been developed.

Dual phase microstructures may have a beneficial effect on the mechanical properties of stainless steels. While increasing the chromium content of Fe-Cr alloys results in improved corrosion resistance, ferritic stainless steels suffer from poor toughness, as was revealed in pioneer research by Binder and Spendelow[29]. The poor toughness results from their sensitivity to interstitial content and the susceptibility to grain growth at temperatures in excess of 1000 °C [10].

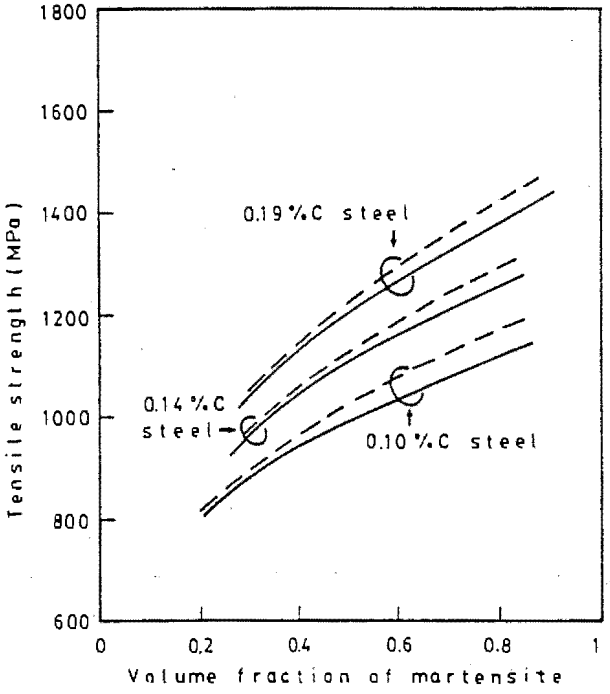

Figure (2.3): The effects of variations in martensite hardness and volume fraction on the tensile strength of a low alloy dual phase steel, and the limited accuracy of calculated values[27].

---------- CALCULATED ———————— EXPERIMENTAL

As grain size decreases the toughness increases, and the ductile to brittle transition temperature (DBTT) decreases ($T_{DBTT} \propto d^{(1/2)}$) [14], despite the fact that the yield strength also increases[30,31]. It has been shown that altering the chemistry of such stainless steels to allow for the presence of some martensite in the microstructure results in much improved toughness as a consequence of a finer grain size[6,7,32] (Fig.(2.4)). The finer grain size results from of the presence of the second phase (austenite) during hot or cold rolling and subsequent heat treatments[33]. The dual phase $\alpha + \gamma$ structure is also beneficial in the welding of heat treated materials in that the growth of fresh austenite at

the ferrite grain boundaries in the heat affected zone, in the temperature range of the $\alpha + \gamma$ loop, retards ferrite grain growth[33]. In low alloy dual phase ferrite-martensite steels a finer ferrite grain size has also been noted to increase the yield strength[30,31]. While there has been some contention as to whether the second phase in dual phase steels should necessarily be tougher than the matrix phase in order for toughening to be effective[6,7], it appears that this factor is strongly related to the alloying elements in solution.

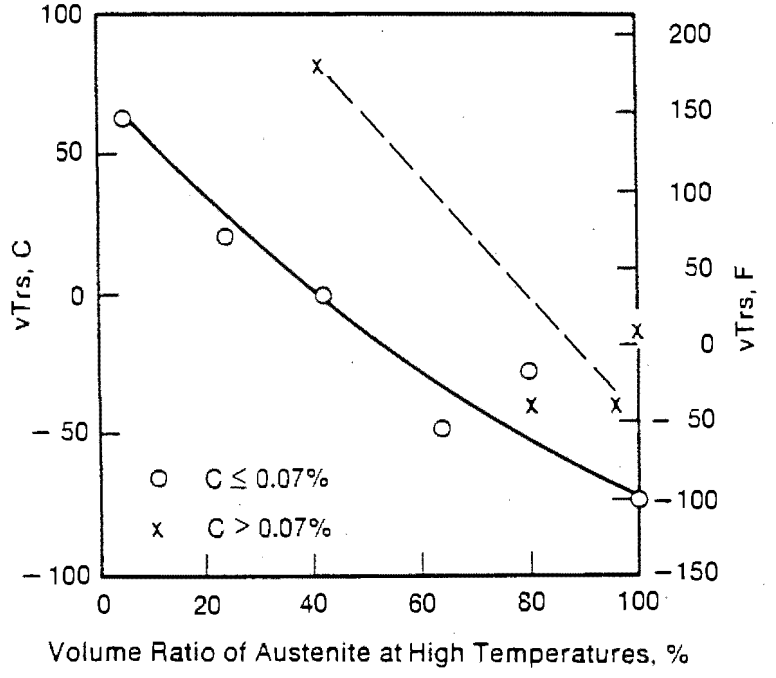

Figure (2.4): Effect of tempered martensite content on the toughness of 17 wt.% Cr alloys after tempering at 800 °C [34]. The increase in toughness as the tempered martensite content is increased is a consequence of a decrease in the ferrite grain size.

2.3.1 LAMELLAR TYPE DUAL-PHASE MICROSTRUCTURES

Some recent research has been directed at lamellar type dual phase microstructures [13,34,35,36]. Lamellar type dual phase microstructures can be formed during intercritical annealing of both low alloy and stainless steels, which promotes the growth of fresh austenite along interlath boundaries within the martensite grains, but prevents a full austenite reversion. Thus packets of martensite laths are transfomed to lamellar composites consisting of alternate layers of α-ferrite (tempered martensite) and austenite. On cooling to room temperature the austenite may transform to martensite, depending on

the chemistry of the alloys. Microstructures have been investigated which contain alternate layers of either ferrite and martensite or martensite and austenite. However, in all cases the general conclusion reached is that fine lamellar microstructures provide good combinations of toughness, ductility and tensile strength. It has been shown that dual phase alloys having a lamellar ferrite/martensite microstructure may have superior strength and ductility to those with an island type martensite mophology[37].

2.4 EFFECTS OF CARBON AND NITROGEN ON THE DEVELOPMENT OF MICROSTRUCTURE IN Fe-Cr ALLOYS

Carbon and nitrogen have generally been frowned upon as alloying elements in high chromium steels where toughness and weldability are important criteria. Both carbon and nitrogen increase the general corrosion rate of ferritic stainless steels when trapped in solid solution (nitrogen to a lesser extent than carbon), and in precipitate form they reduce the chromium content in solution[38].

However, carbon and nitrogen can have advantageous effects on the high temperature equilibrium structure, and may be used as cost reducing substitutes for nickel in stainless steels. These advantages, and the general effects of carbon and nitrogen on the microstructure of stainless steels, are briefly described in the following paragraphs.

Carbon and nitrogen are strong austenite (γ) stabilising elements. In "pure" Fe-Cr alloys, the γ field extends to a limit of approximately 11 wt% chromium (Fig. (2.1)). Increasing the carbon or nitrogen content expands the γ and $\alpha + \gamma$ phase fields to higher chromium levels (Fig. (2.5))[39]. The effect is similar for both carbon and nitrogen. A 17% Cr stainless steel requires as little as 0.03% (C+N) to produce a dual phase ferrite-martensite microstructure when heat treated in the 1000 - 1100 °C temperature range[32]. It has been determined that a 17% Cr steel requires 0.3 wt% nitrogen at 1000 °C or 0.34 wt% carbon at 1150 °C to produce a fully austenitic alloy[40,41].

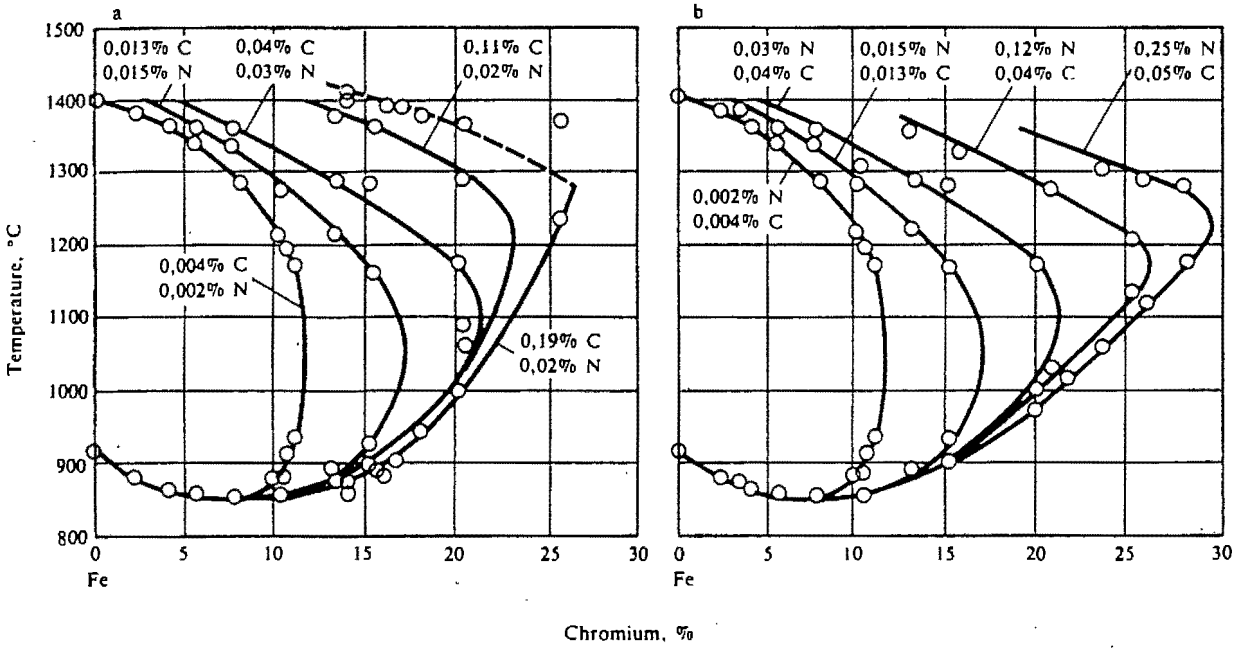

Figure (2.5): Fe-Cr phase diagram illustrating the effects of (a) carbon and (b)nitrogen on the extent of the α + γ phase field[39].

Castro and Tricot[42] found that nitrogen and carbon each have distinguishing effects on the temperature ranges of stability of austenite in 17% Cr alloys. Increasing the nitrogen content (Figure (2.6a)) caused the γ nose (referring to the maximum austenite content for a given interstitial content) to expand along the 1000 °C isotherm. Increasing the carbon content in solution expanded the γ nose from the 1000 °C isotherm at low carbon levels to the 1200 °C isotherm at intermediate to high carbon levels (Figure (2.6b)). Thus at 1000 °C nitrogen appears to have a stronger γ promoting ability than carbon, a possible consequence of the greater stability of carbon based precipitates than nitrogen based precipitates at this temperature[42].

In 17 wt.% Cr alloys carbon has the effect of raising the A_5 temperature (temperature at which 100% δ ferrite is formed) 1.3 times more than an equivalent addition of nitrogen[42]. Significant amounts of both carbon and nitrogen in solution in Fe-Cr alloys would extend the γ + δ phase field over a wide temperature range, and would promote a high A_5 temperature (under equilibrium conditions). A 16 wt.% Cr, 0.1 wt.% N, 0.04 wt.% C alloy[42] has an A_5 temperature of approximately 1350 °C. The higher the A_5 temperature, the narrower the single phase δ ferrite band below the solidus. This is important when considering weldability because rapid grain growth occurs in the δ-ferrite temperature range, which reduces the toughness of the heat affected zone[10,43].

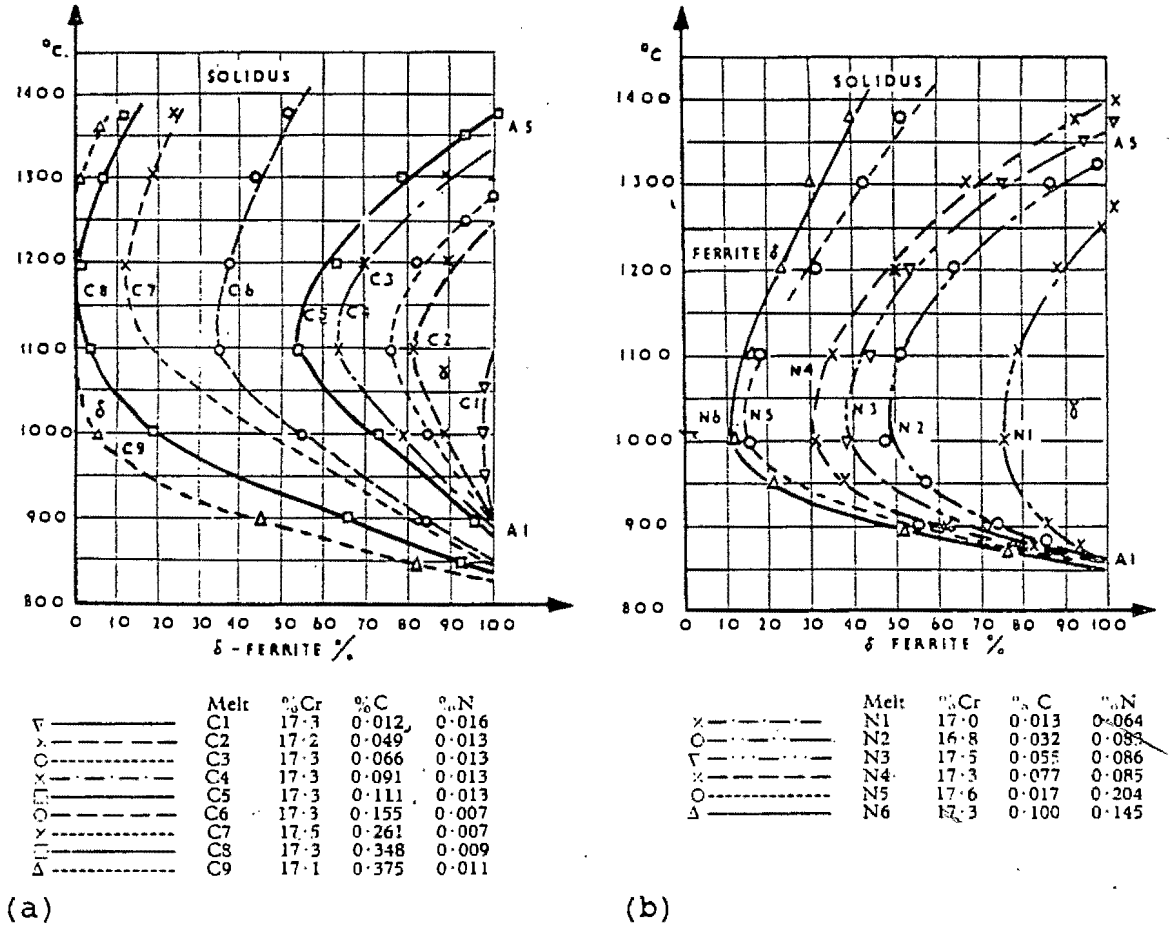

Figure (2.6): (a)Influence of carbon and (b) influence of nitrogen on the austenite content in 17 wt.% Cr stainless steels, in the temperature range of 800 to 1200 °C [42].

In nitrogen alloyed 18% Cr steels the partition coefficient of chromium between ferrite and austenite decreases from approximately 1.2 at low nitrogen levels (± .04) to 1.08 at high nitrogen levels (± .3 %) [42]. This is a consequence of the changing ferrite/austenite ratio as the nitrogen content is increased. The partition coefficient of chromium (between α and γ) is, however, not only a function of nitrogen content, but also the activity of chromium in solution[31,40].

As a result of rapid diffusion of interstitial γ promoting elements, and a low partition coefficient of chromium, the driving force for altering the phase constitution of alloys having a high interstitial content is expected to be high within the $\alpha + \gamma$ phase field, resulting in a narrow dual phase region. On the other hand, partitioning of alloying elements between the ferrite and martensite in dual phase Cr-Ni steels having a low interstitial content is high[13] and the rate of diffusion of nickel (substitutional alloying element) is low, thus the phase changes will be more sluggish than in nitrogen and carbon alloyed steels, thereby resulting in a substantially wider dual phase region.

2.5 HEAT TREATMENT OF STAINLESS STEEL ALLOYS

2.5.1 FE-CR-NI ALLOYS

2.5.1.1 MICROSTRUCTURAL CHANGES ACCOMPANYING HEAT TREATMENT

Dual phase ferrite-martensite microstructures, consisting of between 0 and 100% martensite, can be achieved in low interstitial (C + N < 0.03) 17 wt.% Cr steels with the addition of between 0.5 and 4 wt.% Ni, and air cooling or quenching from between 1000 and 1100 °C [8]. The sluggish rate of diffusion of Cr and Ni prevents any phase changes occurring during air cooling between the solution treatment temperatures and the Ms temperatures in alloys where the interstitial content is low[13].

The boundaries representing the onset and termination of phase transformations occurring during the heat treatment of 16 wt.% Cr alloys with additions of between 2 and 3 wt.% Ni, as determined by dilatometry[13], are represented in Fig. (2.7). This range of Ni contents represents a δ-ferrite content of between 13 and 27%. Tempering between 500 and 600 °C results in softening of the martensite phase as it decomposes to carbides ($M_{23}C_6$, from the residual carbon content), which precipitate on interlath and prior austenite boundaries, and secondary (α) ferrite[13]. A small amount of austenite, rich in nickel, may also form when tempering at 600 °C due to the close proximity of the A_1 temperature. There is no change in the original δ-ferrite phase.

From Fig (2.7) it is evident that heat treating between 600 and 800 °C (inter-critical annealing) results in the transformation of the original martensite into a mixture of secondary ferrite and fresh austenite[13,34]. As the heat treatment temperature is increased from 600 to 800 °C, increasing amounts of austenite are formed. This austenite nucleates on and grows from lath and prior austenite boundaries in the form of parallel lamellar platelets, which join up and eventually engulf the original martensite grains at temperatures above 800 °C. On cooling to room temperature the austenite transforms to martensite. However, the possibility of retained austenite has been noted, especially from heat treatments in the lower part of the inter-critical temperature range where the nickel content of the austenite is high[13,34]. The lamellar ferrite/martensite structure is most prominent after heat treating at 700 °C [13].

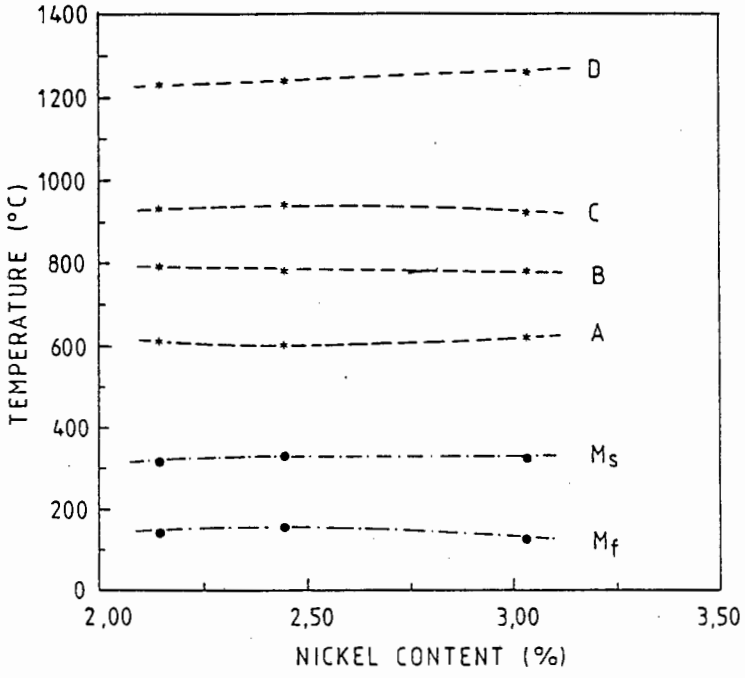

A - Start of γ formation B - γ formation complete
C - Start of δ formation D - δ formation complete

Figure (2.7): Phase transformations occurring during the heating of a number of Fe-16 wt.% Cr alloys having various Ni contents[13].

Both Cr and Ni partition between the austenite and ferrite phases formed in the original martensite while heat treating in the inter-critical temperature range, and thus the transformations are sluggish[13,34]. No change takes place in the δ phase during the above mentioned heat treatments. Figure (2.8) illustrates the phase changes occurring in an alloy containing 84 % martensite after various heat treatments over the inter-critical temperature range.

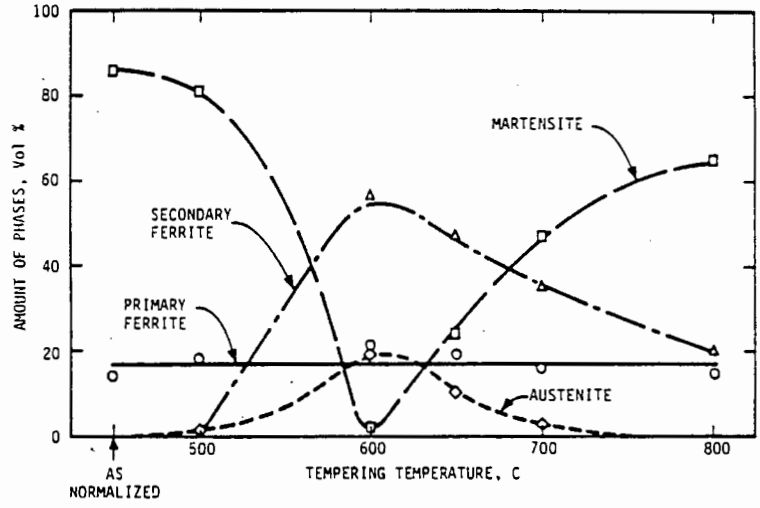

Figure (2.8): Effect of heat treatment on the phase constitution of an alloy containing 16% Cr, 5% Ni and 1.5% Mo[34].

2.5.1.2 MECHANICAL PROPERTIES OF LOW INTERSTITIAL NICKEL ALLOYED DUAL-PHASE STAINLESS STEELS

The effects of heat treatment on the tensile strength and impact resistance of an alloy containing 16 wt.% Cr and 2.5 wt.% Ni are summarized in Table (2.2) [13].

HEAT TREATMENT	Solution Treated	600 °C/ 2 Hours	700 °C/ 2 Hours	800 °C/ 2 Hours
TENSILE STR. [MPa]	1091	821	855	1006
IMPACT STR.* [J]	50	66	85	58

*3/4 SIZED CHARPY SPECIMENS

Table (2.2): Effect of heat treatment on the tensile strength and toughness of a 16% Cr, 2.5% Ni alloy with a low interstitial content (C + N < 0.06) [13].

It is evident from Table (2.2) that while heat treating at 700 °C causes an increase in tensile strength over that observed after tempering at 600 °C, there is also an increase in impact resistance. The increase in tensile strength has been attributed to the presence of new martensite in the microstructure, while the increase in impact resistance has been attributed to the lamellar morphology of the martensite[13,34]. It has been suggested that the lamellar composite (ferrite-martensite) phase resists crack initiation and propagation[13,36].

2.5.2 FE-CR-C-N ALLOYS

Little research has been directed at high nitrogen (> 0.1 wt.%) Fe-Cr alloys. However, the effect of nitrogen in lesser quantities (.01 - .06 wt%) on the precipitation kinetics of carbides and nitrides in these alloys has been approached by various authors. Varying the carbon and nitrogen contents and controlling their distribution and reactions in Fe-Cr alloys leads to a wide scope of possible structures and properties[10,44].

2.5.2.1 PRECIPITATES ENCOUNTERED IN Fe-Cr-C-N SYSTEMS

Carbon and nitrogen can reduce the chromium content in solution by forming precipitates. The precipitates encountered in 12-17% Cr alloys are the body centered cubic $M_{23}C_6$ and $M_{23}(CN)_6$ phases at low carbon activities, hexagonal M_7C_3 at intermediate carbon levels and the hexagonal ϵ phase, M_2N [45,46]. M is usually a mixture of Cr and Fe. The nitride M_2N is predominantly chromium nitride, and since the affinity for nitrogen in this case is high, little carbon is expected to dissolve in it[40]. The $M_{23}C_6$ precipitates assume the following orientation relationship with the matrix[47]:

$(001)_\alpha \parallel (011)M_{23}C_6$,

$(110)_\alpha \parallel (\bar{1}1\bar{1})M_{23}C_6$,and

$(\bar{1}10)_\alpha \parallel (\bar{2}\bar{1}1)M_{23}C_6$,

and are generally found as film-like or globular precipitates on grain boundaries, or as fine globular precipitates within the grains.

The M_2N precipitates grow as clusters of needles in regions of high dislocation density, or as single larger needles, and assume a Burgers orientation relationship with the matrix[48]:

$(0001)Cr_2N \parallel (011)_\alpha$, and

$(11\bar{2}0)Cr_2N \parallel (11\bar{1})_\alpha$.

These precipitates have a <311> growth direction, which corresponds to a minimum interatomic distance mismatch with the matrix lattice. Figures (2.9a) and (2.9b) illustrate the temperature ranges of stability of some of the above-mentioned phases.

The temperature to which carbides and nitrides are stable depends on the carbon and nitrogen content and whether equilibrium is approached (ie time at a given temperature). In type 422 (12% Cr) stainless steel[49], for instance, it was found that the isothermal industrial solution heat treatment of 1038 °C for three hours was not sufficient to dissolve all precipitates formed at the grain boundaries from a 830 °C anneal.

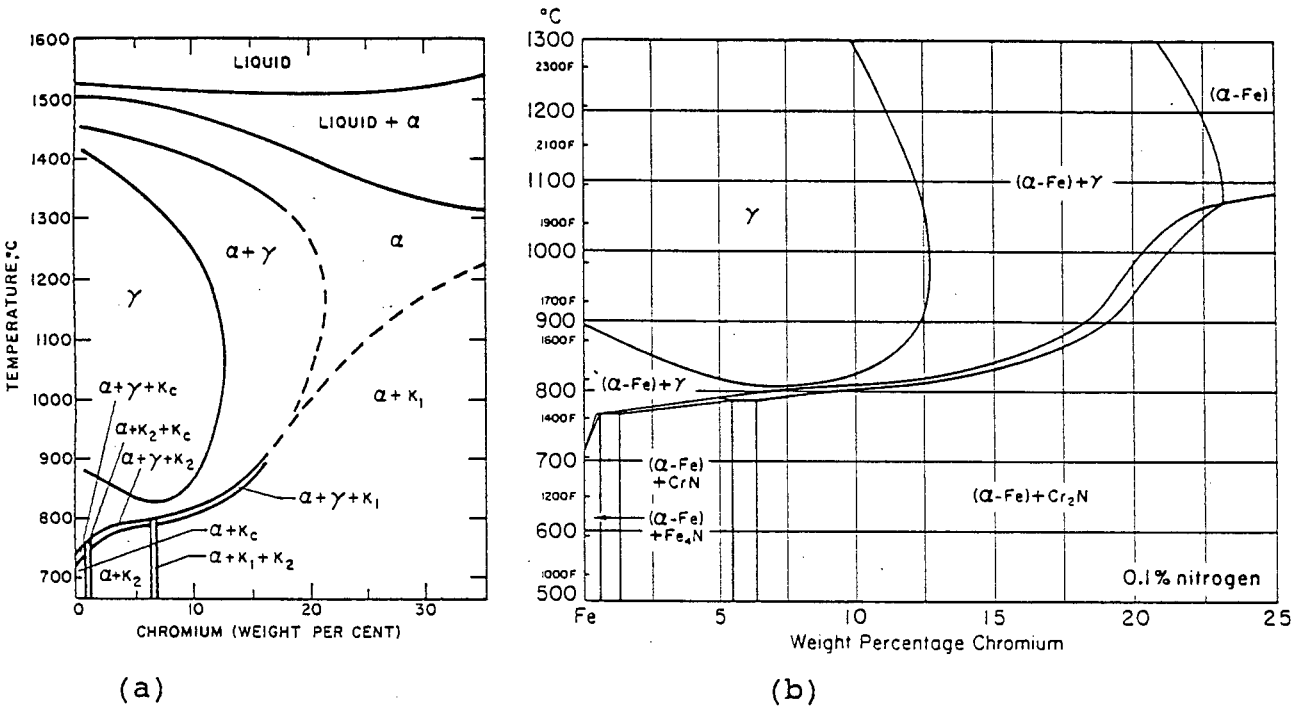

FIGURE (2.9): (a)0.05% carbon[83] and (b) 0.1% nitrogen[50] Fe-Cr phase diagrams illustrating the stability ranges for various precipitates.
$K_1 = M_{23}C_6$; $K_2 = M_7C_3$; $K_c = M_3C$

In 17% Cr alloys, nitrides are expected to dissolve between 950 and 1000 °C, and carbides between 1000 and 1200 °C [42,44].

2.5.2.2 PRECIPITATION OF CARBIDES AND NITRIDES IN STAINLESS STEELS

In Fe-Cr and Fe-Cr-Ni alloys, the size, shape and distribution of phases strongly influences precipitation kinetics[10,15]. Chromium, forming a substantial part of most precipitated phases in Fe-Cr alloys due to its high affinity for nitrogen and carbon, is the slowest diffusing species and thus governs the rate of precipitation and precipitate distribution[38].

(1) PRECIPITATES FORMED DURING COOLING

Heat treating of AISI 430 between 1000 °C and 1100 °C results in a dual phase ferritic austenitic microstructure. During air cooling of such an alloy, from 1100 °C through the precipitation temperature range (430 - 930 °C), $M_{23}C_6$ precipitates were observed to

form primarily on δ-ferrite/δ-ferrite grain boundaries, although similar precipitates of a finer nature were also noted on some δ/γ grain boundaries[51].

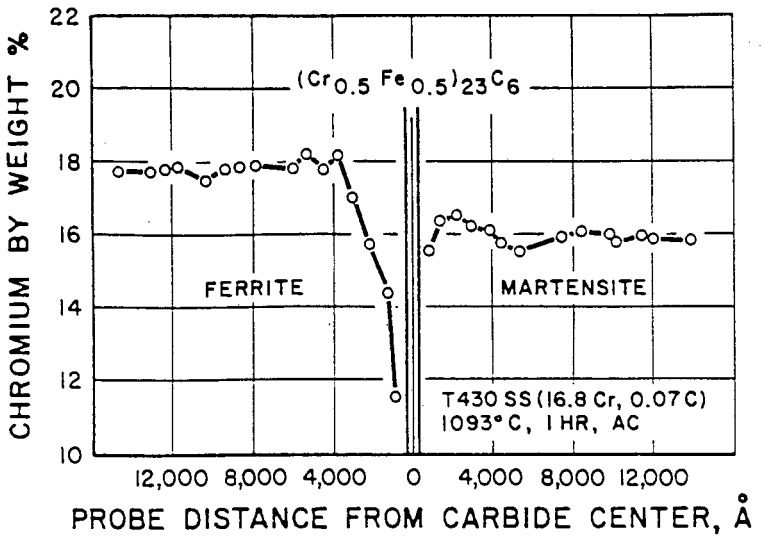

FIGURE (2.10): Chromium depletion to below 11% adjacent to a carbide on the ferrite side of the grain boundary[51].

The diffusion rate of chromium is estimated to be 1000 times higher in ferrite than in austenite at 600 °C [52]. During air cooling through the precipitation range of dual phase stainless steels (430 - 930 °C) the rate of cooling is sufficiently slow for chromium to diffuse through the ferrite to the grain boundaries and leave a narrow chromium depleted zone (Figure (2.10))[51]. Chromium diffusion in austenite is slow, but it has a rich supply of carbon which can diffuse rapidly to the grain boundaries and combine with chromium, which has diffused through the ferrite phase, to form carbides[38,51]. These factors account for the more rapid appearance of precipitates on δ-ferrite/δ-ferrite grain boundaries and the more prominent chromium depleted zone observed in the δ-ferrite phase, adjacent to δ-ferrite/martensite grain boundaries, than in the martensite phase (Fig. (2.10)). It has been noted that water quenching from 1100 °C may not totally prevent precipitation on δ-ferrite grain boundaries[51].

The extent of precipitation and chromium depletion in the ferrite is influenced by ferrite grain size. The larger the grains, the less heterogeneous nucleation sites there are available and the less the extent of carbide precipitation[53]. However, finer grained materials will 'heal' chromium depleted zones more rapidly. Several researchers have found that nitrogen retards nucleation and growth of carbide precipitates, and may reduce the severity of the heat affected zone [38,54].

(2) PRECIPITATES FORMED DURING TEMPERING AND ANNEALING

The phenomenon known as 475 °C embrittlement occurs in both ferritic and martensitic stainless steels. Ferrite, being naturally brittle in stainless steels due to the solid solution strengthening effect of chromium, is embrittled further between 400 and 500 °C by spinodal decomposition of the ferrite phase into chromium and iron rich zones[10]. Carbon and nitrogen intensify this effect by enhancing zone formation[55]. After prolonged heating at 450 °C, ultra fine nitride precipitates have been observed in the central regions of ferrite grains in an essentially martensitic AISI 410 stainless steel[45]. Such precipitates have been noted to cause embrittlement of martensitic stainless steel due to the numerous precipitation sites available in the highly dislocated lath martensite[10].

The acicular Cr_2N precipitates in AISI 410 reportedly increased in size as the tempering temperature was increased to 700 °C [45]. Primary carbides were observed to begin forming at prior austenite and austenite-ferrite grain boundaries at approximately 450 °C (apparent only after long holding times). These precipitates become more apparent in globular form at 600 °C, and at 760 °C the globules appear to coalesce to form continuous bands[38,45]. The precipitates formed in the proximity of 760 °C have been observed to contain a majority of carbon, the bulk of the nitrogen being trapped in the form of Cr_2N. Grain boundary precipitates formed in AISI 430 (which had previously been solution treated at 1100 °C) after heat treating at 700 °C were rich in chromium, having a $(Cr_{0.9}, Fe_{0.1})_{23}C_6$ structure[51], and the intragranular chromium content was 2 % lower than that noted immediately after the solution treatment. In martensite, carbide and nitride precipitates are nucleated within the grains and along lath and prior austenite grain boundaries[44,53]. Above approximately 550 °C, the chromium depleted zone formed in the primary ferrite phase as a consequence of original slow (air) cooling is 'healed' since the rate of depletion of chromium by carbide formation approaches a balance with the rate of bulk diffusion[51]. The peak temperature for grain boundary precipitation in Fe/Cr alloys is approximately 810 °C. At this temperature, in AISI 410[45], the acicular nitride precipitates have dissolved and most of the nitrogen in solution has diffused to the grain boundaries to join up with carbon as continuous film-like $M_{23}(CN)_6$ precipitates.

The tempering of martensite to form secondary ferrite and carbides depends on the transformation kinetics of the precipitation reactions. In turn then, the transformation

kinetics will depend on the martensite morphology. Tempering of lath martensite to obtain a strain free grain structure consists of two stages : recovery and recrystallisation. Recovery involves a rearrangement of dislocations to form a stable configuration, without the motion of large angle lath boundaries. Recrystallisation involves the motion of large angle lath boundaries to form equiaxed grains. These processes are related to packet size (a group of laths having the same spatial orientation) and prior austenite grain size[58].

2.5.2.3 TEMPER RESISTANCE

Alloying elements such as Mn and Ni reduce the solubility of carbides and thus impart a degree of temper resistance[56,57]. Increasing interstitial levels also cause an increase in temper resistance. Irvine et. al.[56] proposed that during heat treatment of 12% Cr stainless steels, precipitation follows the following sequence of events:

$$Fe_3C \rightarrow \begin{Bmatrix} M_2X \\ Cr_7C_3 \end{Bmatrix} \rightarrow Cr_{23}C_6.$$

Fe_3C is not found in 17 wt.% Cr alloys, but in high nitrogen martensitic alloys, the intermediate stage will be prolonged due to the high affinity of chromium for nitrogen, which could slow $M_{23}C_6$ precipitation and thus impart temper resistance to the steel[10,2].

2.5.2.4 EFFECTS OF NITROGEN AND CARBON ON MECHANICAL PROPERTIES

Elements which represent a greater degree of atomic mismatch give rise to a more significant solid solution strengthening effect[14,59]. When trapped in solid solution, interstitial atoms increase the matrix lattice friction stress, and the formation of intergranular precipitates combined with carbon and nitrogen segregation to dislocation sites provides strong barriers to dislocation motion[84].

In Fe-Cr alloys the hardness and strength is increased by the presence of nitrogen and carbon in solution by both a solid solution strengthening effect and by promoting the formation of hard martensite[10,42]. Nitrogen has been shown to have a greater solid solution strengthening effect than carbon, a possible consequence of its greater solubility[57].

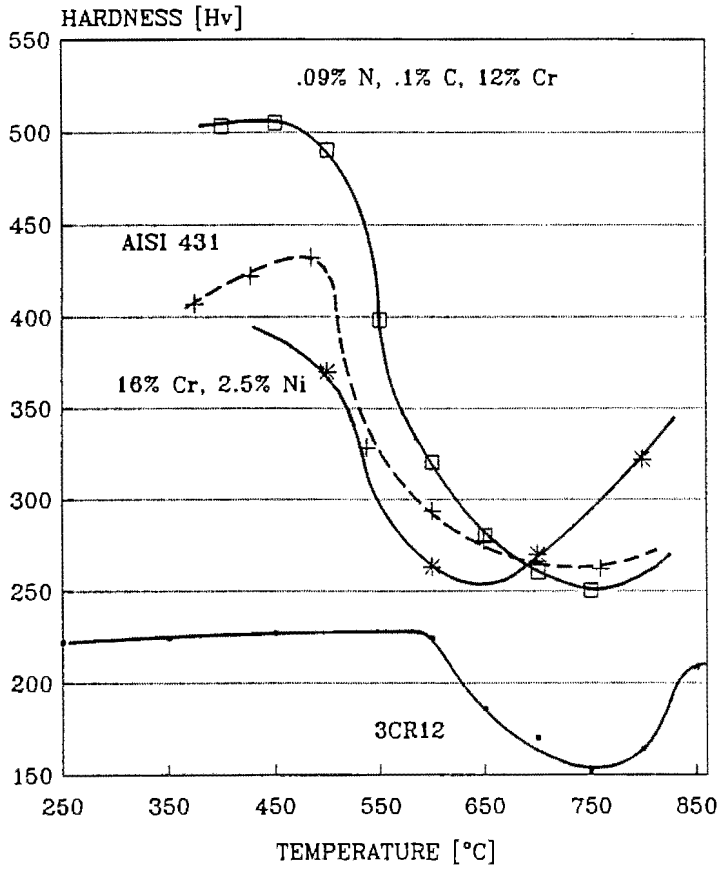

Figure (2.11): Change in hardness accompanying heat treatment of a number of experimental and commercial alloys [9,53,62,63].

Tempering and intercritical annealing of interstitially alloyed steels results in reduced strength and hardness as a result of the removal of carbon and nitrogen from solution[56,17]. The changes in hardness accompanying the heat treatment of two alloys with a low interstitial content (3Cr12[60] and 16Cr, 2.5 Ni[13]) and two alloys with higher interstitial contents (AISI 431[61] and 12Cr, .1C, .09N[56]) are illustrated in Fig (2.11).

The toughness of Fe-Cr alloys is very sensitive to interstitial content, and this becomes more notable as the chromium content increases above 15% [2]. In 17% Cr alloys in the solution treated condition a maximum ductile to brittle transition temperature (DBTT) of approximately 150 °C is obtained at a total carbon and nitrogen content of 0.03% , with little change as the carbon and nitrogen content is increased[32]. The limit of a single phase (ferritic) structure in 17% Cr alloys lies at approximately 0.03%(C+N). Alloys with greater than 0.02%(N+C) [62] in solid solution suffer from low toughness (a DBTT in excess of room temperature) as a consequence of the susceptibility of the ferrite to cleavage fracture, which occurs along soft {100} planes[14].

Ductility can be restored to interstitially alloyed steels by heat treatment. The heat treatment temperatures should be aimed at the dissolution of fine precipitates at

dislocation sites, and the formation of coarse grain boundary and intergranular carbide and nitride precipitates[84]. This stems from the observation that the interstitial concentration in the matrix surrounding fine precipitates on dislocations is expected to be higher than that adjacent to coarse grain boundary precipitates[84], in accordance with the Thomas-Freundlich relationship[63]. The effects of annealing at 800 °C on the ductile to brittle behavior of 17% Cr steel is shown in Fig.(2.12). A maximum in the DBTT (corresponding to a minimum in toughness) can be correlated with the limit of a single phase (δ-ferrite) microstructure[32]. The presence of increasing amounts of tempered martensite, when (C+N)> 0.03%, improves the toughness (depresses the DBTT) as a result of two factors: (1) a reduction in the ferrite grain size as a result of increased amounts of austenite at hot working temperatures[32], and (2) the presence of increased amounts of less cleavage prone tempered martensite in the microstructure[64].

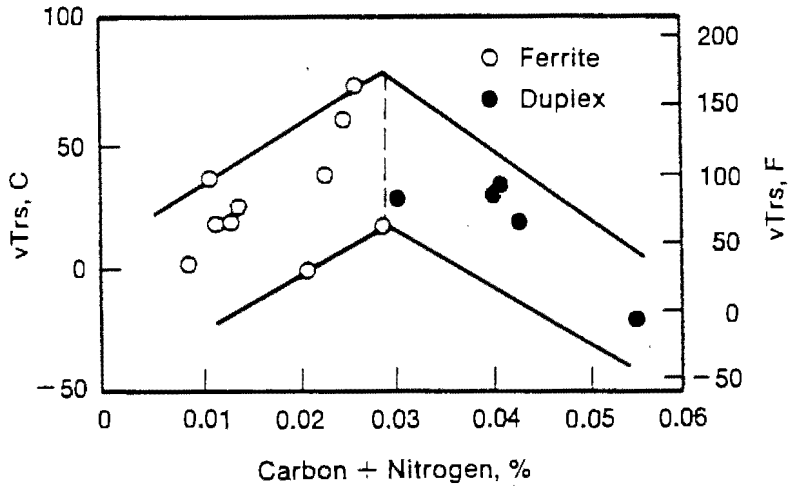

Figure (2.12): Effect of annealing at 800 °C on the impact transition temperature of a 17 wt.% Cr alloy[32]. 0.03 % (C+N) represents the transition between a single phase ferritic and a dual phase ferritic martensitic microstructure.

From Fig.(2.12) it is also evident that the toughness of wholly ferritic alloys ((C+N)<0.03%), after heat treating at 800 °C, decreases as the interstitial level approaches 0.03 wt.%. Intergranular film-like and plate-like precipitates have been shown to degrade the toughness of ferritic steels by providing sites for the nucleation and growth of cracks[65]. The presence of $M_{23}(CN)_6$ precipitates on prior austenite grain boundaries have also been observed to substantially reduce the toughness and elongation of a type 422 martensitic stainless steel[49]. The presence of grain boundary precipitates, and their weakening effect, has been related to the occurrence of transverse splitting in low alloy

steels with a degree of directionality to the microstructure[66]. Acicular intergranular nitride precipitates have been shown to produce embrittling effects in Fe-26% Cr ferritic alloys by providing a large number of crack initiation sites and increasing the flow stress[65].

2.5.2.5 DEVELOPMENT OF NITROGEN ALLOYED STAINLESS STEELS

High nitrogen martensitic 12% Cr stainless steels have been produced with creep resistance and high temperature strengths suitable for advanced turbine applications[67]. Nitrogen has been used extensively in austenitic and duplex stainless steels[52,67,68,69]. As well as a beneficial effect on pitting resistance, nitrogen has a less severe, or even retarding effect on sensitization. It also widens the annealing and hot working temperature ranges for austenitic stainless steels[52].

2.6 MECHANISMS OF DEFORMATION AND FRACTURE OF DUAL PHASE STEELS

2.6.1 YIELDING AND DISLOCATION INTERACTIONS IN DUAL PHASE STEELS

Dual phase ferrite/martensite steels have a low yield stress and commonly exhibit continuous yielding characteristics[18]. These properties have been attributed to the high density of unpinned dislocations in the ferrite phase in the region of ferrite martensite interfaces[26,30,70]. The dislocations are introduced as a result of the 2 to 3% volume change accompanying the martensite transformation, and increase in density as the Ms temperature is lowered[71].

The elimination of yield point elongation (Luders band formation) requires a critical amount of hard phase and a critical strength difference between the hard and the soft phases[70]. The occurrence of continuous yielding in AISI 430 stainless steel has been shown to be dependent on the processing during fabrication, which governs the shape, hardness and distribution of martensite[72]. Continuous yielding characteristics were observed if a rapid solution treatment was employed after cold rolling, before the final anneal. Grushko and Weiss[70] observed that the continuous yielding behavior of a 12% Cr alloy consisting of approximately 90% martensite incorporated two distinct stages (Fig. (2.13)), the first

being related to yielding of the ferrite phase, and the second being attributed to the onset of yielding in the martensite phase. No such behaviour has been observed in the HSLA group of steels, which generally have a much lower martensite content.

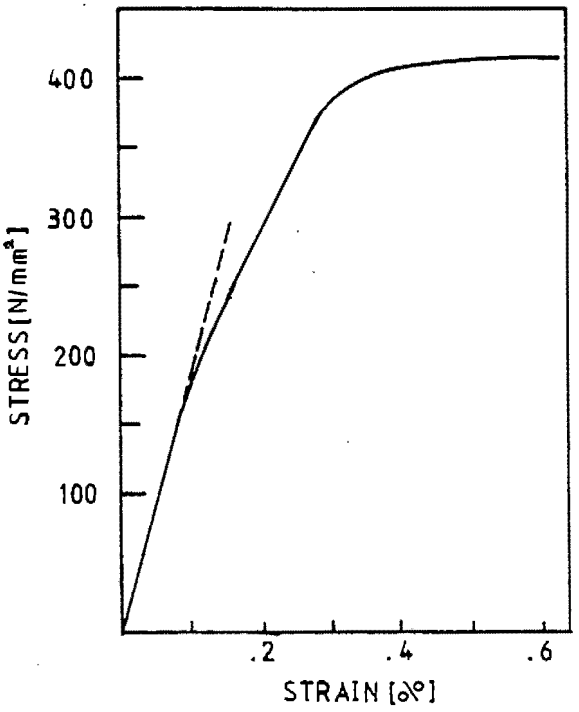

Figure (2.13): The yield behaviour of a dual phase ferritic martensitic 12% Cr steel[70]. Two distinct stages were observed.

The good formability of dual phase steels has been attributed to the high initial work hardening rate[73]. The work hardening of this class of steel has been observed to occur in three distinct stages[73,74,75]:

(1) .1 - .5% strain: Rapid work hardening is observed in the ferrite due to the elimination of residual stresses, and the buildup of back stress in the ferrite phase as a result of plastic incompatibility between the two phases;

(2) .5 - 4% strain: Work hardening rate in the ferrite drops as plastic flow is constrained by undeformed martensite;

(3) 4 - 18 % strain: Dislocation cell structures are formed, and further deformation of the ferrite is governed by dynamic recovery and cross slip and eventual yielding of the martensite phase.

The presence of these three stages has been verified by Jaoul-Crussard analysis of stress/strain tensile test curves[76]. Transmission electron microscope analysis of specimens representing various stages of deformation has shown that while Stage 1 involves interaction of quenched in dislocations and residual stresses with the applied stress, stage 2

is characterised by gradients of dislocation density and configuration across the ferrite grains. This leads to the formation of dislocation cells, which are well defined in stage three. The good formability of dual phase steels has been related to the existence of the second stage[73], in which the rate of decrease of the strain hardening rate is lower than in the other stages.

2.6.2 DEFORMATION AND FRACTURE INITIATION

While the last section described the deformation behaviour of dual phase steels in terms of dislocation motion and interactions, a large amount of the understanding of the deformation and fracture processes of dual phase steels has been derived from the analyses of surface deformation markings and fracture surfaces. Observations made by various authors will be summarized in the following sections.

2.6.2.1 PRE-NECKING DEFORMATION CHARACTERISTICS

As dual phase steels begin to yield slip lines are immediately observed in the ferrite phase (at 45° to the tensile axis)[77,78], which propagate towards the martensite islands. The buildup of slip lines along ferrite/martensite interfaces indicates transfer of load from the ferrite to the martensite phase[77]. The contiguity of the martensite has a strong influence over the type of slip occurring[23,24,77]. In steels with a more inter-connected martensite morphology, a planar slip mode is observed with little evidence of cross slip. An island type martensite morphology results in a more wavy type of slip occurring in the ferrite phase, which bridges between adjacent ferrite grains. The planar slip mode appears to be related to the poor operation of plastic relaxation, while the wavy slip mode is associated with higher plastic relaxation[79]. Increasing the volume of the martensite phase also increases the constraint on plastic deformation in the ferrite phase[23,77].

The onset of yielding in the martensite phase, if it occurs at all, is delayed to higher strains as its volume fraction decreases and hardness increases[77].

2.6.2.2 POST-NECKING DEFORMATION CHARACTERISTICS

The contiguity of the martensite phase has a strong influence on the ductility of, and the mode of fracture occurring in dual phase steels[24,26,80]. Microvoid initiation occurs at a progressively earlier stage in the deformation process as the contiguity increases. This has been shown to result from fracture of the martensite phase (Fig. (2.14)), which leads rapidly into cleavage fracture of the ferrite phase as a result of the high plastic constraint, and possible final fracture before the peak uniform elongation is reached. A comparison of the fracture processes occurring in a steel with a high contiguity and one with a low contiguity (island type) martensite morphology is illustrated in Fig. (2.14).

More generally, conflicting results from various authors as to the main modes of void initiation and crack propagation in dual phase steels suggest that these factors are very sensitive to variations in microstructure produced by differences in alloying element contents and heat treatment procedures. In the following paragraphs, pertinent observations by various authors relating to the fracture processes occurring in dual phase steels are summarized.

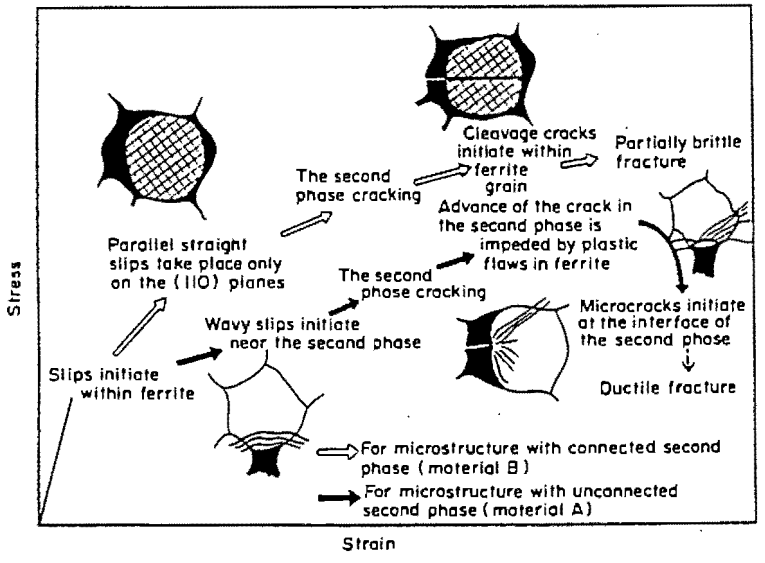

Figure (2.14): Comparison of the process leading to fracture in two dual phase steels, one with an island type and one with an interconnected type martensite morphology[24].

Ray[80] noted that microvoid formation in a low alloy dual phase steel containing 50% martensite occurred in four different ways: (1) interfacial decohesion at ferrite/martensite grain boundaries, (2) decohesion of the interface around large inclusions in the ferrite phase, (3) fracture of the martensite phase, and (4) cleavage fracture of the ferrite phase in

regions of high stress intensity (e.g. sharp martensite corners), and suggested that while (1) and (2) probably occurred first, all four mechanisms could operate simultaneously.

Szewczyk and Gurland[78] found that while occasional void nucleation occurred around MnS inclusions, the most prominent mode in operation was interfacial decohesion at ferrite martensite grain boundaries in regions of high plastic constraint. The former mechanism produced large ductile dimples on the fracture surfaces while the latter resulted in a fine uniform background of dimples.

In determining the effects of martensite hardness on the fracture modes of dual phase steels, Tomota et al[25] found that as the hardness decreased, the mechanism of void initiation changed from one of decohesion at ferrite martensite grain boundaries, resulting in cleavage fracture of the ferrite phase and ductile fracture of the martensite phase, to one of fracture of the martensite phase, which resulted in a purely ductile fracture appearance. Final fracture involved linking of voids formed around small inclusions.

Hayden and Floreen[7] noted that if the harder, tougher phase in Fe-Cr-Ni stainless alloys (martensite) can deform at fairly low stresses, cleavage fracture of the ferrite phase can be prevented. They also observed numerous evidence of plastic blunting of cleavage cracks in the ferrite phase by martensite islands during low temperature tensile and impact testing.

2.6.2.3 FRACTURE OF LAMELLAR DUAL PHASE STEELS

The strength component obtained from a fine lamellar ferrite/martensite composite phase appears to be two fold: it offers more effective barriers to dislocation motion in the ferrite phase, and simultaneously provides more efficient composite strengthening for a fixed volume percent of martensite[26], as given by the theory of discontinuous fibre composites[81].

The mode of fracture occurring in lamellar dual phase steels can possibly be related to the fracture of ferrite/pearlite steels, which has been investigated by Cuddy and Bassim[82]. They noted that dislocation activity in the ferrite regions of pearlite colonies was retarded by the Fe_3C platelets. Microvoid initiation was observed to occur in the pearlite colonies, and it was proposed that this occurred by parting of the Fe_3C platelets under combined

tensile and shear loading, which lead to ductile dimple fracture of the inter-connecting ferrite and crack propagation normal to the pearlite colonies, as illustrated in Fig. (2.15).

This mechanism of fracture is supported by in situ observations of the tensile fracture of a lamellar ferrite/martensite dual phase steel[36]. However, it was also observed that where voids nucleated around inclusions, the lamellar martensite phase retarded crack propagation, and that if the primary slip system acting in the ferrite phase and the direction of the martensite lamellae are parallel, void formation may occur by decohesion of inter-colony boundaries.

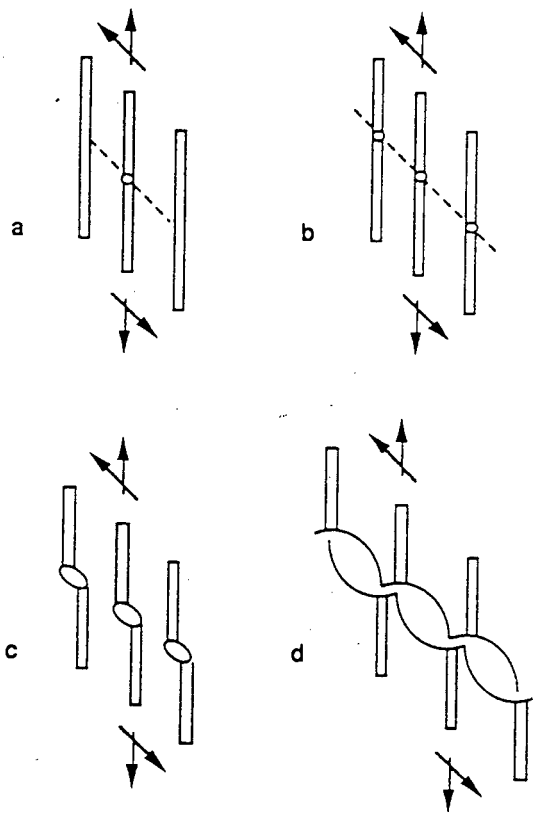

Figure (2.15): Mechanism of fracture initiation in the pearlite colonies of ferrite pearlite steels[82]. (a) Cracking of cementite plate; (b) shear zone developing in ferrite causing cracking in adjacent plates; (c) and (d) void formation and coalescence.

CHAPTER THREE

EXPERIMENTAL AND ANALYTICAL TECHNIQUES

This section outlines the experimental methods used in this investigation. It includes descriptions of the specimens and procedures used for tensile and impacting of the experimental and standard steels, and of the rolling procedures used in order to refine the microstructures of a number of the alloys analysed in this investigation.

3.1 MATERIALS USED

3.1.1 EXPERIMENTAL ALLOY COMPOSITIONS

The experimental alloys used in this project were manufactured in the laboratories at Middleburg Steel and Alloys, Transvaal. The materials were received in the hot rolled condition (Starting temperature between 1000 and 1100 °C, and finishing temperature between 780 and 880 °C) as plate of 8 mm to 10 mm in thickness. The chemical compositions of the heats received from Middleburg Steel and Alloys are listed in Table (3.1).

ALLOY	%Cr	%Ni	%Mn	$\%N_2$	%C	%Si	%S	%P
A	16.36	2.55	1.05	0.01	0.02	0.45	.012	.021
C	16.85	0.52	0.98	0.121	0.05	0.63	.009	.019
D	16.04	0.13	0.94	0.067	0.032	0.51	.011	.021
E	15.69	1.12	0.93	0.116	0.026	0.25	.005	.013

Table (3.1): Chemical compositions of the experimental alloys, expressed as weight percent.

3.1.2 COMMERCIAL ALLOY COMPOSITIONS

A number of commercially available alloys were incorporated in the test program. The compositions of these alloys, as determined in the Middleburg Steel and Alloys laboratories, are listed in Table (3.2). While AISI 304 and 431 were purchased from local (Cape Town) distributors, as 12mm plate and 25mm bar respectively, the AISI 430 material was supplied as 8mm plate off a production run at the Middleburg mill, as it was not locally available in thickness greater than 4mm. A minimum 8mm in thickness was required of all the materials tested in order to meet suitable test specimen requirements.

AISI DESIG.	%Cr	%Ni	%Mn	$\%N_2$	%C	%Si	%S	%P
304	18.44	8.21	1.59	.045	.023	.37	.007	.026
430	16.61	.16	.61	.041	.063	.66	.005	.029
431	15.71	1.61	.44	.035	.186	.31	.007	.024

Table (3.2) Chemical compositions of the standard stainless steel grades AISI 304, 430 and 431.

3.2 METALLOGRAPHY

The microstructures of the alloys studied in this thesis were characterized by both conventional light microscopy, using a REICHERT MeF2 optical microscope, and scanning electron microscopy (SEM), using a CAMBRIDGE S200 instrument.

For the purposes of optical microscopy and SEM analysis, samples were prepared by conventional metallographic techniques and finished either by mechanical polishing with 0.25 μm diamond paste, or by electropolishing after mechanical polishing with 3 μm diamond paste.

The various etching procedures used in specimen preparation for conventional light microscopy and SEM analysis are described below.

PROCEDURE A: Dip etch in a solution of 10 ml HNO_3, 20 ml HCl and 30 ml H_2O cooled to below 20 °C for 90 to 180 seconds;

PROCEDURE B: Dip etch for 5 to 15 seconds in a solution of 100 ml 1:5 vol/vol HCl, 2g $NH_4F.HF$ and 1g $K_2S_2O_5$;

PROCEDURE C: Electrolytic polish for 1 minute in a solution containing 25g Cr_2O_3, 7 ml H_2O and 133 ml CH_3COOH, at a potential difference of 20 Volts, and maintained below 20 °C in an ice bath. This is followed by etching in the same solution at a potential difference between 3 and 6 Volts for 1 to 3 minutes.

The combination of Procedure A followed by Procedure B proved effective in distinguishing between martensite, ferrite and austenite phases in the high nickel alloys, while with the high nitrogen alloys a satisfactory etch was achieved using either Procedure A or Procedure C. Procedure A emphasized carbide and nitride precipitates, while Procedure C attacked the same precipitates. As a standard procedure all specimens for microscopic analysis were etched on the planar face L-ST, as described in Fig. (3.1).

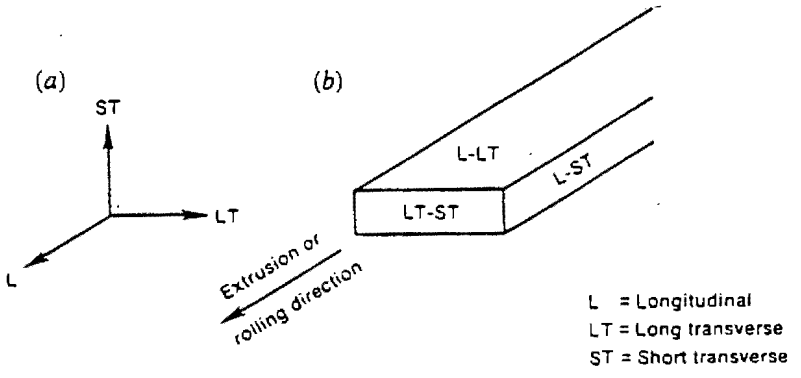

Figure (3.1) Definitions of (a) axis and (b) planar section notation for a rolled microstructure[13].

3.3 ELECTRON MICROSCOPY

Scanning Electron Microscopy, using a Cambridge S200 with a Tracor Northern Energy Dispersive X-Ray Spectroscopy (EDS) attachment, was employed in order to characterise both microstructural changes accompanying heat treatments and fractography produced during mechanical testing. While polished and etched specimens were imaged using a 30 kV primary accelerating voltage, for the purposes of fracture surface analysis and EDS an accelerating voltage of 20 kV was employed. Either secondary electron, or mixed secondary electron and back scattered electron imaging modes were used.

Transmission electron microscopy (TEM) was also used to characterise the precipitation reactions occurring during the heat treatment of a high nitrogen stainless steel alloy. Disc specimens (3 mm diameter) were punched from demagnetised 0.25 mm sheet. The discs were then ground to 0.1 mm on 800 grit grinding paper using an adjustable hand held grinding jig. Electropolishing was done in a Struers Tenupol 2 jet polisher using a solution containing 80 ml glycerol, 300 ml methanol and 20 ml perchloric acid, which was mixed and maintained at -10 °C. Electropolishing was done at a potential difference of 57.5 Volts and a flow rate of 3.1 . The specimens were analyzed in a JEOL 200 CX electron microscope at an operating voltage of 200 kV.

3.4 HEAT TREATMENTS

Heat treatments were performed in a NABER chamber furnace. For any particular heat treatment the temperature was allowed to settle with a deviation of no more than 5 °C above or below the stated temperature. Specimens for mechanical testing were heat treated after machining, and thus they were coated with a zirconia based ceramic film (ISOMOL 100) prior to heat treatment in order to reduce surface damage. All metallographic and mechanical testing specimens were solution treated for 1 hour at 1000 °C before any form of testing or further heat treatments were performed on the specimens.

3.5 HARDNESS MEASUREMENTS

All hardness measurements were made on the planar face L-ST, as described in Figure (3.1). Bulk hardness measurements were made using a Vickers diamond pyramid indenter at a load of 30 Kgf. Each value quoted is an average of at least five indentations.

Microhardness measurements were performed on a SHIMADZU microhardness tester. A Vickers diamond pyramid was used, at a load of either 50 gf, 100 gf or 200 gf for a period of five seconds, and each value quoted is an average of a minimum of ten microhardness indentations.

3.6 MECHANICAL TESTING

3.6.1 TENSILE TESTS

Tensile tests were performed on a ZWICK universal tensile testing machine equipped with a 200 kN load cell and a clip on extensometer. The tensile tester was interfaced with a computer and equipped with a ZWICK data acquisition program.

Two types of tensile specimens were used. The round type (Fig. (3.2a)) was used for testing the original plate or bar material and represents a scaled down version of an ASTM E8 standard tensile specimen. The gauge length used (18mm) was 4 times the gauge diameter, and allowed easy accommodation of the extensometer. Flat specimens (Fig. (3.2b)) were used for tensile testing sheet material which had been rolled down to 1mm in thickness. This specimen shape was designed around the limited width of the rolled material (as a result of the low load capacity of the rolling apparatus).

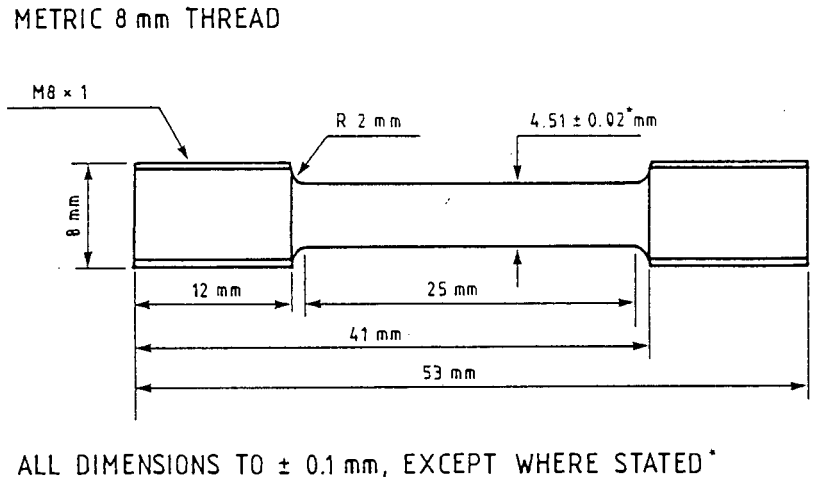

(a)

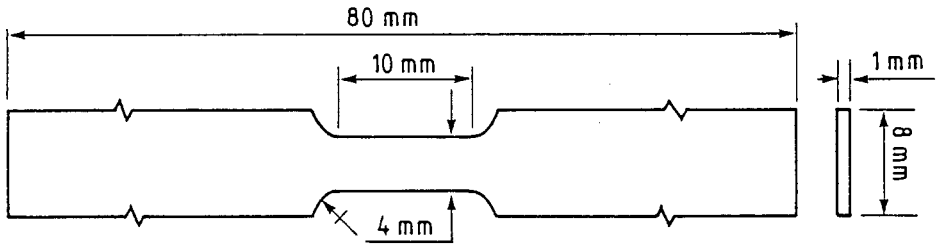

(b)

Figure (3.2): Two Types of Tensile Specimen were used: (a) a round type and (b) a flat type.

All tensile specimens were machined parallel to the rolling direction, and were tested in duplicate at an initial strain rate of 10^{-3} s^{-1}.

3.6.1.1 Interrupted Stage Tensile Testing

This was done using the flat type specimens, and with the extensometer arms in position. The gauge lengths of the specimens were polished and etched before testing. The specimens were loaded to a particular percentage strain, unloaded and then examined in the SEM. This was repeated throughout the duration of a tensile test, up to the point of fracture. To monitor progressive stages of plastic deformation, positions on the gauge length were marked using microhardness indentations. Sequences of photographs, depicting the progressive stages of surface deformation, were constructed by taking photographs of the marked positions during interruptions of the tensile test.

3.6.2 IMPACT TESTS

Impact resistance was measured using sub-size Charpy V notch specimens. All specimens had the dimensions 7.5mm x 10mm x 53mm. The thickness of the specimens was limited by the thickness of the original experimental heats, supplied in plate form and varying in thickness between 8 and 11 mm. The length of the specimens was restricted by the limited quantity of some of the experimental heats. Thus the specimens were 2mm shorter than recommended in the standard testing methods (ASTM E8). However several random comparisons were made between the shortened specimens and the full length specimens. With the exception of AISI 304, no difference in impact energy was detected, as plastic deformation was limited to the immediate vicinity of fracture. All specimens were machined with the long axis in the direction of rolling and with the notch in the L-ST planar face (described in Fig (3.1)). Where testing temperature is not stated it can be assumed that the tests were performed at room temperature.

3.7 LABORATORY ROLLING SCHEDULES

3.7.1 ROLLING PROCEDURES

Rolling was performed on a DINKEL laboratory rolling apparatus. The small load capacity of the apparatus (due to spring loaded mill wheels) limited the specimen size which could be rolled, and a maximum reduction of 0.25mm per pass during cold rolling or 0.5 mm per pass during hot rolling was employed during rolling of the stainless steel specimens. A particular rolling schedule was developed for each class of alloy, and was designed to take into account factors such as splitting and high hardness. The final thickness was 1mm, and all materials, except for AISI 431, went through 75 % cold deformation before a final recrystallisation heat treatment. The mechanical processing of each alloy is summarized in Table (3.3).

3.7.2 HEAT TREATMENTS

The temperatures at which the alloys were recrystallised, and the times required at the specific temperatures, are shown in Table (3.3). The recrystallisation treatment for AISI 430 was chosen to allow for full recrystallisation of the microstructure (no further change in microhardness with increased heat treatment time), which produced an equiaxed grain structure while maintaining a fine grain size.

Alloy	Initial Rolling Procedure/s	Final Rolling Procedure	Recryst. Temp [C]	Time [Mins]
A	H/R 8mm → 4mm; Starting 1000 °C	C/R 4mm → 1mm, no intermediate H/T	1000 A/C	120
AISI 430	C/R 8.2mm → 7mm → 5.8mm → 4mm Intermediate heat treatments of 830 °C/ 5 mins.	C/R 4mm → 1mm	830 W/Q	3
AISI 431	H/R 4mm → 1mm, starting temp. 1000 °C; one intermediate H/T at 1000 °C for 30 mins.		1040 A/C	40

H/R= HOT ROLLED, C/R= COLD ROLLED, H/T= HEAT TREATED

Table (3.3): Summary of the thermomechanical treatments performed on a Alloy A, AISI 430 and AISI 431.

The heat treatment temperature and time for AISI 431 was based on the point at which dissolution of carbide precipitates was complete. The heat treatment used for Alloy A was based on attaining a fully recrystallised, equiaxed grain structure.

3.8 DILATOMETRY

Dilatometry was employed primarily to determine the temperature at which the austenite transforms to martensite (Ms temperature) during cooling, but was also used to identify the approximate temperatures at which phase transformations started to occur during heating. Specimens of dimensions 4mm x 4mm x 50mm were used, and heating was performed at a rate of 4 °C per minute while cooling was uncontrolled (furnace switched off). All tests were performed in an argon atmosphere. The A_{c1} and A_{c3} temperatures, which were determined from the traces, refer the onset and completion of austenite formation.

3.9 NICKEL COATING OF FRACTURED SPECIMENS

Fractured tensile and impact specimens were electrolytically coated with nickel in order to prevent edge damage during sectioning, grinding and polishing. The specimens were coated in a solution containing 500 ml H_2O, 125 g Ni_2SO_4, 25 g $NiCl_2$, and 20 g H_3PO_3, maintained at 60 °C. Prior to coating the specimens were cleaned with the following procedure: ultra-sound in Arklone, wash with distilled water, dip in ammonia solution for ten seconds, wash with distilled water, dip in 30% HCl solution for 5 seconds, wash with distilled water, dip in 30% H_2SO_4 solution for 10 seconds, and finally rinse thoroughly with alcohol. The specimen to be coated was then immediately placed in the coating solution and connected to the power supply as the cathode, while a piece of almost pure nickel was connected as the anode, and a potential difference of 1 V was applied across the terminals. This resulted in a current of between 0.08 and 0.1 Amps. A coating time of approximately 24 hours was employed.

CHAPTER FOUR

RESULTS

4.1 MICROSTRUCTURAL CHARACTERISATION OF EXPERIMENTAL AND STANDARD ALLOYS

4.1.1 ALLOY A

In the solution treated condition alloy A consists of 71% martensite and 29% ferrite (Fig.(4.3)). The extent of partitioning of Cr, Ni and Mn between the ferrite and martensite phases is shown in Table (4.1). The hardness in the solution treated condition is 333 Hv_{30}.

	ELEMENT PARTITIONING(wt %)			
ELEMENT	MARTENSITE		FERRITE	
Chromium	15.6	±0.1	18.8	±0.3
Nickel	2.7	±0.2	1.4	±0.2
Manganese	1.1	±0.1	1.0	±0.1

Table (4.1): The extent of partitioning in Alloy A in the solution treated condition, as determined by EDS. [20 kV].

The A_{c1}, A_{c3} and M_s temperatures for alloy A, as determined by dilatometry (Fig. (4.1)), are 635, 795 and 218 °C respectively.

The variation in hardness accompanying heat treatment for one hour in the temperature range 500 - 900 °C is illustrated in Fig. (4.2) . Heat treating for two hours at the various temperatures did not substantially alter the hardness from that observed after one hour, although the microstructural transformations (observed optically) appeared more advanced after a two hour treatment. Thus for the purpose of mechanical testing, two hour heat treatments were employed.

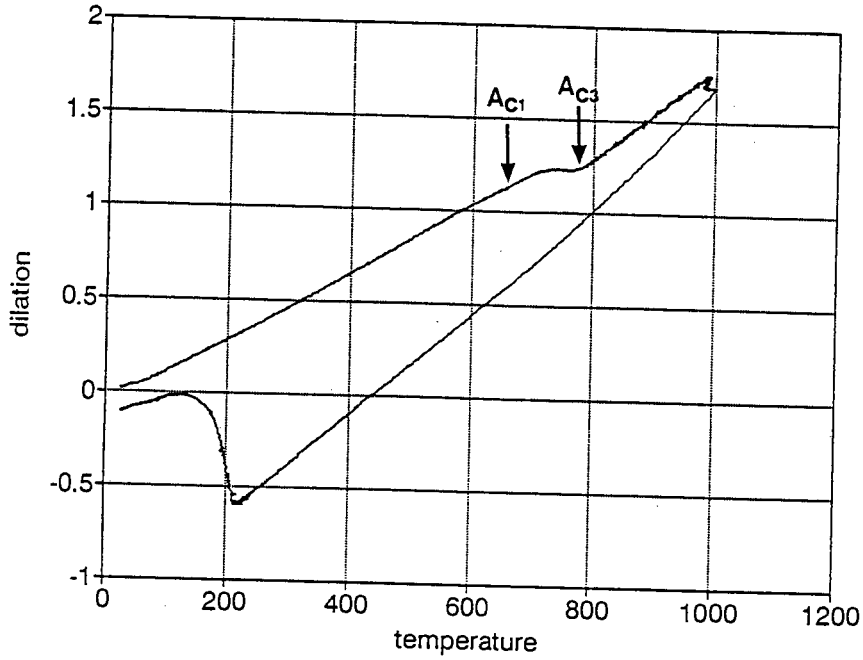

Figure (4.1): Dilatometric trace for alloy A. The heating rate was 4 °C/minute

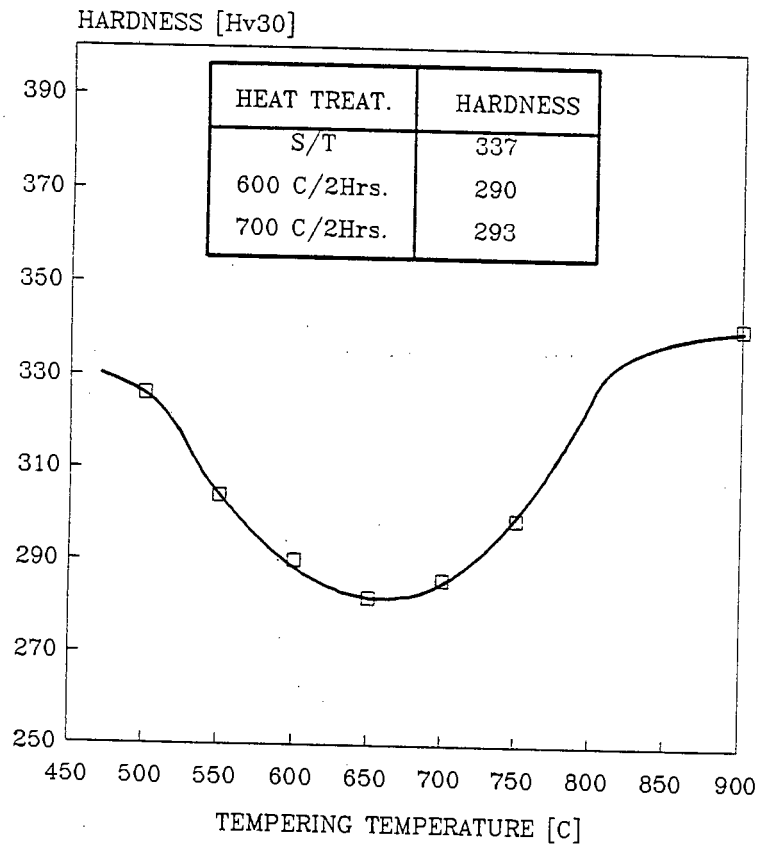

HEAT TREAT.	HARDNESS
S/T	337
600 C/2Hrs.	290
700 C/2Hrs.	293

Figure (4.2): Effect of heat treating for one hour at various tempereatures on the hardness of alloy A. The hardness values in the solution treated condition and after tempering at 600 and 700 °C for two hours are inset.

Tempering for two hours at 600 °C results in softening of the alloy, as seen by a drop in hardness from 333 Hv_{30} in the solution treated condition to 279 Hv_{30}. Microstructural analysis revealed that the martensite phase has broken down to form secondary ferrite with some fine intergranular and interlath precipitation (Fig.(4.3b)). While some $M_{23}C_6$ precipitation is expected, the appearance of Fig. (4.3b) suggests that there is also a small amount of austenite formed (larger white spots), since the low interstitial content would prevent the formation of such large carbide precipitates.

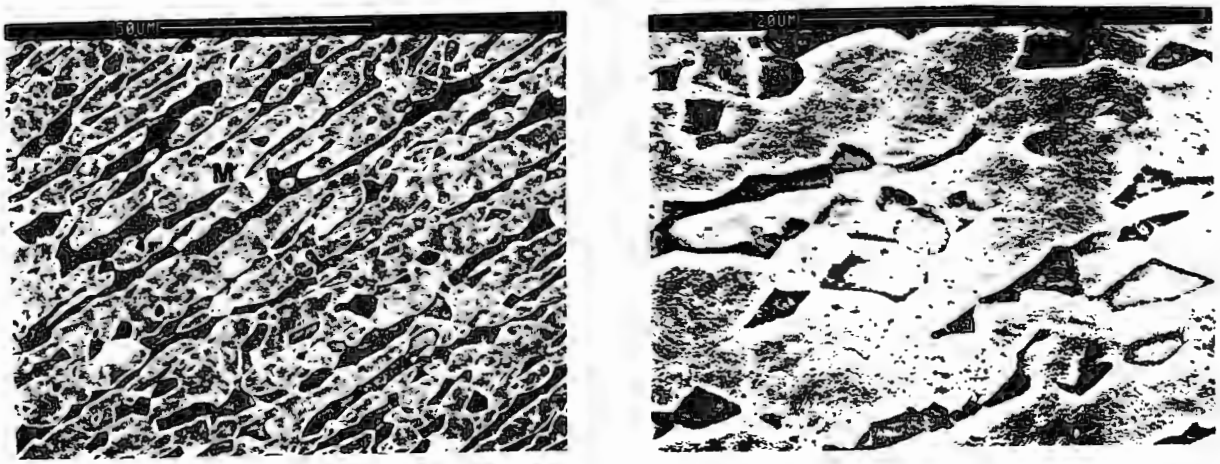

(a) (b)

Figure (4.3): Appearance of the microstructure of Alloy A (a) in the solution treated condition, and (b) after tempering at 600 °C for two hours, illustrating the effect of tempering on the microstructure of the martensite phase.

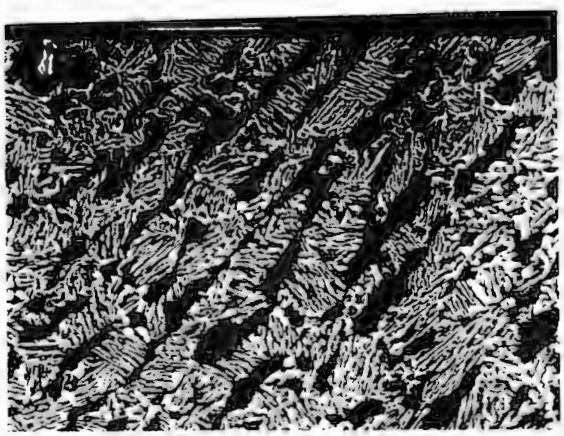

Figure (4.4): Appearance of the microstructure of Alloy A after Tempering at 700 °C for 2 hours.[F = δ-ferrite, L = lamellar ferrite/martensite composite phase]

Inter-critical annealing at 700 °C (which is above the A_{C1} temperature) for two hours results in nucleation and growth of austenite (white regions, Fig. (4.4)) in the original martensite phase, to form a lamellar composite structure. At room temperature, this composite consists of lamellar martensite and inter lamellar secondary (α) ferrite. The δ-ferrite phase remains substantially unchanged during these heat treatments.

4.1.1.1 ISOTHERMAL TREATMENT AT 700 °C

In order to assess the rate at which the lamellar composite phase forms and how it affects the hardness, the isothermal response of alloy A to heat treatment at 700 °C was investigated. There is a substantial drop in hardness in the first eight minutes at 700 °C (Fig.(4.5)). In this time there is little progress made in the austenite reversion (Figs. (4.6a) and (4.6b)), except for regions of fine austenite nucleated on lath and prior austenite boundaries of the original martensite phase.

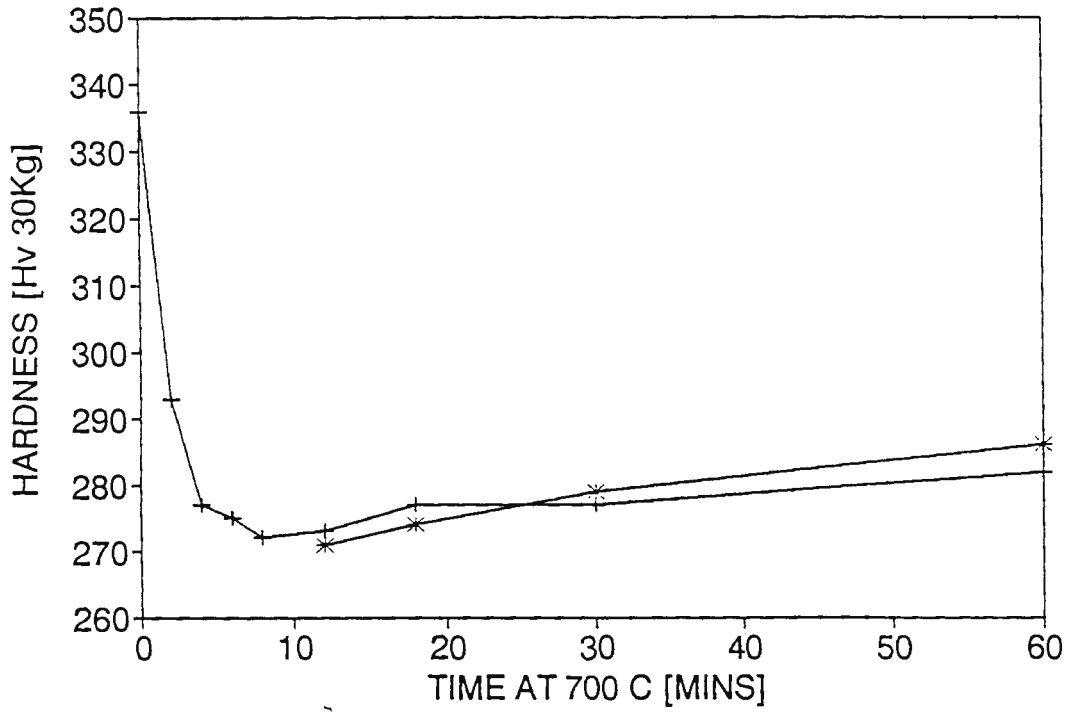

* - SUB-ZERO COOLED

Figure (4.5): Variation in hardness of alloy C with heat treating time at 700 °C, and the effect of cooling the specimens to -70 °C on the hardness.

Subsequent increases in heat treatment time result in a gradual increase in hardness as the microstructure contains progressively larger amounts of martensite. The difference in the microstructures after tempering at 700 °C for 1 hour and 2 hours can be observed by comparing fig. (4.6c) and fig. (4.4).

In order to determine if any austenite was retained to room temperature after quenching from 700 °C, several specimens were cooled to approximately -70 °C in a mixture of alcohol and dry ice. As illustrated in Fig.(4.5) there is little change in hardness after sub zero cooling, indicating that little or no austenite was retained to room temperature. During the course of the isothermal treatments no change was observed to occur in the δ-ferrite phase.

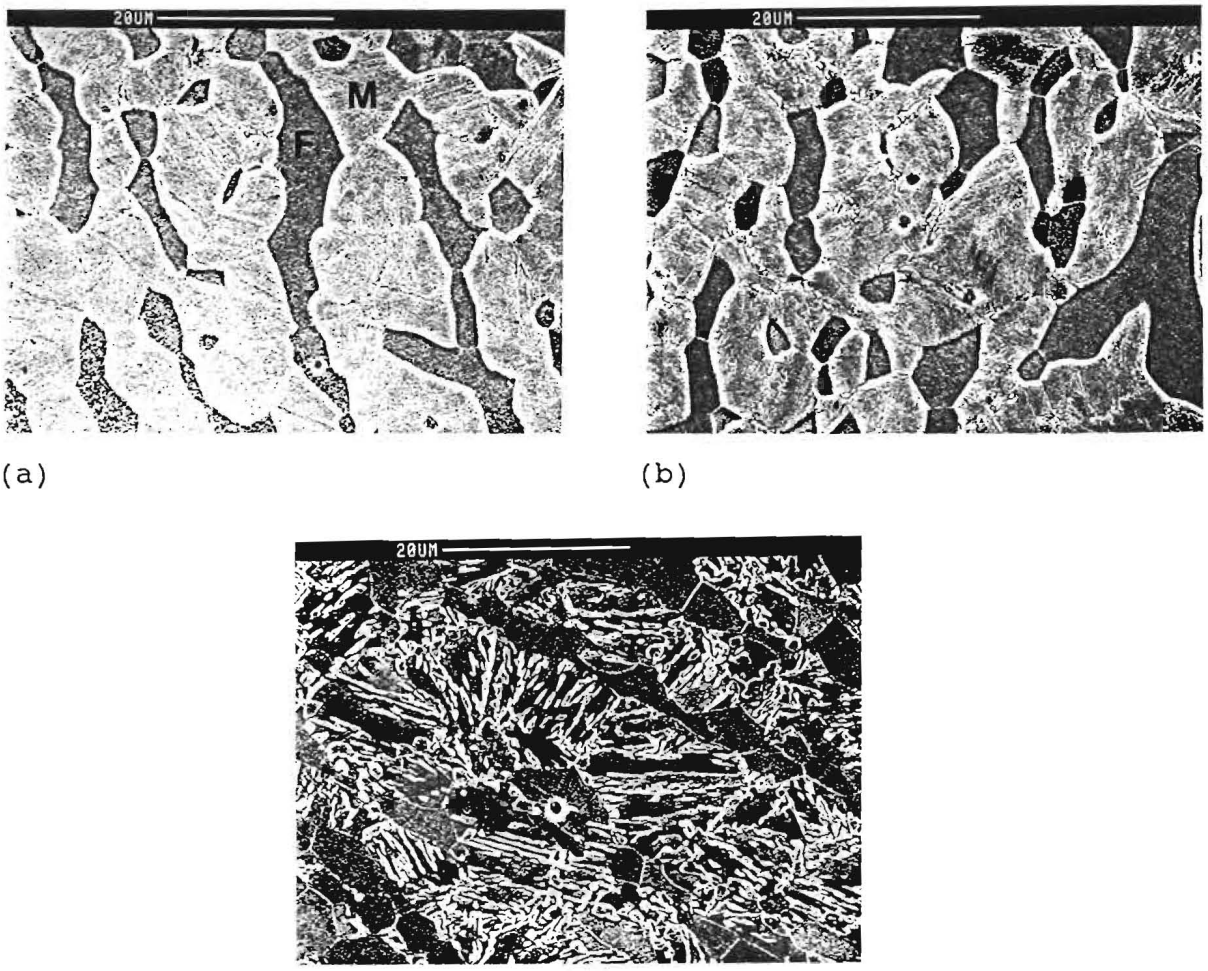

Figure (4.6): Appearance of the microstructure of Alloy A after inter-critical annealing at 700 °C for (a) 4, (b) 8 and (c) 60 minutes.

4.1.2 ALLOY C

The microstructure of Alloy C consists of 64% martensite, as elongated bands, in a ferrite matrix. The average grain diameter of the martensite phase is 22 μm, while the ferrite grain size varies from 10 to 50 μm in thickness and 20 to 120 μm in length. The combined average grain diameter for the alloy is 38 μm. The hardness in the solution treated condition is 346 Hv_{30}. The extent of partitioning of Cr, Ni and Mn between the two phases in alloy C in the solution treated condition is indicated in Table (4.2).

	ELEMENT PARTITIONING (wt %)			
ELEMENT	MARTENSITE		FERRITE	
Cromium	16.2	±.2	18.1	±.4
Nickel	0.5	±.1	0.2	±.2
Manganese	1.2	±.2	0.9	±.1

Table (4.2): Partitioning of alloying elements between the ferrite and martensite phases of Alloy C in the solution treated condition as determined by EDS [20 kV].

The M_S an A_{C1} temperatures, as determined by dilatometry (Fig. (4.7)), are 182 and 833 °C respectively. The A_{C3} temperature is not clearly defined, but hardness measurements on heat treated specimens suggest that the transformation to austenite is more or less complete at 900 °C.

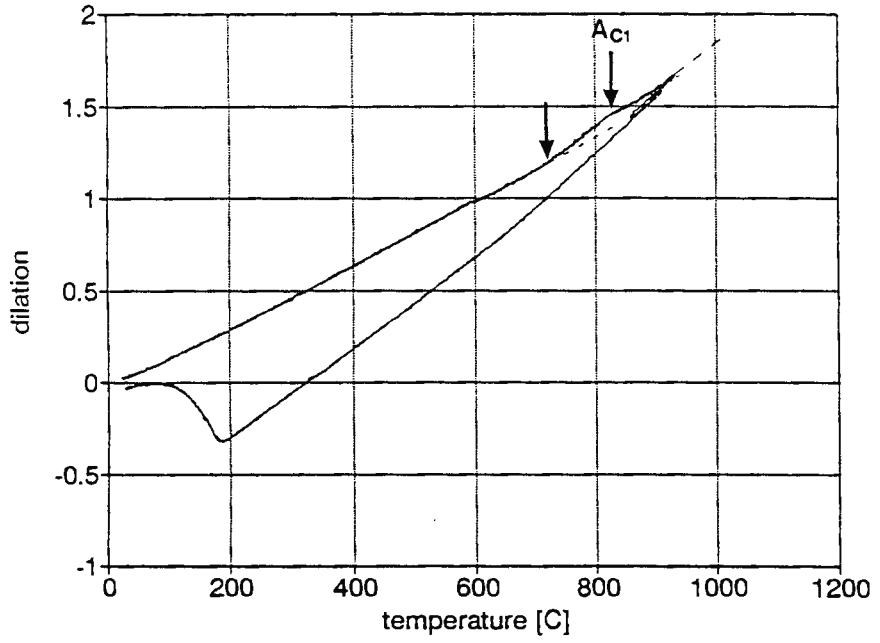

Figure (4.7): Dilatometric trace for alloy C. The trace was performed at a heating rate of 4 °C/minute.

The changes in hardness accompanying heat treatment of alloy C at various temperatures between 400 and 1000 °C are illustrated in Fig. (4.8).

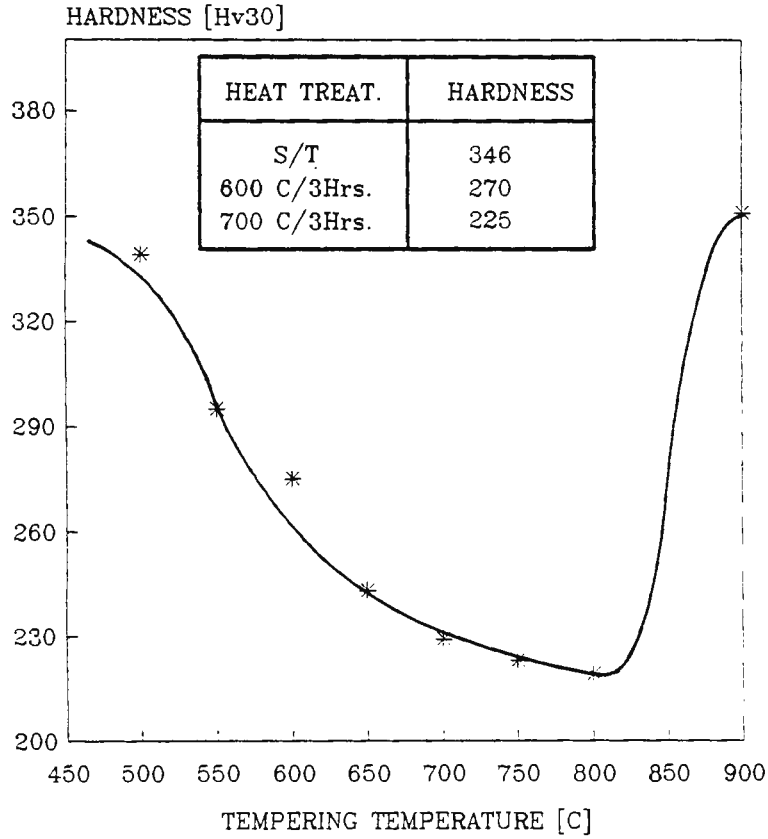

Figure (4.8): Hardness variation accompanying the heat treatment of alloy C for one hour at various temperatures. Inset is the hardness in the solution treated (S/T) condition, and after 3 hours at 600 and 700 °C.

The appearance of the microstructure of alloy C in the solution treated condition is illustrated in Fig. (4.9a). Heat treating at 500 °C for one hour results in some fine grain boundary precipitation, and ultra fine interlath precipitation. No precipitation occurs within the ferrite grains. After one hour at 600 °C fine blocky type precipitates are in evidence on most δ-ferrite grain boundaries. Precipitates are also evident as fine films and globules on δ-ferrite/martensite and prior austenite grain boundaries (Fig.(4.9b)). The precipitates on δ-ferrite grain boundaries coarsen after 3 hours at 600 °C, but still have blocky shapes, while fine precipitates were clearly visible along lath boundaries within the martensite phase. Very fine acicular precipitates are visible in some ferrite grains after tempering at 600 °C for three hours when analysed in the SEM.

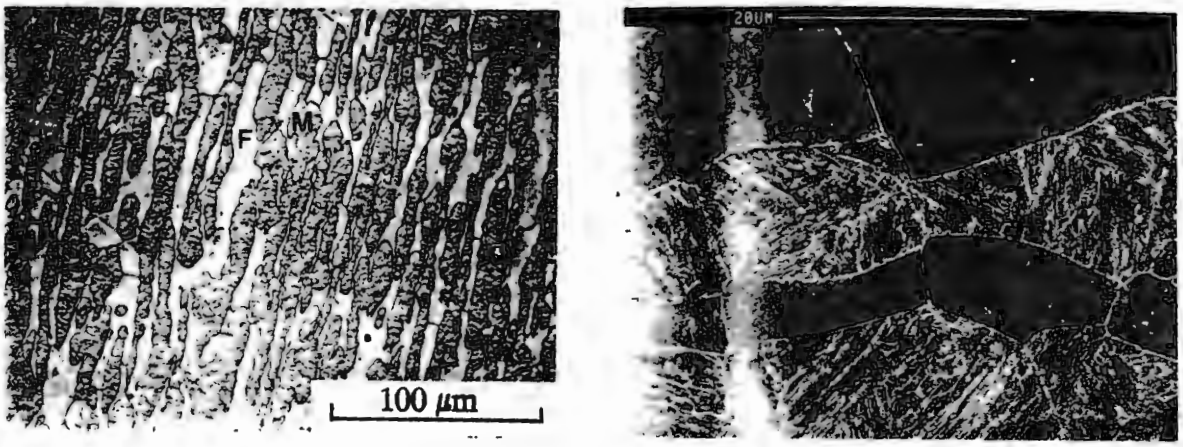

Figure (4.9): (a) Appearance of the microstructure of alloy C in the solution treated condition, indidcating elongated martensite islands in a ferrite matrix, and (b) appearance of the microstructure after tempering at 600 °C for one hour.

Heat treating at 700 °C for one hour results in a further coarsening of grain boundary precipitates, which form as semi-continuous films and globular arrays along δ-ferrite and δ-ferrite/martensite boundaries (Fig. (4.10a)). A dense distribution of fine acicular precipitates is visible in δ-ferrite grains, as shown in Fig. (4.10b), which are thought to be nitrides due to their distinctive shape.

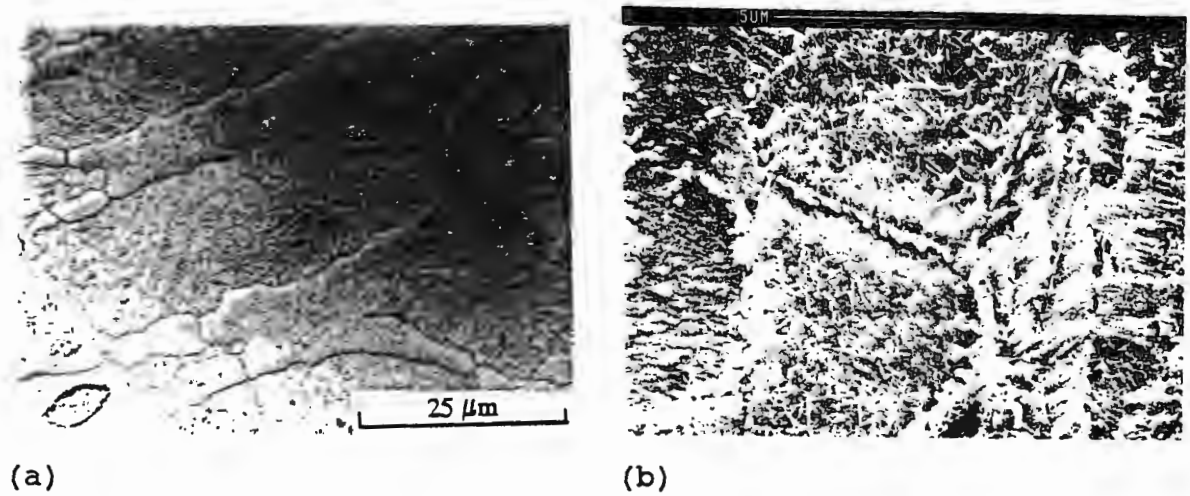

Figure (4.10): Appearance of the microstructure of alloy C after tempering at 700 °C for (a) 1 hour and (b) 3 hours.

A three hour heat treatment at 700 °C produced very little change in the appearance of the microstructure from that observed after one hour. The effects of heat treatment at 600 and 700 °C on the microhardness of the ferrite and martensite phases of alloy C are illustrated in Fig. (4.11).

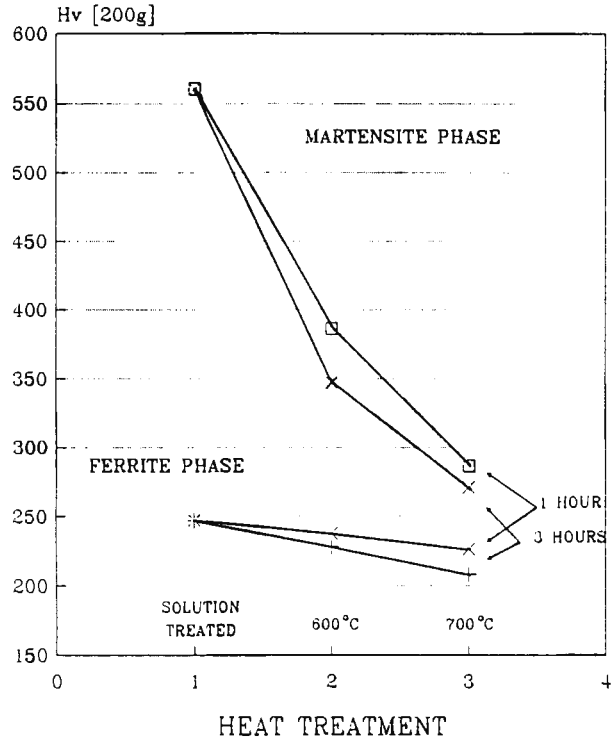

Figure (4.11): Variation in the microhardness of the ferrite and martensite phases of alloy C after heat treating at 600 and 700 °C for one and three hours.

Tempering at 800 °C for one hour results in a minimum in the bulk hardness (Fig. (4.8)). Grain boundaries appear decorated with large globular precipitates. The precipitates in the ferrite phase are predominantly spherical in shape and smaller than the acicular precipitates noted in this phase after heat treating at 700 °C. The microstructure of alloy C after heat treating at 900 °C is similar to that in the solution treated condition, although the δ-ferrite and δ-ferrite/martensite grain boundaries contain fine filmy precipitates.

The effect of tempering at 600 °C, 700 °C and 800 °C on the chromium content of the ferrite and martensite phases is illustrated in Table (4.3).

	CHROMIUM CONTENT [wt %] AFTER A PARTICULAR HEAT TREATMENT [°C]			
PHASE	Solution Treated	600/3HRS	700/3HRS	800/1HR
Ferrite	18.2 ±.3	18.1 ±.3	17.9 ±.3	17.8 ±.4
Martensite	16.1 ±.2	16.3 ±.2	16.2 ±.4	16.3 ±.3

Table (4.3): The extent of partitioning of chromium between the ferrite and tempered martensite phases in alloy C in various heat treated conditions, as determined by EDS [20 keV].

4.1.2.1 TEM ANALYSIS OF THE TEMPERED MICROSTRUCTURE OF ALLOY C

In order to compare the starting microstructure with a fully tempered structure, Tranmission Electron Microscopy was used to analyse specimens in the solution treated condition and after tempering at 700 °C for 3 hours.

In the solution treated condition there is no evidence of precipitation on grain boundaries or within the martensite or ferrite phases. The martensite is primarily of the lath type, but a small amount of twinned martensite is also present. Tempering at 700 °C for 3 hours converts the original martensite phase to a structure consisting of fine sub-cells which contain a low dislocation density (Fig.(4.12)).

Figure (4.13a) illustrates the nature of the precipitates formed in the ferrite phase of alloy C after tempering at 700 °C for three hours. The precipitates are acicular in shape, up to 3 μm in length, and several layers of atoms thick. From the diffraction pattern (Fig. 4.13b) the precipitates were determined to be the hexagonal close packed Cr_2N phase with an orientation relationship:

$$(0001)_{Cr2N} \parallel (011)_{\alpha}$$

and

$$[0110]_{Cr2N} \parallel [112]_{\alpha}.$$

This orientation relationship is a variant of the Burgers relationship and is in accordance with the finding of Bywater and Dyson[48].

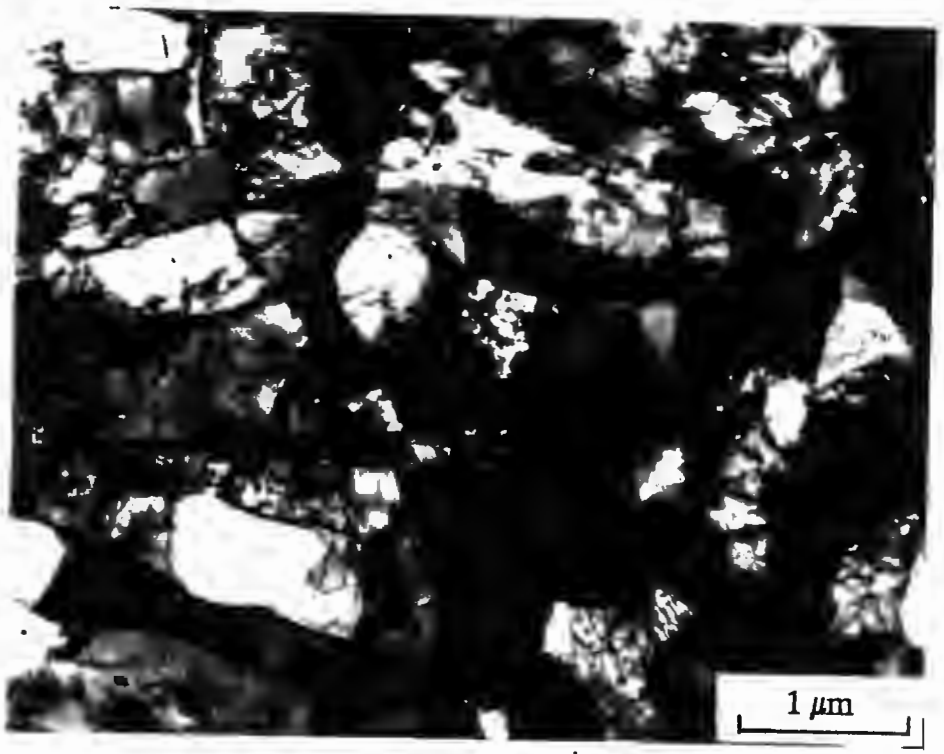

Figure (4.12): TEM micrograph illustrating the nature of the tempered martensite phase of alloy C.

Figure (4.13a): TEM micrograph of the ferrite phase, showing the presence of Cr2N precipitates.

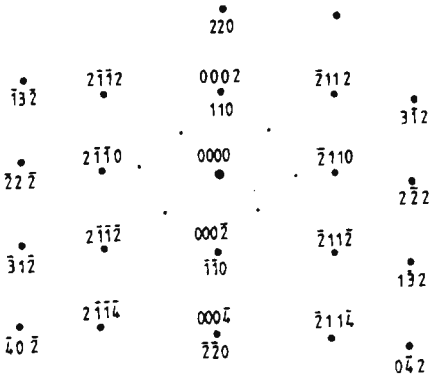

Figure (4.13b): Zone axis diffraction pattern, illustrating the presence of a hexagonal close packed phase in the BCC ferrite phase.

TEM analysis was also performed on a specimen tempered at 600 °C for one hour. The dislocations on the interior of the ferrite grains appeared free from precipitates. However in the regions of ferrite grains immediately adjacent to the ferrite/tempered martensite interfaces fine (sub-micron) precipitates were observed, assumed to be Cr_2N.

4.1.2.2 ISOTHERMAL TREATMENT OF ALLOY C AT 700 °C

In an attempt to understand the tempering reactions and how the products formed, an isothermal treatment at 700 °C was performed on Alloy C. The change in hardness experienced by the alloy (initially oil quenched from 1000 °C) as the heat treatment time was increased is illustrated in Fig.(4.14).

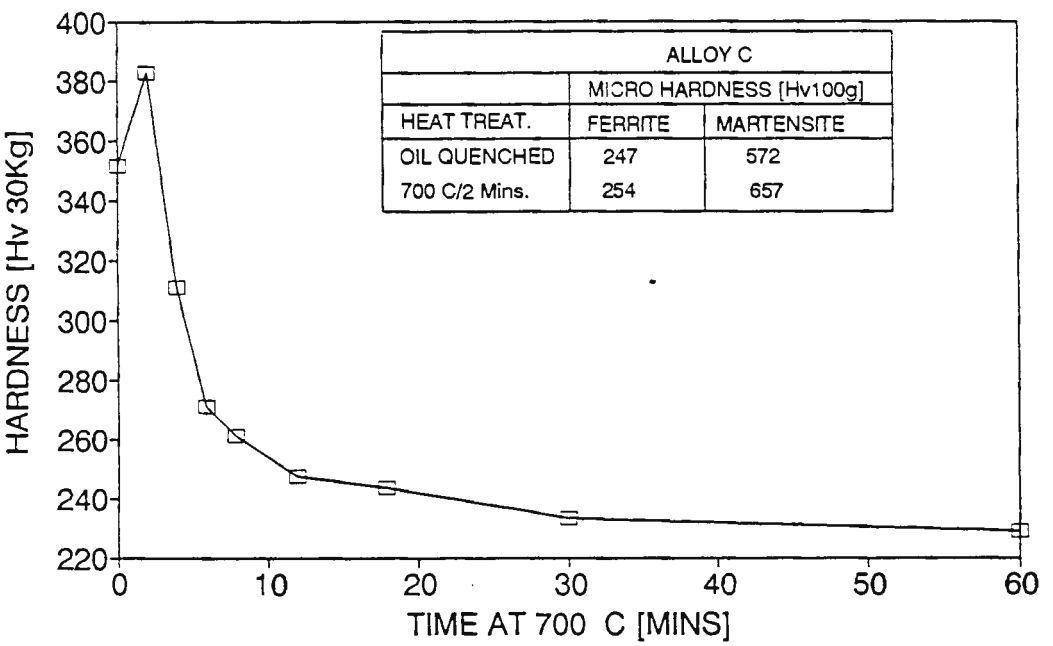

Figure (4.14) : Hardness change accompanying isothermal heat treatment of Alloy C at 700 °C.

After two minutes at 700 °C there is a sharp rise in hardness. From light microscopy there was no evidence leading to an explanation of the increased hardness. Inset in Fig.(4.14) is the microhardness of the respective phases in the oil quenched condition and after 2 minutes at 700 °C. The increase in hardness is thus attributed to hardening of the martensite phase, most probably as a result of fine precipitation within these regions of high dislocation density.

A four minute treatment at 700 °C produces a large drop in hardness (70 Hv_{30}). The light micrograph (Fig.(4.15a)) indicates that grain boundary precipitation has begun to occur. Six minutes at temperature marks the onset of precipitation on lath and packet boundaries (Fig.(4.15b)), and a scattering of ultra-fine precipitates are visible within the ferrite grains.

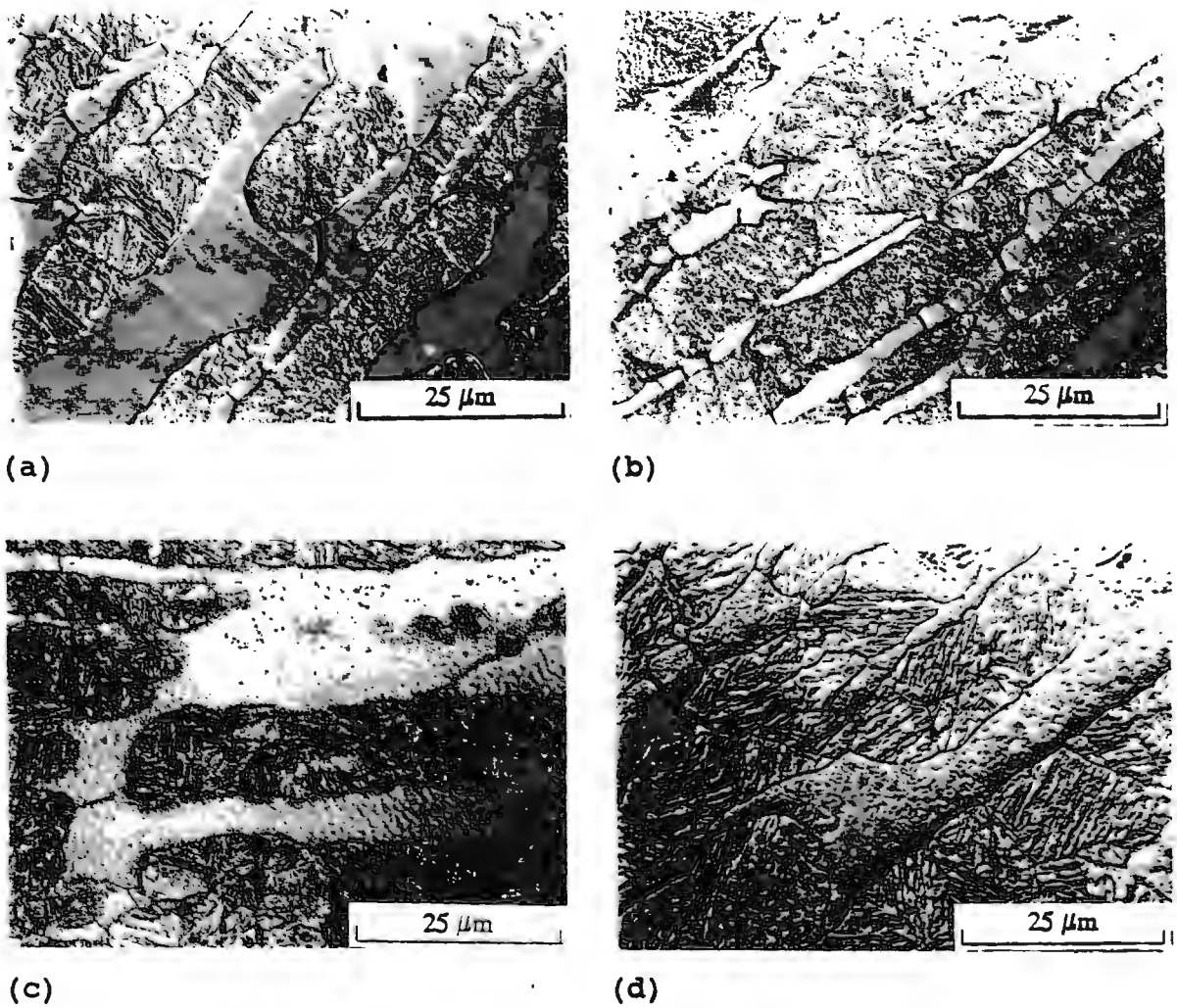

Figure (4.15): Light micrographs of alloy C tempered at 700 °C for (a)4 minutes, (b)6 minutes, (c)8 minutes and (d) 1 hour.

After 6 minutes at 700 °C the rate of loss of hardness rapidly tapers off as a result of gradual coarsening of precipitates in the martensite phase. After 8 minutes at temperature the precipitates in the ferrite appear denser and more defined, although primarily in the regions surrounding martensite islands (Fig.(4.15c)).This suggests that the initial precipitates occurring in the ferrite are nucleated on dislocations, the high dislocation density surrounding the martensite grains accounting for the predominance of precipitation in that region. With increased time at 700 °C the density of precipitates in the ferrite phase increases to a uniform concentration, as seen after one hour at temperature (Fig.(4.15d)).

4.1.3 ALLOY D

The microstructure of Alloy D in the solution treated condition consists of martensite islands (38% of the alloy) in a ferrite matrix, with a bulk hardness of 253 Hv_{30}. The extent of partitioning of Cr and Mn between the two phases in the solution treated condition is illustrated in Table (4.4).

	ELEMENT PARTITIONING(wt %)			
ELEMENT	MARTENSITE		FERRITE	
Chromium	15.4	±0.2	17.0	±0.3
Manganese	1.2	±0.2	0.90	±0.1

Table (4.4): The extent of partitioning in Alloy D in the solution treated condition as determined by EDS [20 keV].

The ferrite and martensite grains are elongated as a consequence of rolling (Fig. (4.18a)) and extend up to 180 μm in length and 70 μm in thickness. The average grain diameter is 43 μm. The M_S, A_{C1} and A_{C3} temperature for the alloy were 220, 858 and 918 °C respectively, as indicated in the dilatometry trace in Fig. (4.16).

The change in hardness of alloy D with heat treatment temperature is illustrated in Fig.(4.17).

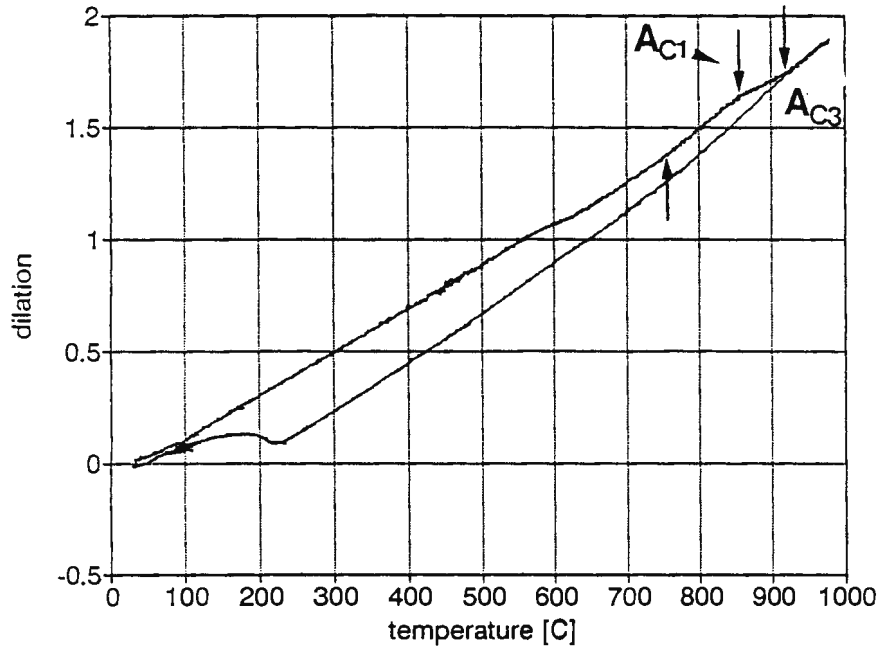

Figure (4.16): Dilatometry trace for alloy D. The trace was performed at a heating rate of 4 °C/minute.

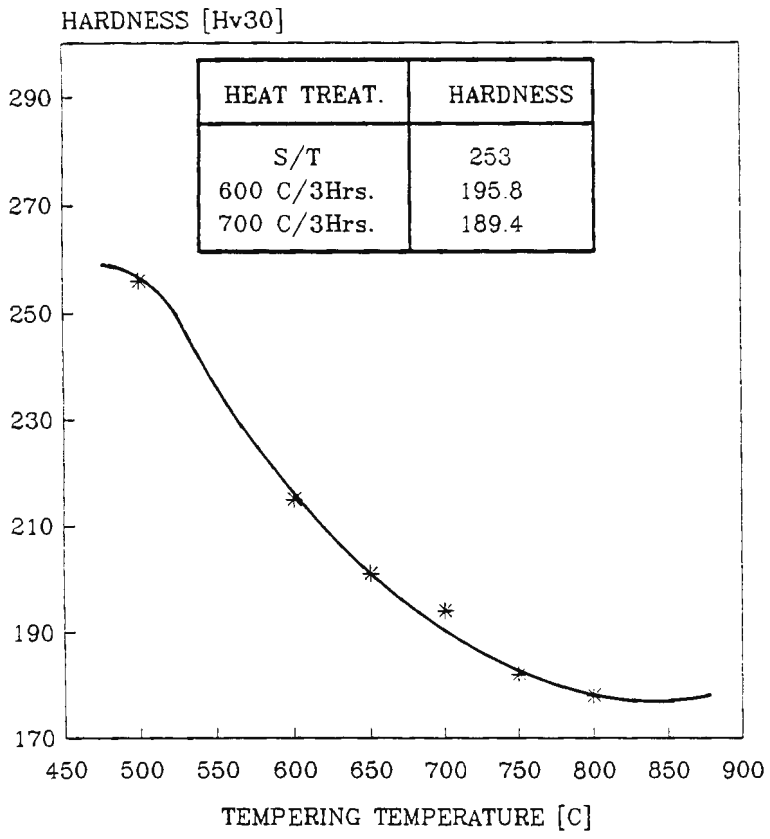

Figure (4.17): Hardness changes accompanying heat treatment of Alloy D for one hour at various temperatures. The effect of a 3 hour heat treatment at 600 °C and 700 °C is inset.

The first evidence of tempering, as determined by dilatometry (Fig. (4.16)), is observed at approximately 570 °C. Tempering for one hour at 600 °C results in precipitation on prior austenite grain boundaries, and fine very fine interlath precipitation. The reduction in hardness as a result of tempering for three hours at 600 °C is associated with the observation of more advanced precipitation of carbonitride precipitates on grain boundaries, and growth of the fine interlath precipitates in the martensite phase (Fig(4.18b)). There is no evidence of precipitation in the ferrite phase after a prolonged treatment at 600 °C.

Tempering at 700 °C for one hour marks the onset of precipitation in the ferrite phase in Alloy D (Fig.(4.19)). However this acicular phase, believed to be chromium nitride, appears less dense in Alloy D than that observed in Alloy C. Semi-continuous film and blocky precipitates are observed to form on the majority of δ-ferrite grain boundaries, while larger globular precipitates form on the δ-ferrite/martensite grain boundaries and in the martensite phase.

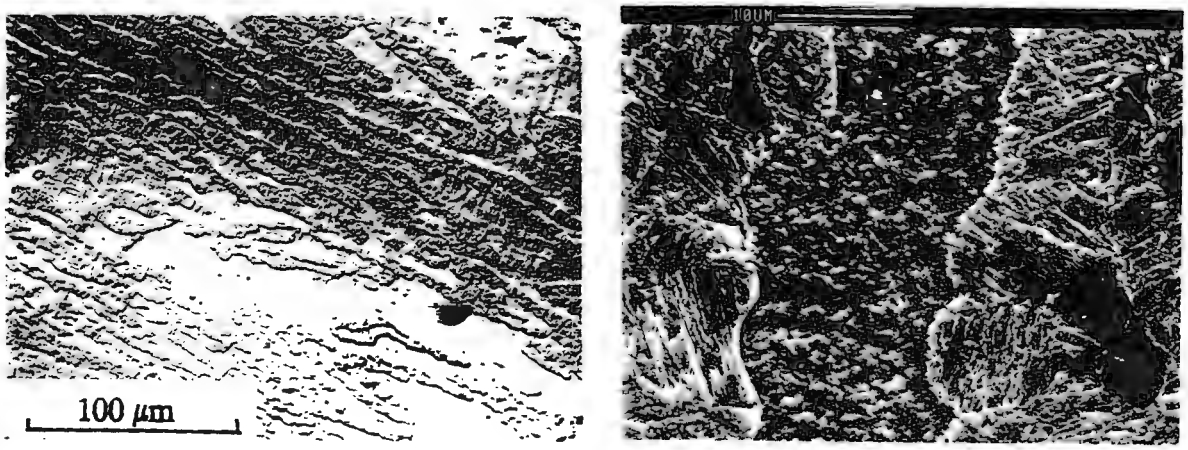

Figure (4.18): Appearance of the microstructure of alloy D in (a) the solution treated condition and (b) after three hours at 600 °C.

There is little further change in the appearance of the microstructure after 3 hours at 700 °C. This is reflected in only a small change in hardness after a 3 hour temper (Fig. (4.17)).

Figure (4.19): SEM micrograph of alloy D tempered at 700 °C for one hour.

4.1.4 ALLOY E

Alloy E has a a dual phase microstructure consisting of 89% martensite and 11% ferrite (Fig.(4.22a)), with M_S, A_{C1} and A_{C3} temperatures of approximately 233, 765 and 842 °C respectively, as measured by dilatometry (Fig. (4.20)).

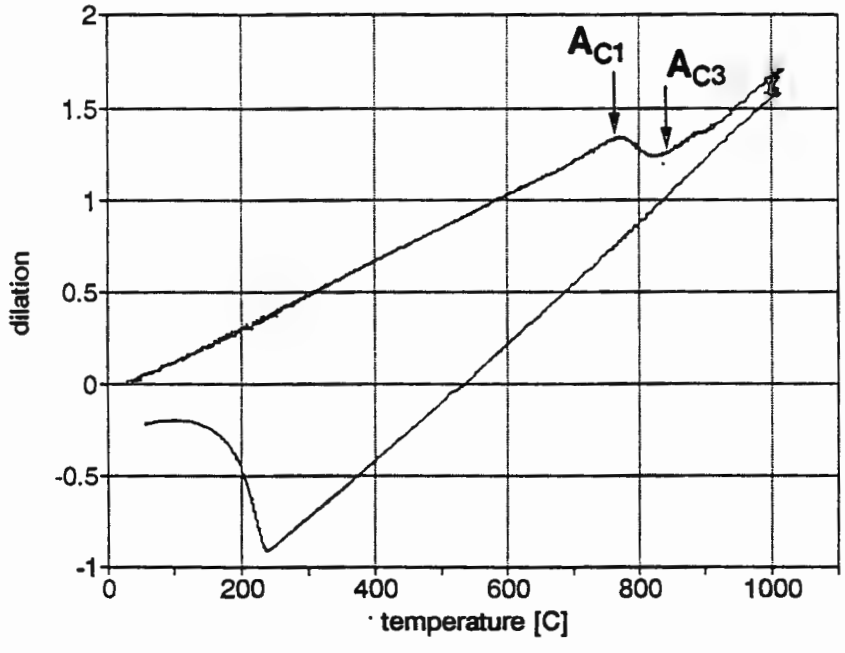

Figure (4.20): Dilatometry trace for alloy E. The test was performed at a heating rate of 4 °C/minute.

The average ferrite grain size is 7 μm and martensite grain size is 27 μm. The extent of partitioning of chromium, nickel and manganese within the alloy in the solution treated condition is illustrated in Table (4.5).

	ELEMENT PARTITIONING(wt %)			
ELEMENT	MARTENSITE		FERRITE	
Chromium	15.5	± 0.2	18.0	± 0.3
Nickel	1.0	± 0.2	0.6	± 0.1
Manganese	1.1	± 0.1	0.9	± 0.1

Table(4.5). The extent of partitioning in Alloy E in the solution treated condition, as determined by EDS (20 keV beam).

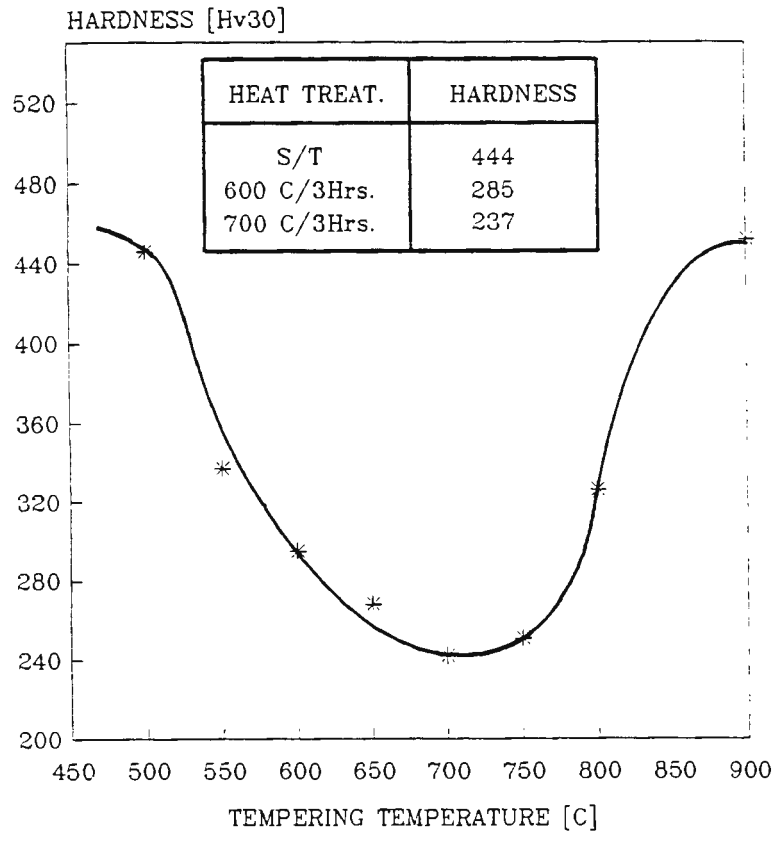

Figure (4.21): Variation in hardness of alloy E after tempering at various temperatures for 1 hour. The effect of a three hour heat treatment at 600 and 700 °C is inset.

The variation in hardness with a one hour heat treatment at various temperatures is illustrated in Fig. (4.21). Fine precipitation on some δ-ferrite and prior austenite grain

boundaries, and ultra fine precipitation on interlath boundaries is observed after tempering at 500 °C for one hour.

After tempering at 600 °C for one hour the grain boundary and interlath precipitates are more clearly visible, but still very fine (Fig. (4.22b)). The microstructure of alloy E is not considerably altered after three hours at 600 °C, and this is reflected in only a small difference in hardness between the one hour and three hour heat treatments (Fig, (4.21)). Tempering at either 600 or 650 °C has no effect on the appearance of the δ-ferrite grains.

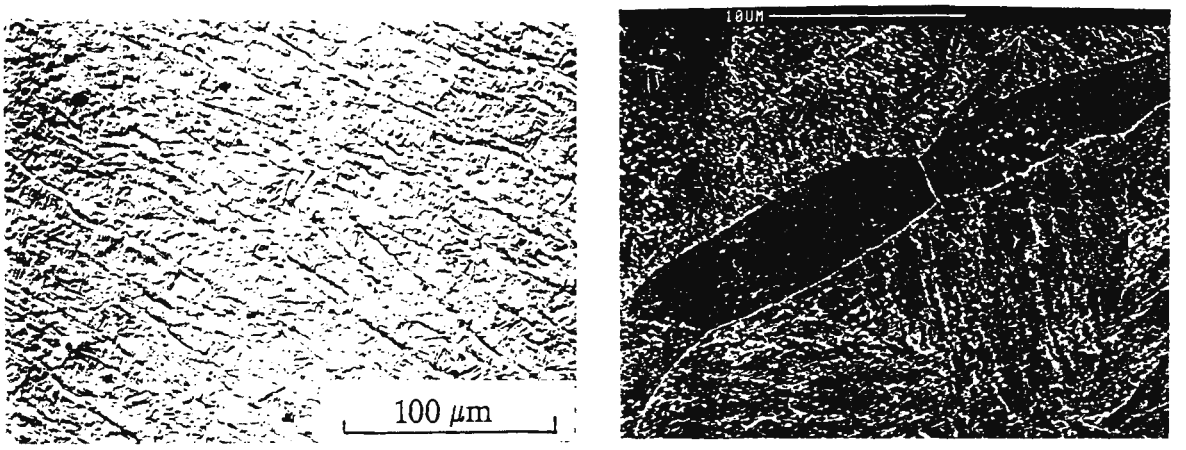

Figure (4.22): (a) Light micrograph of Alloy E in the solution treated condition (b) SEM micrograph of Alloy E after tempering at 600 °C for 1 hours.

After tempering for one hour at 700 °C fine, acicular precipitates are visible in high concentrations in the δ-ferrite grains (Fig (4.23a)). Grain boundary precipitates occur as both globular or "blocky" type structures and as semi-continuous films. Tempering at 700 °C for three hours produces little additional change in the microstructure of the alloy.

The slight increase in hardness when tempered at 750 °C for one hour (Fig. (4.21)) can be attributed to a partial austenite reversion in the alloy, the austenite transforming to fresh martensite when cooled to room temperature. This is in approximate agreement with data from dilatometric analysis (Fig.(4.20)), which indicates that the A_{c1} temperature is 765 °C. The austenite reversion is more advanced after heat treating at 800 °C for one hour, and manifested itself in the form of narrow lamellae on interlath boundaries of the original martensite phase (Fig (4.23b)), similar to that noted in Alloy A when tempered at 700 °C for 2 hours. The extent of partitioning of alloying elements between the ferrite and martensite of the lamellar composite phase is illustrated in Table (4.6).

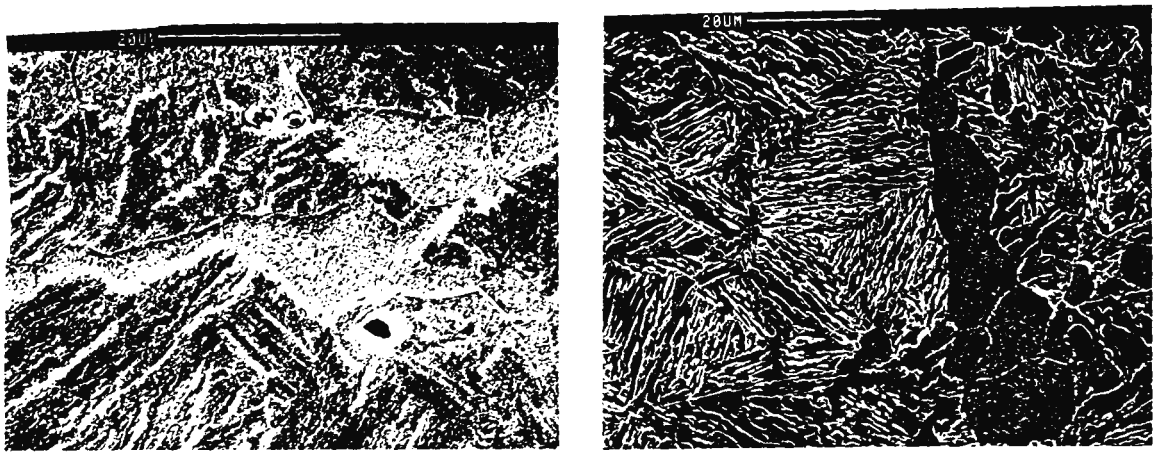

(a) (b)

Figure (4.23): Appearance of the microstructure of Alloy E after tempering for 1 hour at (a)700 °C, and (b) 800 °C.

While there is still evidence of nitride precipitates, occurring as both acicular and spherical precipitates in the ferrite phase and as globular precipitates on most grain boundaries, after heat treating at 800 °C for one hour, the increase in hardness (Fig. (4.21)) suggests that some nitrogen is dissolved during the heat treatment.

	Wt. % OF ELEMENT	
ELEMENT	FERRITE	MARTENSITE
Cr	16.0 ±.3	15.3 ±.3
Ni	0.7 ±.1	1.3 ±.2
Mn	0.8 ±.1	1.3 ±.1

Table (4.6): Partitioning of elements between the ferrite and martensite phases in the lamellar composite formed at 800 °C, as determined by EDS [20keV].

4.1.5 STANDARD STAINLESS STEELS

The effects of various heat treatments on the microstructures of AISI 304, 430 and 431 are summarised in Table (4.7). The captions within the table describing the appearance of the

microstructures in the various heat treated conditions refer to the micrographs in Fig. (4.24).

ALLOY	Heat Treatment	Hardness Hv_{30}	Grain Size	Comments On Microstructural Characteristics
AISI 304	AS REC.	160	30 - 40 μm	Similar in both heat treated conditions - ±4 % δ-ferrite as elongated bands in a large grained austenite matrix (Fig. (4.24a))
	SOLUTION TREATED[1]	158		
AISI 430	AS REC.	195	10 - 160 μm	Large grained ferritic microstructure containing coarse grain boundary and intragranular precipitates (Fig (4.24b))
	SOLUTION TREATED[2]	243	5 - 120 μm	Bands of equiaxed martensite islands (35 vol.%) in a ferrite matrix (Fig (4.24c)).
	600 °C/ 2 Hrs	203	5 - 120 μm	Fairly coarse blocky type carbides on ferrite and prior austenite grain boundaries; fine interlath precipitation within the martensite phase (Fig (4.24d)).
	700 °C/ 2 Hrs	190	5 - 120 μm	Further coarsening of grain boundary precipitates, to form globular arrays; fine acicular and spherical precipitates evident in δ-ferrite grains (Fig (4.24e)).
AISI 431	AS REC.	277	20 - 40 μm	Tempered martensite consisting of large carbide precipitates in a ferrite matrix
	SOLUTION TREATED[1]	557	20 - 40 μm	Microstructure composed of both lath and acicular martensite (Fig (4.24f)), and ± 4% δ-ferrite.
	600 °C/ 2 Hrs	317	20 - 40 μm	Fine carbide precipitates on interlath and prior austenite (Fig (4.24f)),boundaries (Fig (4.24g)).
	700 °C/ 2 Hrs	305	20 - 40 μm	Fine lamellar martensite (white regions, Fig (4.24h)) on interlath boundaries of the original martensite phase, in a tempered martensite matrix.

Table (4.7): Summary of the effects various heat treatments on the microstructures AISI 304, 430 and 431.
(1 - 1040/40mins/quenched 2 - 1000/1Hr/air cooled)

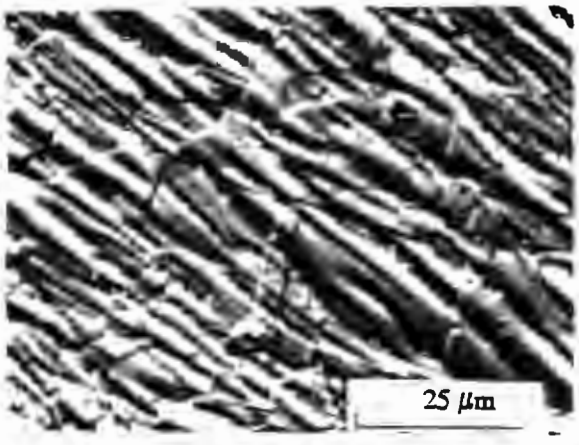

(a)

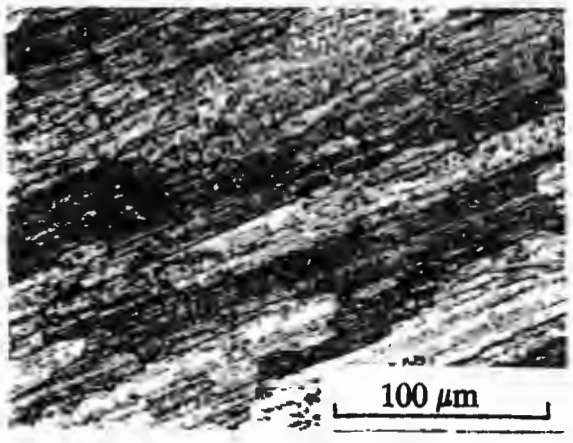

(b)

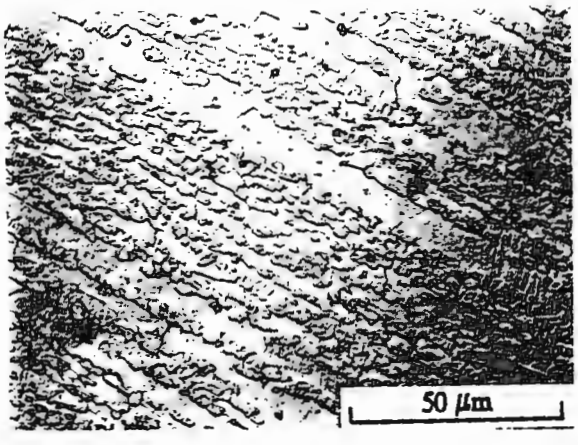

(c)

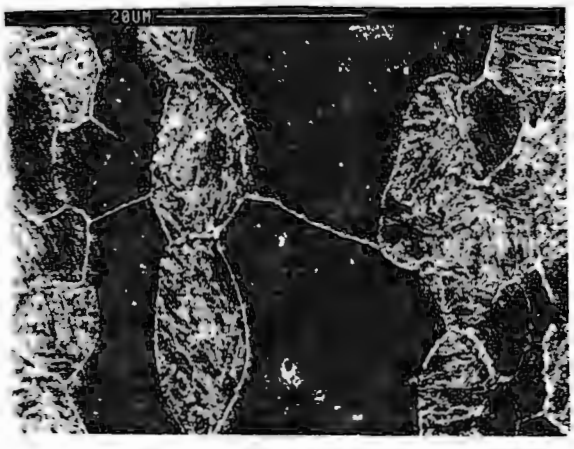

(d)

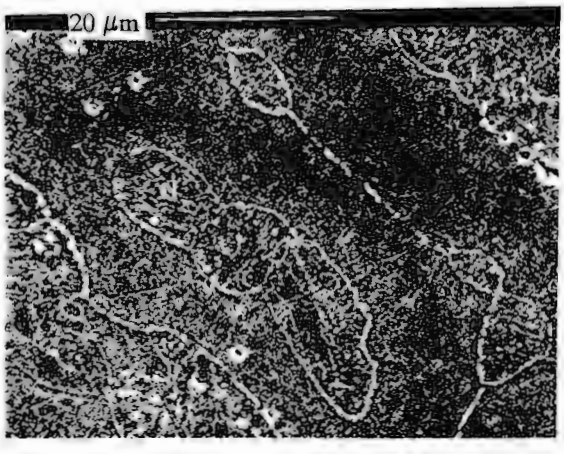

(e)

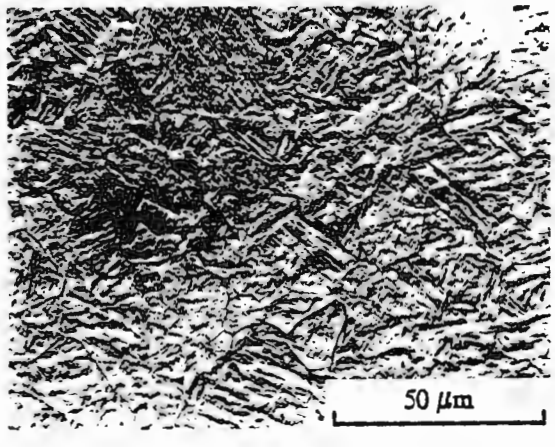

(f)

..... / Fig. (4.24)

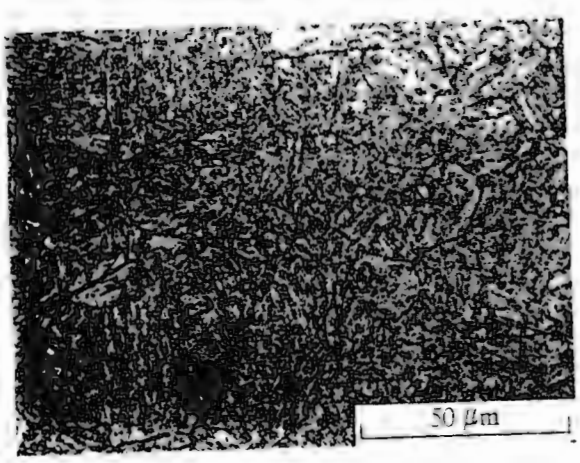

(g)

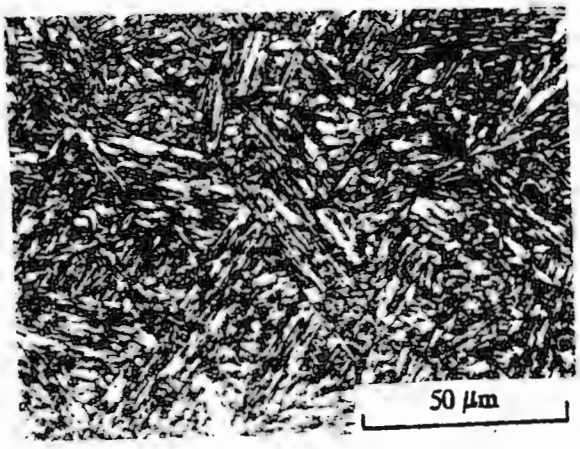

(h)

Figure (4.24) Appearance of the microstructures of AISI 304, 430 and 431 in various heat treated conditions: (a) 304 solution treated, (b) 430 as received, (c) 430 solution treated, (d) 430 tempered at 600 °C/2 hours, (e) 430 tempered at 700 °C/2 hours, (f) 431 solution treated, (g) 431 tempered at 600 °C/2 hours, (h) 431 tempered at 700 °C/2 hours.

4.2 MECHANICAL PROPERTIES AND FRACTOGRAPHY

4.2.1 ALLOY A

4.2.1.1 MECHANICAL PROPERTIES

The mechanical properties of alloy A in the solution treated condition, and after soaking at 600 and 700 °C for two hours are listed in Table (4.8). The tensile deformation curves for alloy A in its various heat treated conditions are illustrated in Fig. (4.25).

HEAT TREATMENT	σ_{UTS} [MPa]	$\sigma_{0.2\%}$ [MPa]	$\sigma_{0.5\%}$ [MPa]	Elong. [%]	Charpy [J]	Hardness Hv_{30}
S/T	990	759	908	18.5	62.5	337
600 °C/2Hrs	814	745	756	22.0	80.9	290
700 °C/2Hrs	821	621	724	19.3	84.9	293

S/T = SOLUTION TREATED

Table (4.8): Mechanical properties of Alloy A in various heat treated conditions.

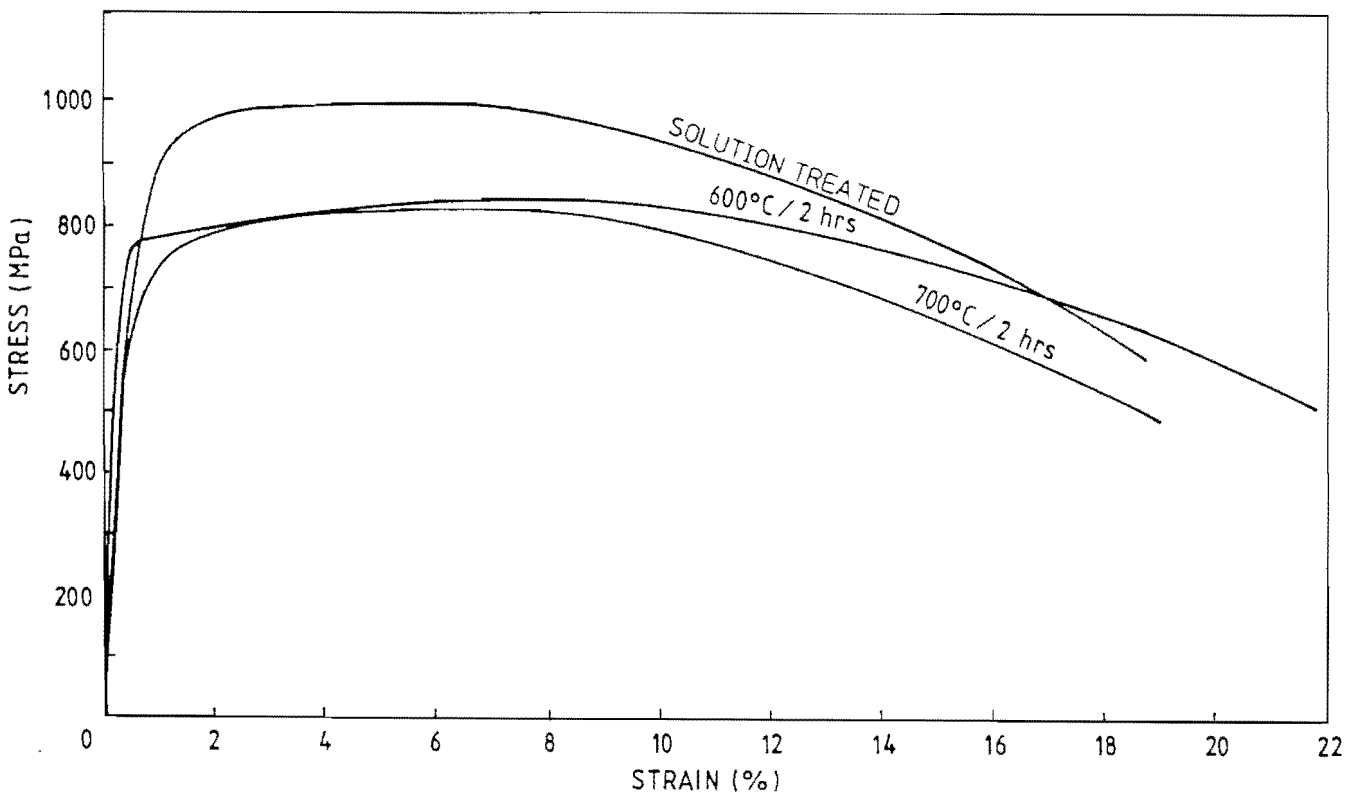

Figure (4.25): Tensile deformation curves for Alloy A in the solution treated condition, and after heat treating at 600 and 700 °C for two hours.

In both the solution treated and 700 °C tempered condition the alloy exhibited continuous yielding characteristics, while in the 600 °C tempered condition a more defined yield point was in evidence. Hence the small gap between the 0.2% and 0.5% yield strengths in the 600 °C tempered condition (Table (4.8)).

4.2.1.2 FRACTOGRAPHY

During tensile testing a common feature preceding final fracture was lateral cracking (Fig. (4.26)). This manifested itself audibly as a sharp crack during the final stages of necking. Cross sections of tensile fracture surfaces revealed that lateral cracks propagate in a predominantly intergranular mode. The fracture surfaces of tensile and impact specimens in each of the three heat treated conditions in which they were tested have ductile appearances, with no signs of brittle cleavage markings.

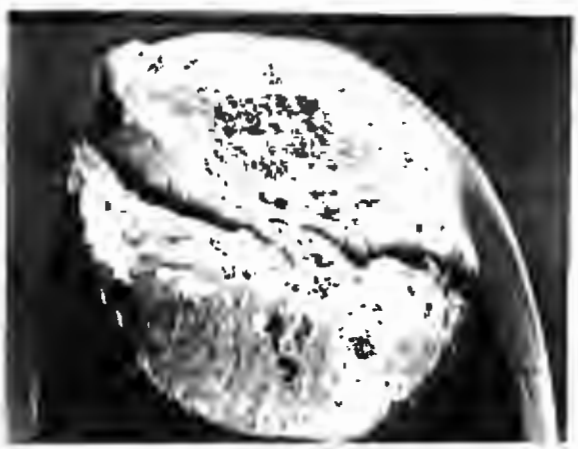

Figure (4.26): Central delamination crack in a tensile specimen of alloy A in the 600 °C tempered condition

The fracture mode was strongly influenced by the large quantity of non-metallic inclusions, located predominantly in the δ-ferrite phase and at δ-ferrite/martensite interfaces. Inclusions were either in the form of fine precipitates rich in aluminium and silicon, or as larger manganese based oxide and sulphide precipitates, and were common to all the experimental alloys.

Analysis of cross sections of tensile specimens of alloy A in the solution treated condition revealed that voids are often associated with the martensite phase and ferrite/martensite interfaces (areas arrowed in Fig. (4.27a)). SEM analysis of the tensile fracture surfaces revealed that inclusions are contained within many of the large ductile dimples, and the fracture surfaces are generally characterised by mixed regions of large and fine ductile dimple formations (Fig. (4.27b)). Surface deformation markings on the region of the gauge

length of tensile specimens of alloy A (in the solution treated condition) near the fracture surface revealed that while strain is inhomogeneously distributed between the ferrite and martensite phases, the martensite phase shows a limited capacity for plastic deformation, and evidence of microvoid initiation around inclusions was observed.

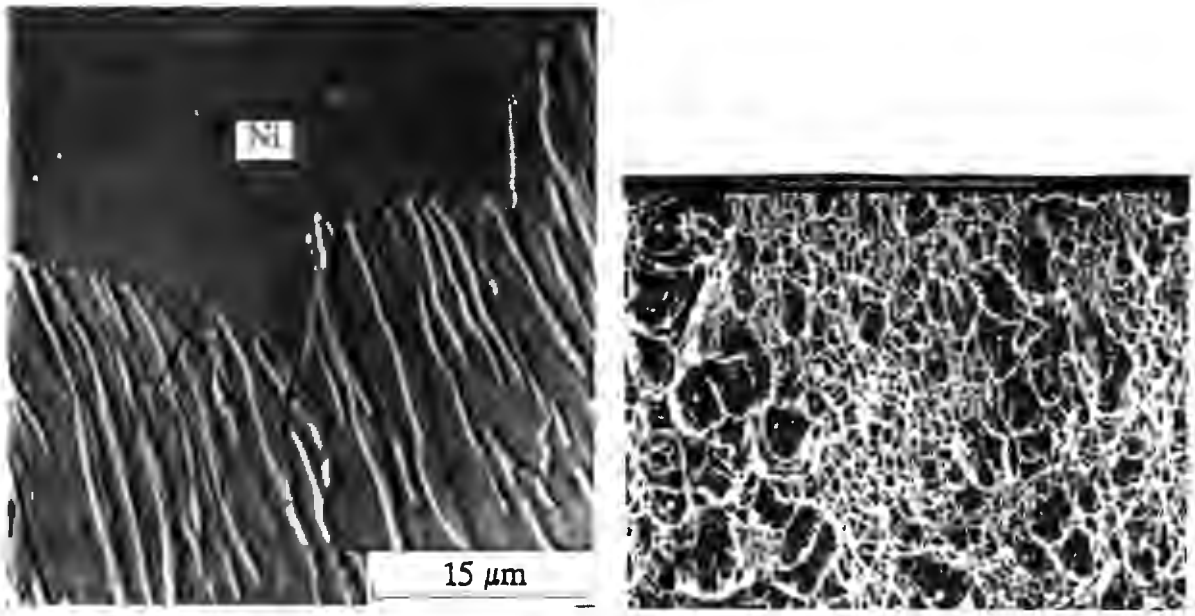

Figure (4.27): (a) Cross section of fractured tensile specimen of alloy A in the solution treated condition; (b) SEM micrograph of the fracture surface.[F = ferrite, M = martensite, Ni = nickel plating]

In the 600 °C tempered condition the tensile fracture surfaces have a more feathery appearance and ductile dimple formations appear on a finer scale. Regions of ductile tearing are also in evidence, possibly resulting from fracture of the δ-ferrite phase.

The tensile fracture surfaces in the 700 °C tempered condition consist of large ductile dimples formed around inclusions (most likely in the ferrite phase), surrounded by fine, evenly dispersed ductile dimple formations (Fig. (4.28a)). These regions of fine microvoid formations form from fracture of the lamellar martensite/α-ferrite composite phase, as was revealed by analysis of cross sections of fracture surfaces, whereas the fractured δ-ferrite generally has a smoother fracture profile. Lateral cracks pass predominantly through ferrite grains or along the δ-ferrite/ lamellar composite phase boundaries (Fig. (4.28b)), and are normally deviated when confronted with lamellar martensite/α-ferrite colonies.

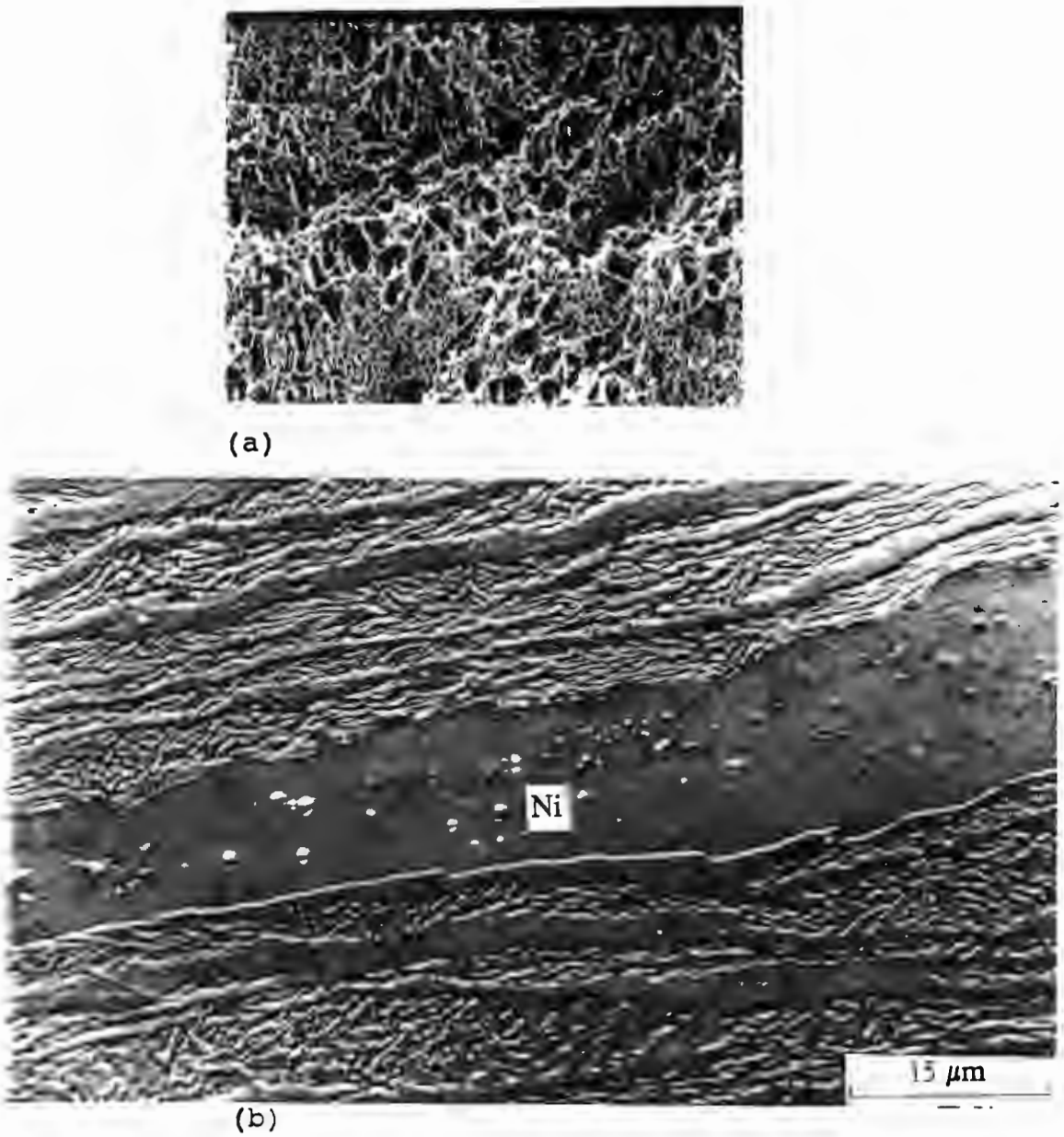

Figure (4.28): (a) Appearance of the tensile fracture surface, and (b) the path of a lateral crack in a fractured tensile specimen of alloy A in the 700 °C tempered condition. [F = ferrite M/F = lamellar composite phase, Ni = nickel plating]

Microscopic examination of the impact fracture surfaces revealed that they are similar in character to the tensile fracture surfaces. In the solution treated condition regions of coarse (centered around inclusions) and fine dimple formations cover the fracture surfaces. Generally very little evidence of sub-surface cracking is observed in cross sections of impact specimens, however there is some evidence suggesting microvoid formation at ferrite/martensite grain boundaries (areas arrowed in Fig. (4.29a)) and within the martensite phase.

Fracture surfaces of impact specimens in the 600 °C tempered condition have a fine feathery appearance due to a combination of fine microvoid formation and extensive ductile tearing. After intercritical annealing at 700 °C, the appearance of the impact fracture surfaces is similar to that of the the tensile fracture surfaces. However the fine, evenly spaced ductile dimple colonies appeared to predominate over the larger inclusion related dimples.

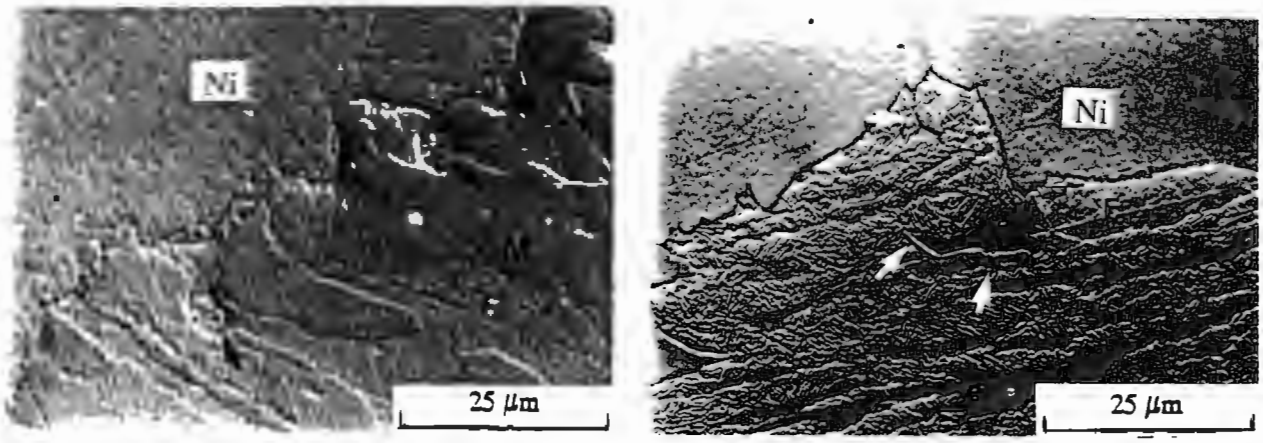

Figure (4.29): (a) Cross section through an impact specimen of alloy A in the solution treated condition indicating microvoid formation at ferrite/martensite grain boundaries, and (b) Cross section through a fractured impact specimen of alloy A in the 700 °C heat treated condition, illustrating the blunting of cracks propagating through the δ-ferrite phase by the lamellar composite phase. [F = ferrite F/M = lamellar composite phase, Ni = nickel coating]

Analysis of cross sections of fracture surfaces revealed that the regions of fine microvoid formations result predominantly from fracture of the lamellar martensite/ferrite composite phases, and that the lamellar composite phase has good crack blunting properties, as is illustrated in Fig. (4.29b).

4.2.2 ALLOY C

4.2.2.1 MECHANICAL PROPERTIES

The mechanical properties of alloy C in the solution treated condition, and after tempering at 600 and 700 °C for 1 hour are listed in Table (4.9).

HEAT TREATMENT	σ_{UTS} [MPa]	$\sigma_{0.2\%}$ [MPa]	$\sigma_{0.5\%}$ [MPa]	Elong. [%]	Charpy [J]	Hardness Hv_{30}
S/T	1199	707	908	14.0	2.5	346
600 °C/1HR	810	644	689	19.8	36.8	283
700 °C/1HR	705	524	539	27.5	56.0	229
700 °C/3HRS	687	485	495	28.5	59.7	225

S/T = SOLUTION TREATED

Table (4.9): Mechanical properties of Alloy C in various heat treated conditions.

The tensile deformation curves for alloy C in various heat treated conditions are illustrated in Fig. (4.30).

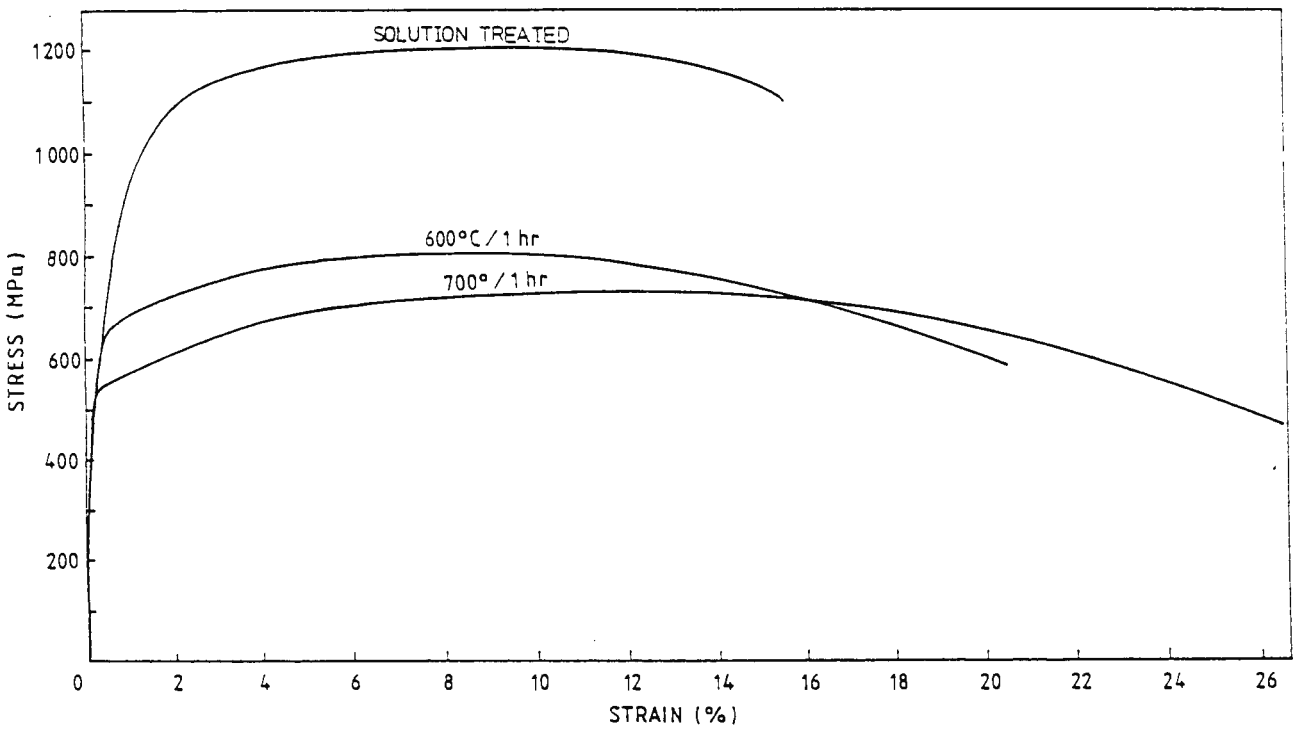

Figure (4.30): Tensile deformation curves for alloy C in various heat treated conditions.

4.2.2.2 FRACTOGRAPHY

In the solution treated condition tensile fracture surfaces have a brittle appearance. The ferrite phase fails by transgranular cleavage fracture, while the martensite phase exhibits quasi-cleavage (fine cleavage facets mixed with fine ductile lips) and fine ductile dimple fracture modes (Fig. (4.31a)). The martensite phase appears the tougher of the two phases, regularly blunting and diverting cleavage cracks propagating through the ferrite phase. However the martensite exhibits little plastic behavior, and analysis of the deformation markings on polished gauge lengths of fractured tensile specimens (Fig. (4.31b)) revealed that the two most common modes of microvoid nucleation were fracture of the martensite phase (labelled R) and interfacial decohesion between the ferrite phase and the martensite phase (labelled D).

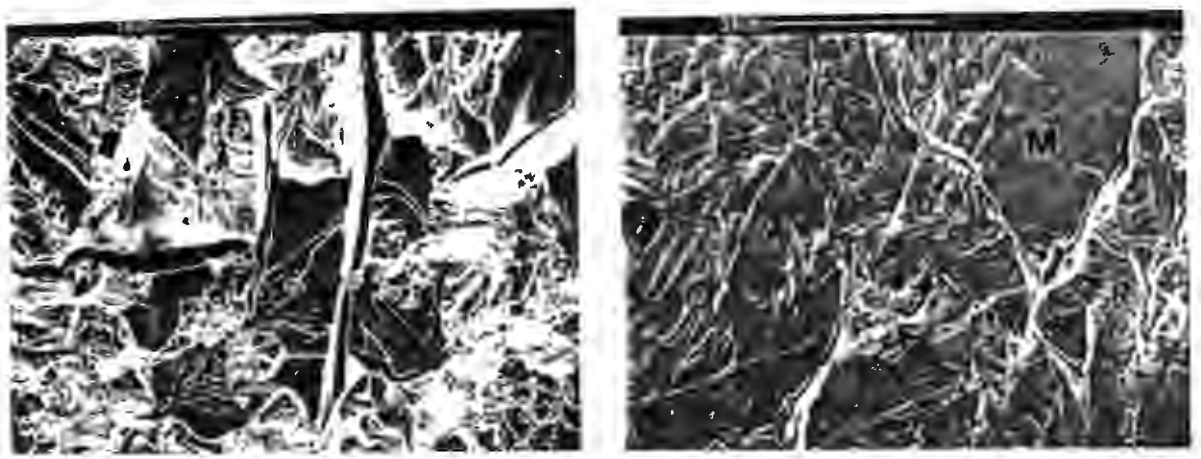

Figure (4.31): (a) Tensile fracture surface of alloy C and (b) strain markings on the gauge length of the alloy in the solution treated condition. (The identity of the phases was determined by EDS analysis) [F = ferrite, M = martensite, D = interfacial tearing, R = fracture of the martensite phase].

As expected from the low impact energy, Charpy impact fracture surfaces in the solution treated condition exhibit entirely brittle features. In the 600 °C tempered condition ductility is improved, although deformation in the ferrite phase is still partially constrained, as is reflected in the limited amount of wavy slip observed in the ferrite phase on the polished gauge lengths of fractured tensile specimens. Cross sections of fractured specimens revealed that lateral cracks followed an intergranular path, and intergranular rupture was frequently observed across the profile of the tensile fracture surface. Charpy fracture surfaces in the 600 °C tempered condition exhibit a combination of cleavage fracture and a feathery type of ductile tearing, and a small amount of intergranular rupture.

The tensile fracture surfaces of alloy C are similar in appearance in the 600 and 700 °C tempered conditions. Regions of very fine ductile dimple formations are associated primarily with fracture of the tempered martensite phase (Fig. (4.32a), labelled M). The predominant fracture mode of the ferrite phase appears to be fine ductile tearing, but evidence of cleavage fracture is also observed. There is also evidence of intergranular separation (Fig (4.32a), labelled I). Analysis of the surface deformation markings on polished gauge lengths of alloy C in the 700 °C tempered condition revealed that a common mechanism of microvoid initiation is intergranular rupture (Fig. (4.32b)) at ferrite/tempered martensite (FM) and ferrite/ferrite (FF) grain boundaries, while occasional evidence of fracture in the tempered martensite phase and around inclusions was also noted.

(a) (b)

Figure (4.32): (a) Tensile fracture surface of alloy C in the 700 °C tempered condition, and (b) deformation markings on the surface of a tensile specimen in a region below the fracture surface.[FF = fracture between ferrite grains, FM = fracture between ferrite and tempered martensite grains, I = intergranular rupture, M = fracture of the tempered martensite phase]

A small amount of transgranular cleavage fracture is observed on the fracture surfaces of fractured Charpy specimens after tempering at 700 °C for one hour, although very fine ductile dimple formations resulting in larger scale ductile features (Fig. (4.33a)), and intergranular rupture, are prevalent. It is believed that the regions arrowed in Fig. (4.33a) may be related to fracture of the ferrite phase, the uniform arrays of ultra fine microvoids resulting from parting along the length of nitride precipitates. Cross sections of fracture surfaces revealed that the tempered martensite is effective in the blunting of cracks propagating through the ferrite phase, and that cracks commonly follow an intergranular

path (Fig. (4.33b)).

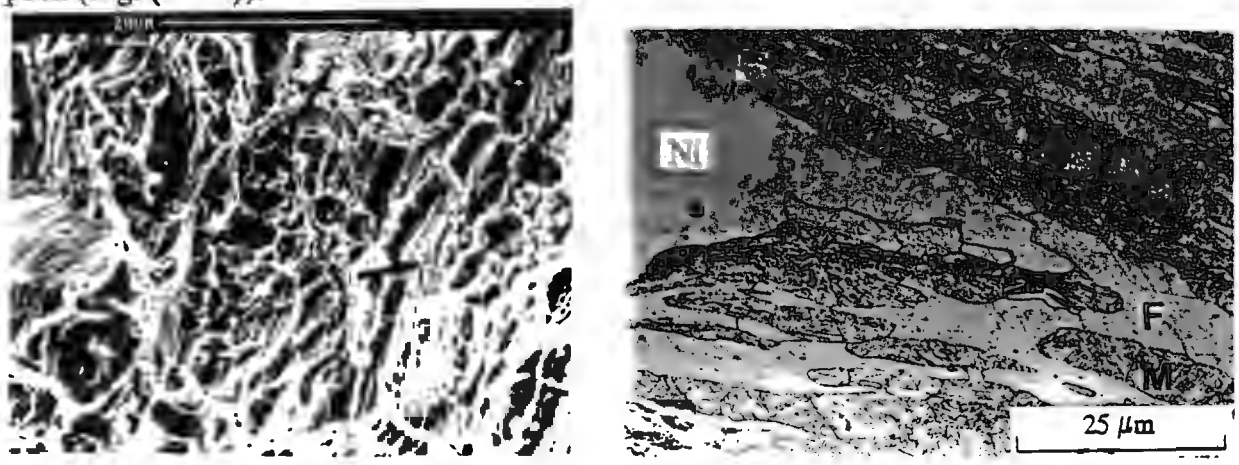

Figure (4.33): (a) Charpy fracture surface in the 700 °C tempered condition, and (b) a cross section through the fracture surface. [F = ferrite, M = martensite, Ni = nickel plating]

4.2.3 ALLOY D

4.2.3.1 MECHANICAL PROPERTIES

The tensile and impact properties of alloy D in various heat treated conditions are listed in Table (4.10).

HEAT TREATMENT	σ_{UTS} [MPa]	$\sigma_{0.2\%}$ [MPa]	$\sigma_{0.5\%}$ [MPa]	Elong. [%]	Charpy [J]	Hardness Hv_{30}
S/T	829	456	617	19.21	2.70	253
600 °C/1HR	628	461	489	27.20	35.83	215
700 °C/1HR	562	382	399	29.33	70.35	194

S/T = SOLUTION TREATED

Table (4.10): Mechanical properties of Alloy D in various heat treated conditions.

The small difference between the 0.2 and 0.5 % proof strengths in the 600 and 700 °C tempered conditions (28.1 MPa and 16.9 Mpa respectively, Table (4.10)) indicates a more defined yield point than in the solution treated condition, and this is reflected in the shape of the tensile deformation curves (Fig. (4.34)).

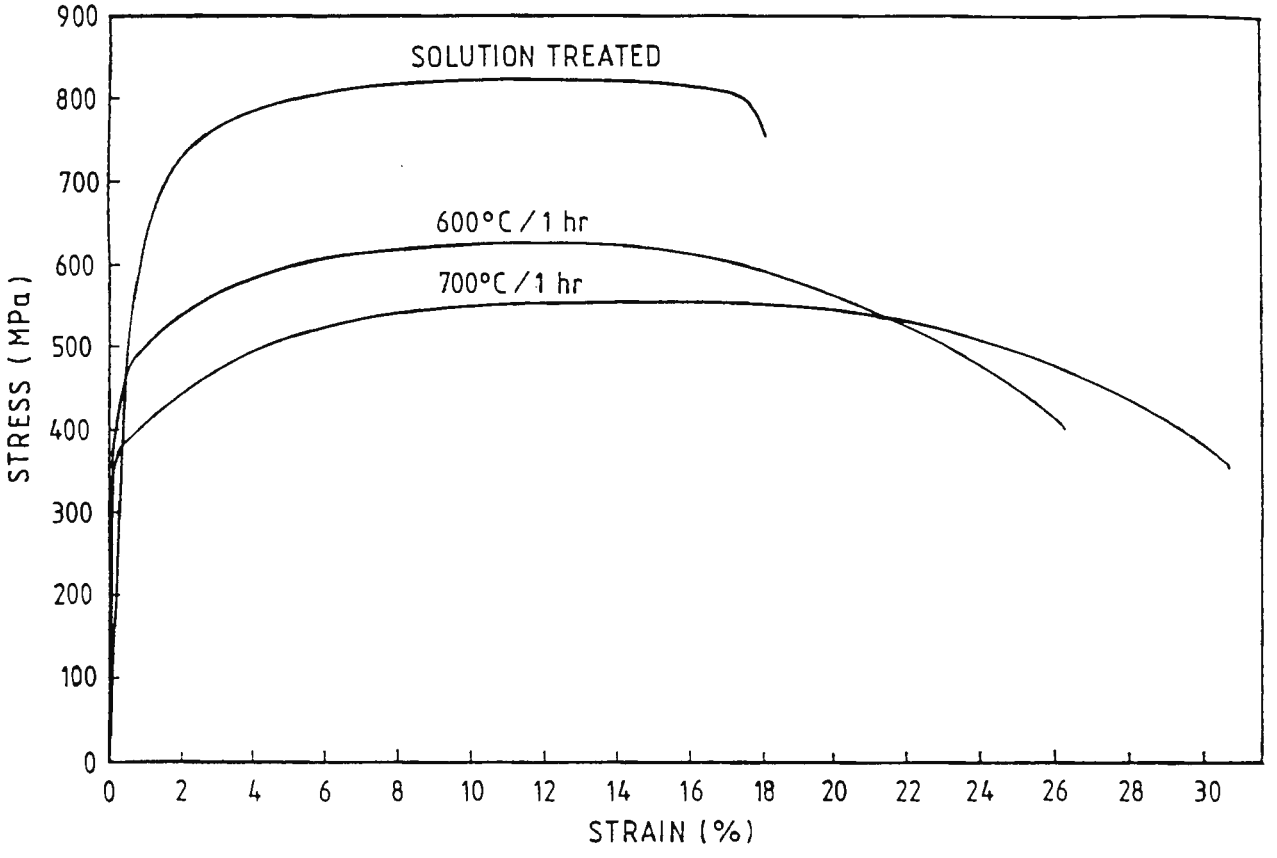

Figure (4.34): Tensile deformation curves for alloy D in various heat treated conditions.

4.2.3.2 FRACTOGRAPHY

Analysis of fractured tensile specimens in the solution treated condition revealed that the ferrite phase exhibits a purely cleavage fracture mode, while the martensite failed in a brittle to ductile dimple fashion, with numerous examples of crack blunting associated with the martensite phase (Fig.(4.35a)). Examination of deformation markings on polished gauge lengths indicate that plastic flow occurs almost entirely in the ferrite phase, in the form of wavy slip, which builds up around the less deformable martensite phase and often lead to intergranular tearing (Fig. (4.35b), labelled D). There is also evidence which suggested that microvoid initiation occurs by fracture of the martensite phase (labelled R). In the 600 °C tempered condition the alloy is susceptible to lateral cracking, and tensile fracture surfaces have a feathery appearance as a result of regions of intergranular rupture, and fine ductile tearing (Fig. (4.36)). Analysis of surface deformation markings revealed little information as to the mechanisms leading to fracture, except for occasional evidence of fracture within the tempered martensite phase.

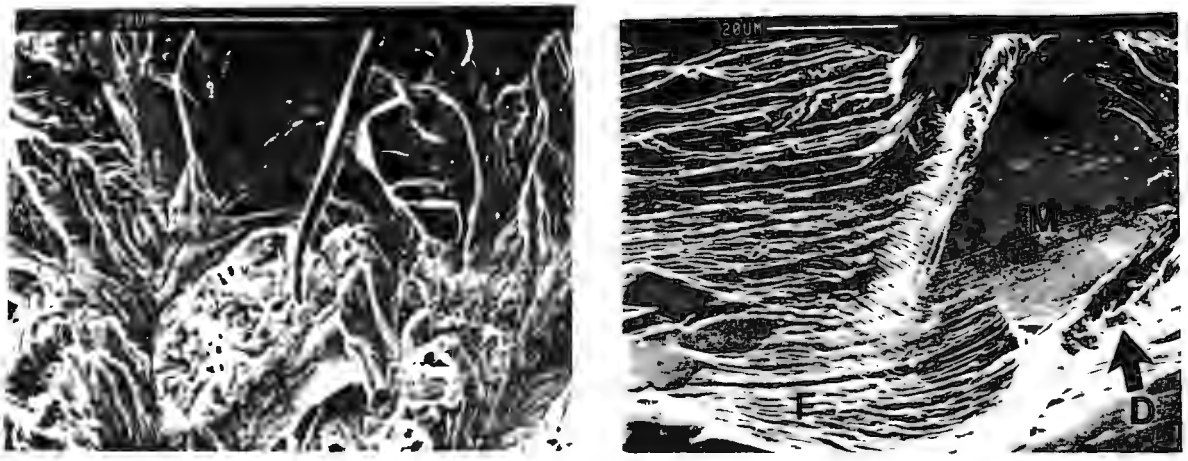

(a) (b)

Figure (4.35): (a) Cleavage fracture of the ferrite phase, and blunting of a crack by the martensite phase of Alloy D in the solution treated condition; (b) surface deformation markings on the gauge length of the same specimen. [F = ferrite, M = martensite, D = interfacial decohesion, R = fracture within the martensite phase]

In the 700 °C tempered condition the overall appearance of tensile fracture surfaces is similar to that in the 600 °C tempered condition. Analysis of surface deformation markings, although made difficult by the high ductility of the alloy, revealed some evidence of fracture initiation around inclusions and in the tempered martensite phase.

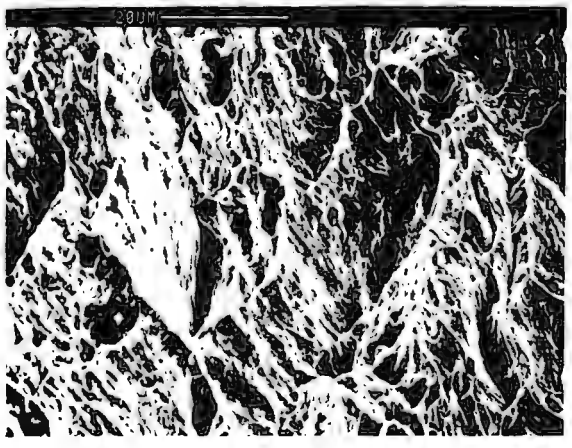

Figure (4.36): Appearance of the tensile fracture surface of alloy D after tempering at 600 °C.

In the solution treated condition the low impact resistance is accompanied by a brittle, faceted fracture surface. Ductility is improved by tempering at 600 °C, although the ferrite

phase still appears to be susceptible to cleavage fracture and a small amount of intergranular rupture is observed (Fig.(4.37a)).

While impact fracture surfaces of alloy D in the 700 °C tempered condition consist primarily of inclusion related ductile dimple formations and feathery, fibrous tearing, the ferrite phase is still susceptible to cleavage fracture.

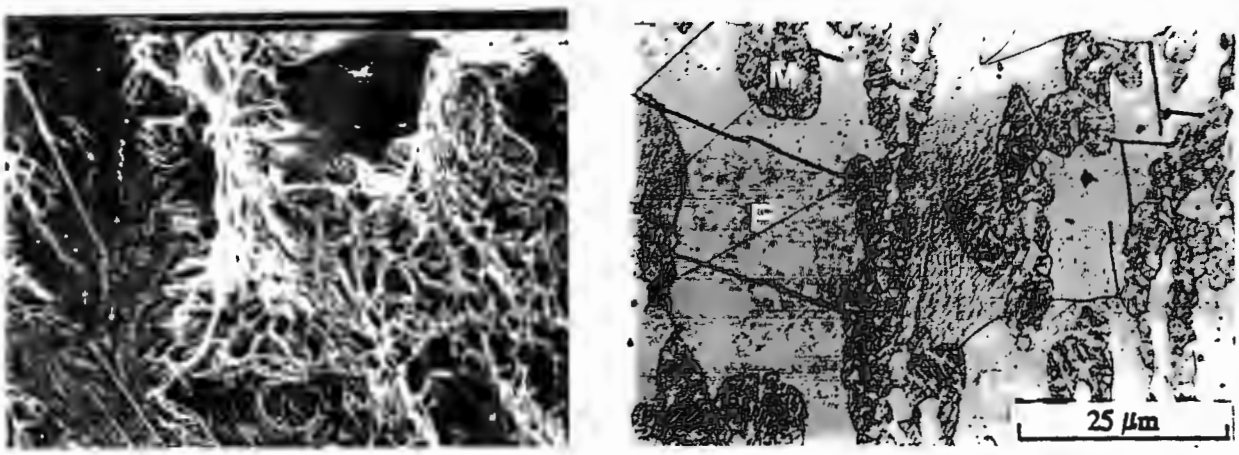

(a) (b)

Figure (4.37): (a) Appearance of the fracture surface of a Charpy specimen in the 600 °C tempered condition and (b) sub-surface cleavage cracks in the ferrite phase of a fractured Charpy specimen in the 700 °C tempered condition.

Light microscope analysis of cross sections of the fracture surface revealed transgranular cleavage cracks in the large ferrite grains which more often than not are blunted at the tempered martensite interface (Fig. (4.37b)). Little evidence of intergranular rupture is observed in the profile of the fracture surface of impact specimens after cross sectioning (Fig. (4.38)).

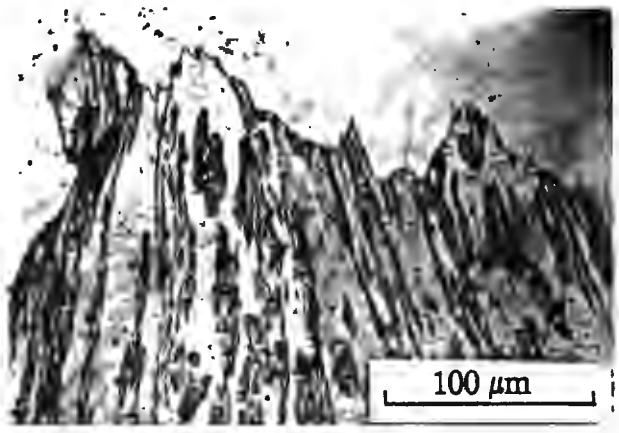

Figure (4.38): Cross section through a fractured Charpy specimen in the 700 °C tempered condition, indicating little evidence of intergranular fracture at the fracture surface.

4.2.4 ALLOY E

4.2.4.1 MECHANICAL PROPERTIES

The microstructural analysis of alloy E indicated a rapid response to heat treatment, which can be attributed to the high interstitial content of the alloy. As a consequence, a one hour soak period is sufficient to produce significant changes in mechanical properties as a function of heat treatment temperature (Table (4.11)).

HEAT TREATMENT	σ_{UTS} [MPa]	$\sigma_{0.2\%}$ [MPa]	$\sigma_{0.5\%}$ [MPa]	Elong. [%]	Charpy [J]	Hardness Hv_{30}
S/T	1309	976	1175	13.8	5.2	444
600 °C/1HR	937	861	866	17.7	32.4	295
700 °C/1HR	750	630	633	24.0	72.3	242
800 °C/1HR	923	668	781	21.6	37.8	326

S/T = SOLUTION TREATED

Table (4.11): Mechanical properties of Alloy E in various heat treated conditions.

The extent of the gap between the 0.3% and 0.5% proof strengths in the solution treated condition, and after heat treating at 600, 700 and 800 °C for one hour is 199, 4.3, 3 and 113 MPa respectively (Table (4.11)). These values reflect the nature of yielding occurring in the

alloy, as illustrated in Fig. (4.39).

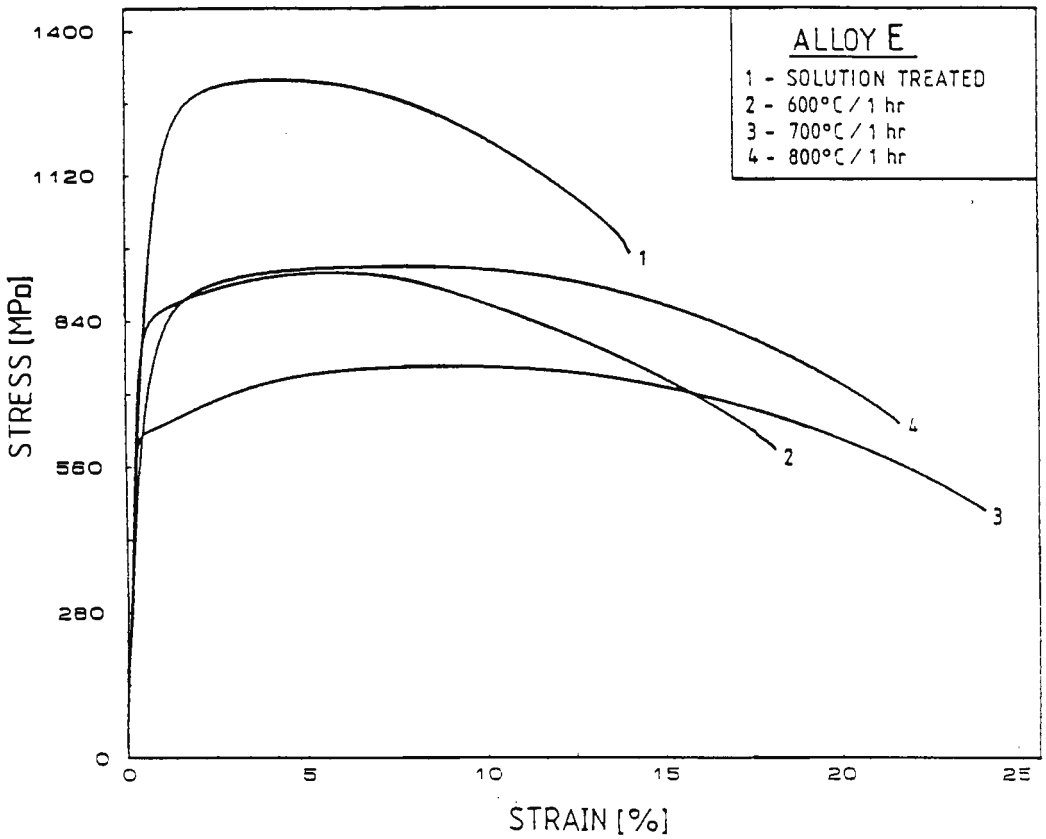

Figure (4.39): Tensile deformation curves for alloy E in various heat treated conditions

4.2.4.2 FRACTOGRAPHY

In the solution treated condition fractured tensile specimens exhibit partial ductility (as fine ductile lips) combined with fine cleavage fracture (Fig. (4.40a)). Tempering at 600 °C results in a moderate increase in ductility and the fracture surfaces of tensile specimens consist primarily of large ductile dimples, nucleated around inclusions, and fine quasi-ductile tearing (Fig. (4.40b)). In the 700 °C tempered condition the tensile fracture surfaces are similar in appearance to those observed in the 600 °C tempered condition, but with a more uniform ductile dimple character. Cross sections of tensile fracture surfaces in the 700 °C tempered condition indicate that the δ-ferrite grains have little effect on the fracture mode due to the low δ-ferrite content. Fractured ferrite entities generally have a smooth profile in cross section, and a small amount of intergranular rupture between the ferrite and tempered martensite phases is observed.

The lamellar martensite/ferrite composite phase formed after heat treating at 800 °C

results in tensile fracture surfaces consisting of very fine ductile dimples surrounding larger inclusion related dimples (Fig. (4.41a)). These fine dimples often have a marked degree of directionality.

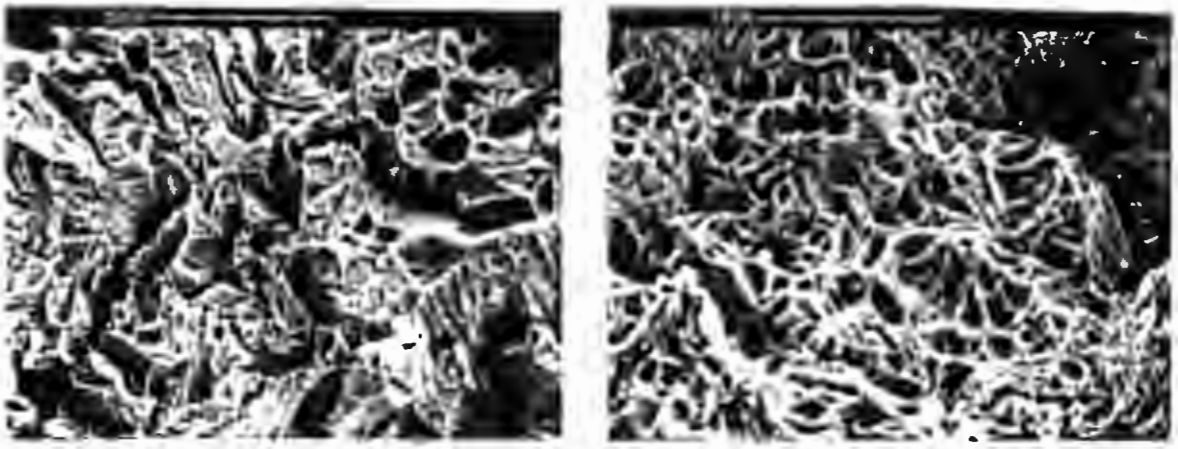

(a) (b)

Figure (4.40): Appearance of the tensile fracture surface of Alloy E in (a) solution treated condition, and (b) after tempering at 600 °C for one hour.

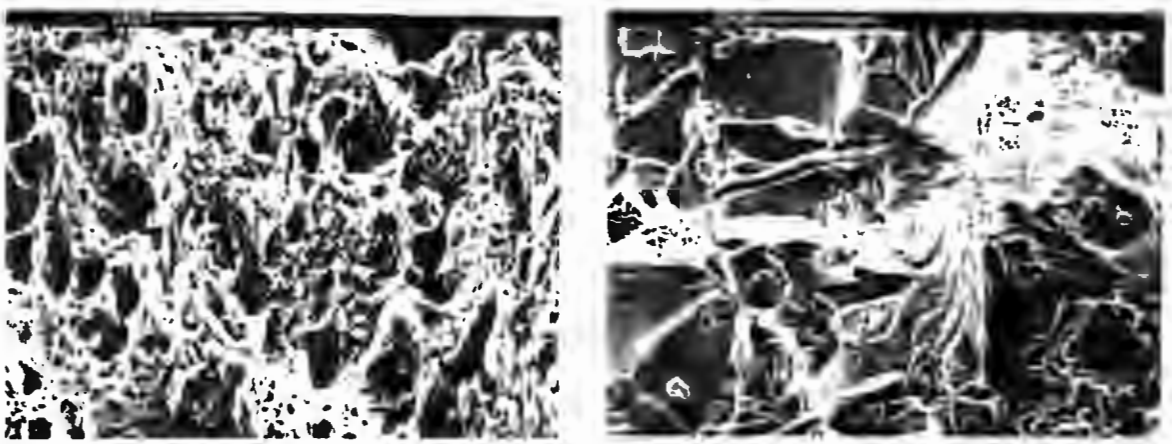

(a) (b)

Figure (4.41): (a) Tensile fracture surface appearance after heat treating at 800 °C for one hour, and (b) Appearance of a Charpy fracture surface of alloy E after tempering at 600 °C for one hour.

In the solution treated condition the low impact resistance is accompanied by a brittle, cleavage prone fracture surface. A considerable improvement in impact resistance is noted after tempering at 600 °C. However, the fracture surfaces still have a partially brittle appearance (Fig. (4.41b)), presenting a combination of fine ductile tearing and transgranular and intergranular cleavage fracture. Fracture surfaces of impact specimens in

the 700 °C tempered condition consist of large ductile dimple networks formed around what appear (from EDS analysis) to be primarily SiO_2 and Al_2O_3 inclusions.

Heat treating at 800 °C results in a reduction in impact resistance below that exhibited in the 700 °C tempered condition. Fracture surfaces are characterized by fine cleavage type fracture (in the order of the size of the lamellar martensite rib spacing), and inclusion related ductile dimple fracture on shear lips and scattered across the fracture surfaces. Lateral tearing is also observed, and the walls of the cracks are covered by fine ductile dimple formations in somewhat regular arrays (Fig. (4.42a)). Analysis of cross sections of fracture surfaces revealed that the fine cleavage facets on the fracture surfaces are related to the deviated nature of cracks passing through the lamellar composite grains, and evidence of blunting of sub-surface cleavage cracks in δ-ferrite grains by the lamellar composite phase was noted (Fig. (4.42b)).

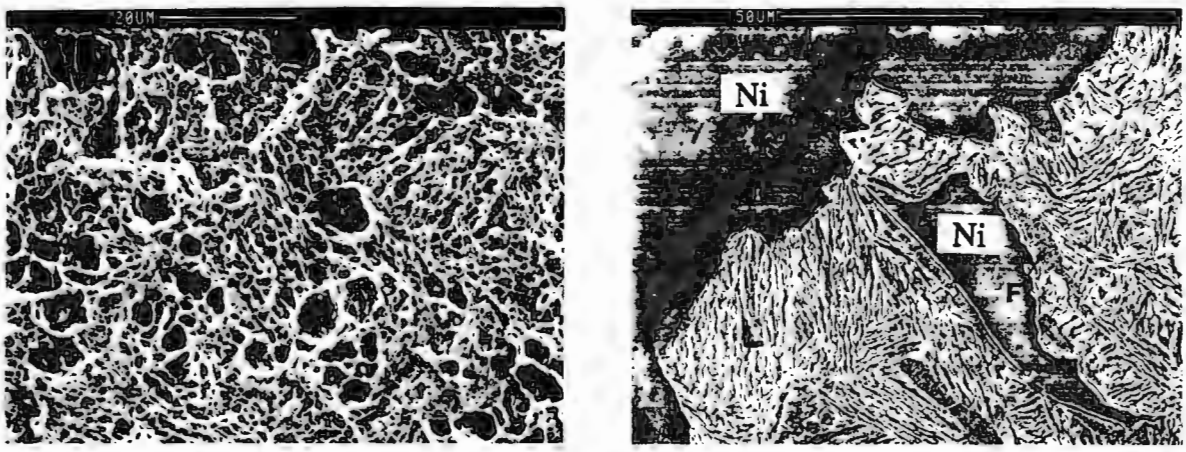

Figure (4.42): (a) Appearance of the wall of a lateral crack in a specimen impacted after heat treating at 800 °C, and (b) a cross section through the same specimen after nickel plating. [F = Ferrite, L = lamellar composite phase, Ni = nickel plating]

4.2.5 STANDARD STAINLESS STEELS

4.2.5.1 MECHANICAL PROPERTIES AND FRACTOGRAPHY

The tensile and impact properties of AISI 304, 430 and 431 in various heat treated conditions are listed in Table (4.12).

STEEL (AISI)	HEAT TREAT.	σ_{UTS} [MPa]	$\sigma_{0.5}$ [MPa]	$\sigma_{0.2}$ [MPa]	Elong [%]	Charpy [J]	Hv_{30}
430	AS REC.	531.4	488.3	475.6	26.5	30.4	195
"	S/T	691.7	467.4	406.8	15.7	2.25	253
"	600/2Hrs	610.1	466.0	436.5	18.2	29.0	203
"	700/2Hrs	572.1	404.2	386.6	26.7	46.1	190
431	AS REC.	820.1	695.0	693.1	23.9	37.0	277
"	S/T	1731.2	1488.9	1245.3	8.1	7.80	557
"	600/2Hrs	938.1	798.7	755.7	19.8	15.2	317
"	700/2Hrs	900.0	742.4	665.0	21.26	54.9	305
304	AS REC.	695.0	276.7	229.5	71.4	188.0	160
"	1040/WQ	688.3	265.0	234.6	69.3	289.0	158

* 1040/40 MINS, AIR COOLED

Table (4.12): Mechanical properties of AISI 304, 430 and 431 in various heat treated conditions.

4.2.5.1.1 AISI 304

In the as received and 1040 °C/water quenched conditions the tensile deformation curves of AISI 304 were virtually identical, and fracture surfaces exhibited comparatively large and uniform ductile dimple features. Impact specimens did not show complete fracture, and the extent of blunting of the crack propagating from the notch of the impact specimen was higher in the solution treated condition than in the as received condition.

4.2.5.1.2 AISI 430

AISI 430 did not exhibit yield point elongation (Luders extension) in the as received condition or in any of the heat treated conditions in which it was tested (Fig. (4.43)). In the solution treated condition, tensile fracture surfaces are characterised by regions of transgranular cleavage fracture and fine ductile dimple features, and a small amount of intergranular rupture. Impact fracture surfaces consist entirely of fine and coarse cleavage facets. In the as received condition tensile and impact surfaces consisted of very fine, fairly uniform ductile dimple features (Fig(4.44)), with occasional evidence of intergranular separation and transgranular cleavage fracture on impact fracture surfaces.

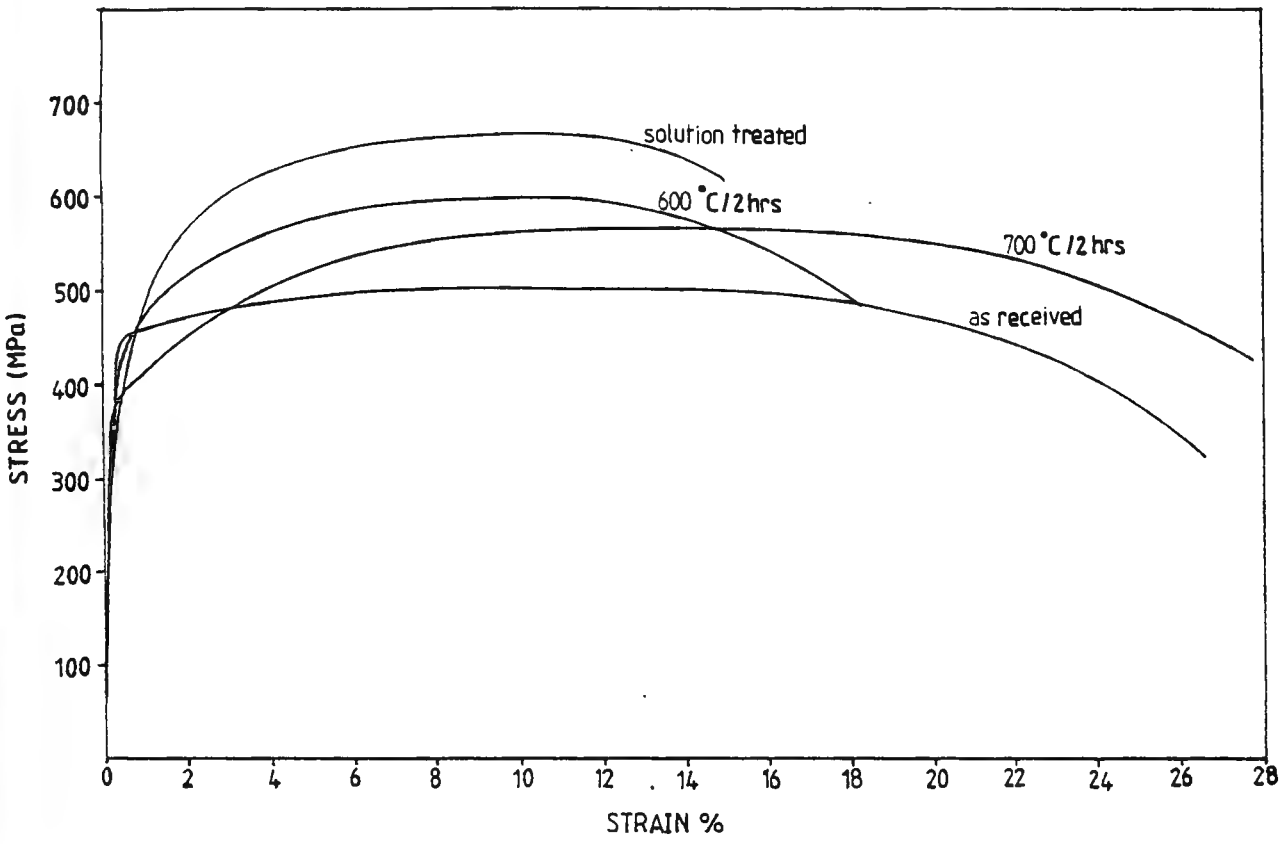

Figure (4.43): Tensile deformation curves for AISI 430 in various heat treated conditions.

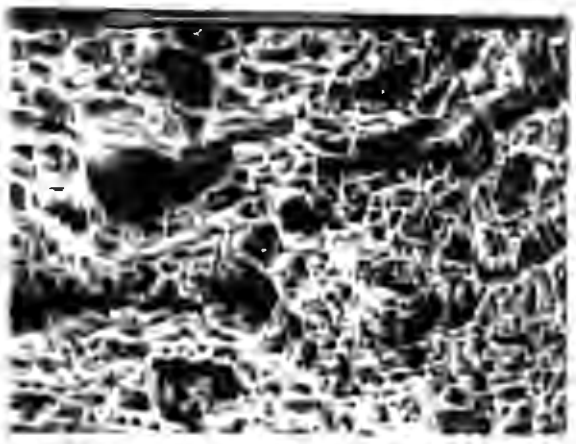

Figure (4.44): Tensile fracture surface appearance of AISI 430 in the as received condition.

Susceptibility to intergranular fracture is highest in the 600 °C tempered condition, and

fracture surfaces are characterised by smooth features associated with intergranular separation, and fine ductile tearing (Fig. (4.45a)). The susceptibility to intergranular fracture is markedly reduced after tempering at 700 °C for two hours, and fracture surfaces consist predominantly of fine, fairly uniformly sized ductile dimple features (Fig. (4.45b)).

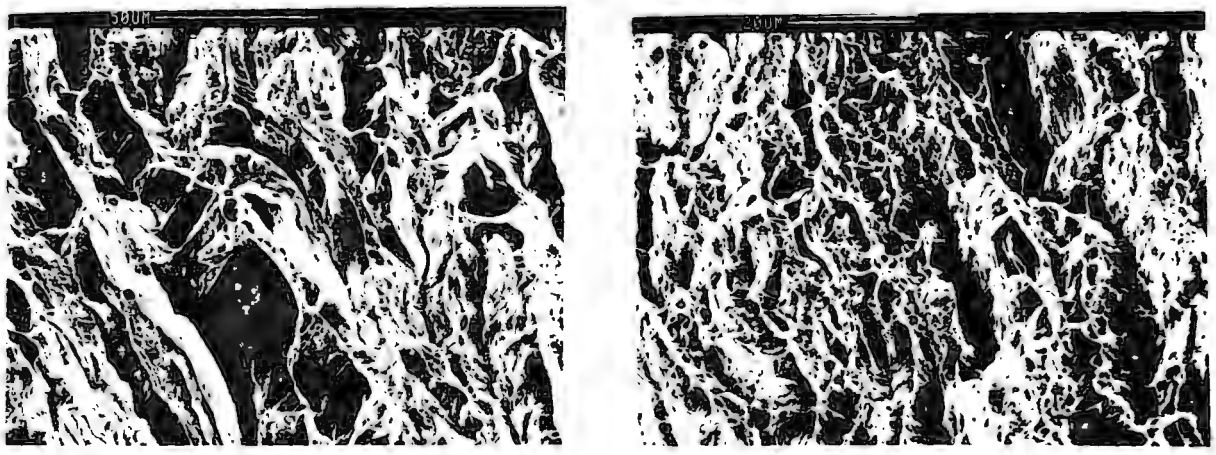

(a) (b)

Figure (4.45): Appearance of the tensile fracture surfaces of AISI 430 after heat treating at (a) 600 °C and (b) 700 °C for two hours after solution treating.

4.2.5.1.3 AISI 431

In the as received condition AISI 431 exhibits yield point elongation (Luders extension) during tensile testing (Fig. (4.46)), and tensile and impact fracture surfaces exhibited very fine ductile dimple features. In the solution treated condition the impact surfaces are characterised by fine cleavage facets and fine shear lips in the order of the size of the martensite laths. The tensile fracture surfaces exhibited occasional evidence of fine cleavage fracture, but consisted predominantly of uniform, comparatively large ductile dimple features (Fig. (4.47a)). In the 600 °C tempered condition tensile fracture surfaces consist of fine ductile dimple features, although the impact fracture surfaces are characterised almost entirely by intergranular and transgranular cleavage fracture (Fig. (4.47c)). In the 700 °C heat treated condition, tensile fracture surfaces are characterised by fine, uniform ductile dimple features (Fig. (4.47b)), although the appearance of impact fracture surfaces still reflected a susceptibility to intergranular rupture.

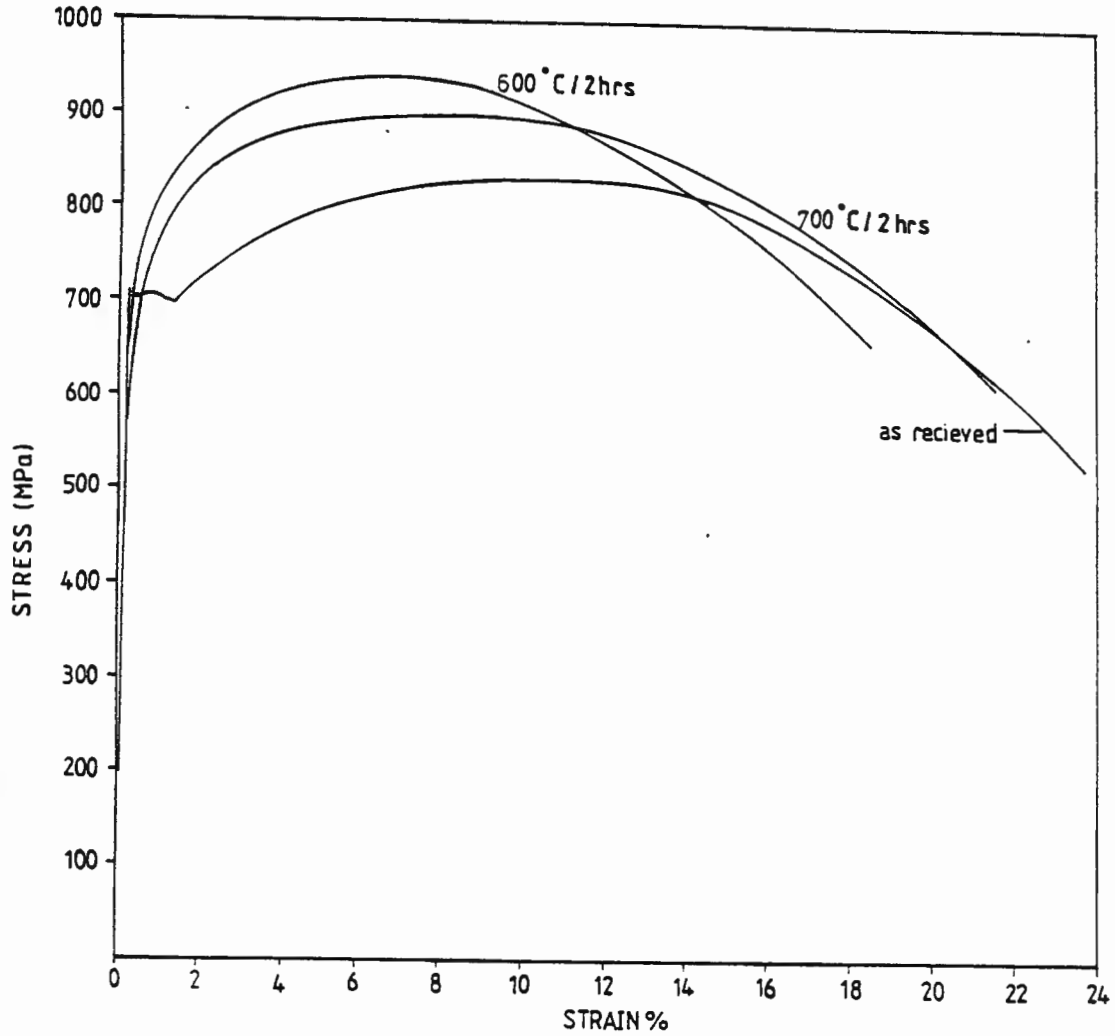

Figure (4.46): Tensile deformation curves for AISI 431 in various heat treated conditions.

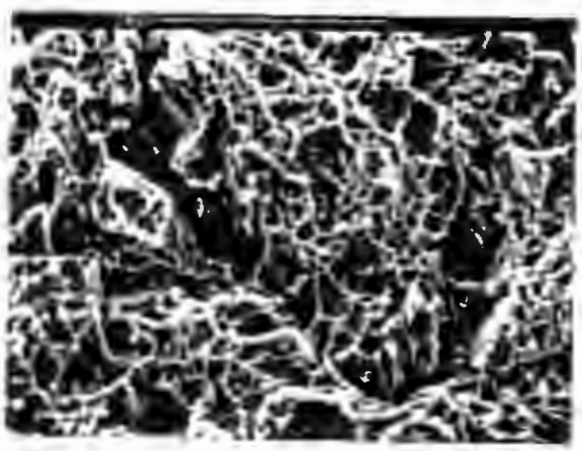

(a)

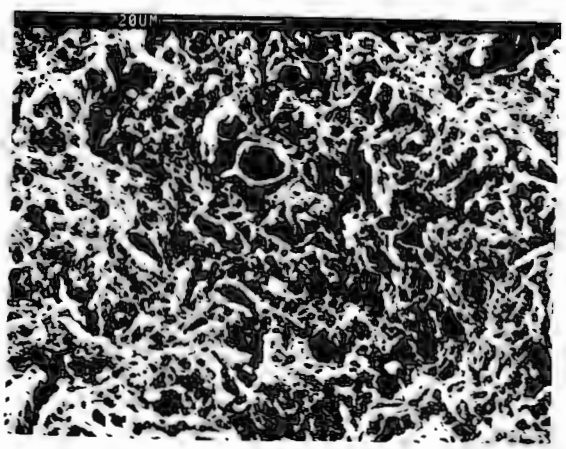

(b)

..... / Fig. (4.47c)

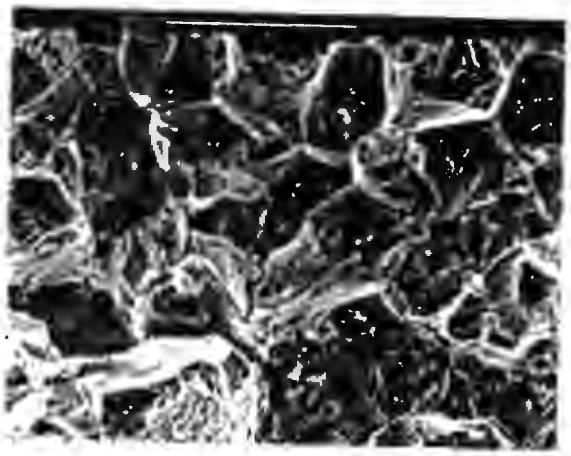

(c)

Figure (4.47): Appearance of tensile fracture surfaces of AISI 431 (a) in the solution treated condition, and (b) after tempering at 700 °C for two hours, and (c) the appearance of an impact fracture surface of the alloy after heat treating at 600 °C for two hours.

4.3 DUCTILE TO BRITTLE TRANSITION BEHAVIOR OF ALLOYS A, C AND E

The effect of temperature on the impact resistance of Alloys A, C and E (Fig. (4.48)) was investigated in order to assess how the variations in microstructure and composition effect ductile to brittle transition characteristics. The ductile to brittle transition temperatures (Table (4.13)) are taken to be the points where the transition curves intersect the 40 J energy level.

ALLOY	Heat Treatment	Transition Temp.
ALLOY A "	Solution Treated 700 °C/2 Hours	-25 -52
ALLOY C	700 °C/1 Hour	-14
ALLOY E "	700 °C/1 Hour 800 °C/1 Hour	-61 36

Table (4.13): 40 J transition temperatures for alloys A, C, and E in various heat treated conditions.

4.3.1 ALLOY A

The fracture surface features of alloy A in the solution treated condition exhibit a transition from a relatively large, uniform ductile dimple character after impacting at 72 °C to a brittle character after impacting at -65 °C, with only a small amount of plastic

deformation, as fine ductile lips, occurring within the martensite phase (Fig. (4.49a)).

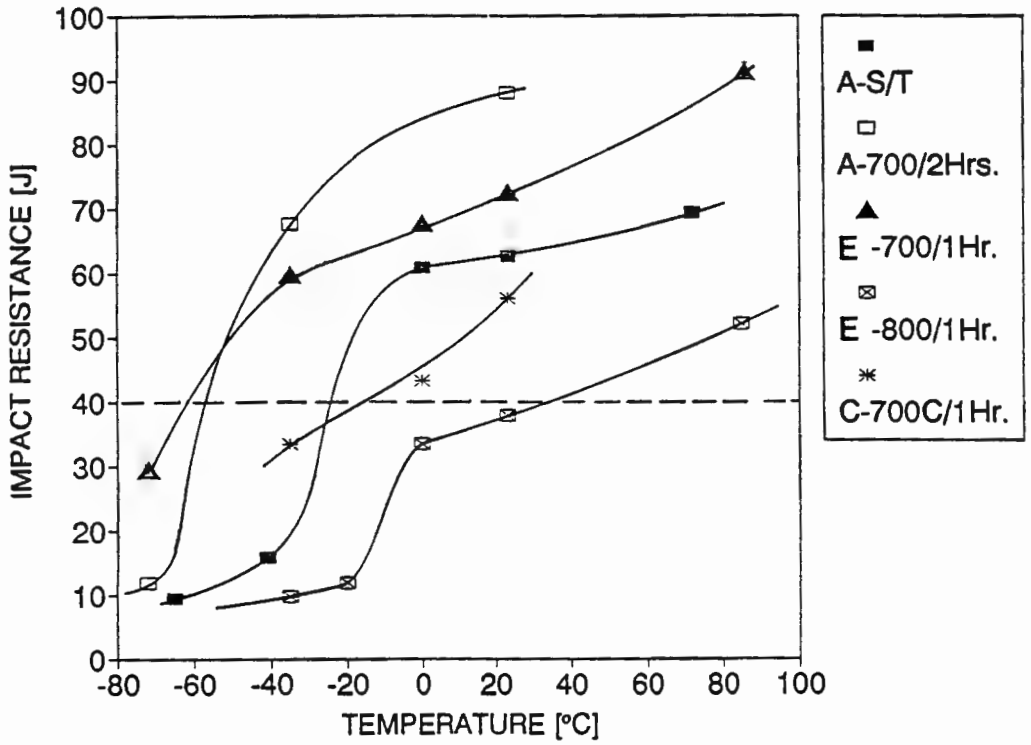

Figure (4.48): The effect of temperature on the impact resistance of alloys A, C, and E in particular heat treated conditions

The appearance of the fracture surface after impacting at -35 °C is similar to that after impacting at -65 °C, except for the presence of ductile lateral cracks.

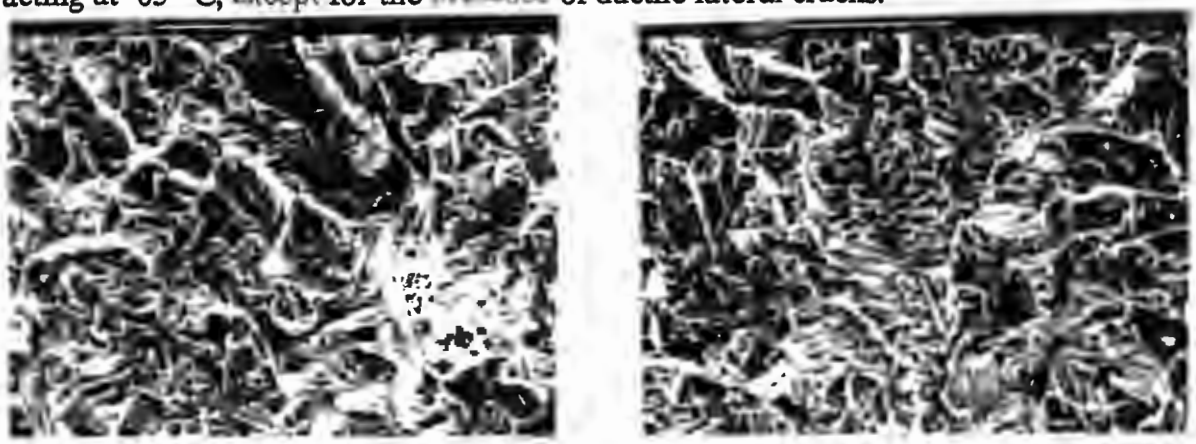

(a) (b)

Figure (4.49) : (a) Appearance of Charpy fracture surfaces of alloy A, in the solution treated condition, after impacting at -65 °C, and (b) appearance of the fracture surface, in the 700 °C heat treated condition, after impacting at -72 °C.

The appearance of a fracture surface of Alloy A in the 700 °C heat treated condition, after impacting at -35 °C, is similar to that after impacting at room temperature, and consists of large inclusion-related ductile dimples, surrounded by a network of finer dimples. Impacting at -72 °C results in a predominantly brittle fracture process, and the fracture surface has a serrated appearance as a consequence of the varied orientation of the fine cleavage facets (Fig.(4.49b)).

4.3.2 ALLOY C

In the solution treated condition, Alloy C has a 40J transition temperature well above room temperature, as is indicated by its low impact resistance (2.5 J). Tempering at 700 °C, however, reduced the transition temperature below 0 °C (Table (4.13)).

When impacted at 0 °C, Alloy C (in the 700 °C tempered condition) exhibits a fracture appearance similar to that at room temperature (refer to Fig (4.33)). The specimen impacted at -35 °C has a fracture surface appearance similar to that after impacting at 0 °C, although a larger amount of transgranular cleavage fracture is observed in the δ-ferrite grains (Fig.(4.50)).

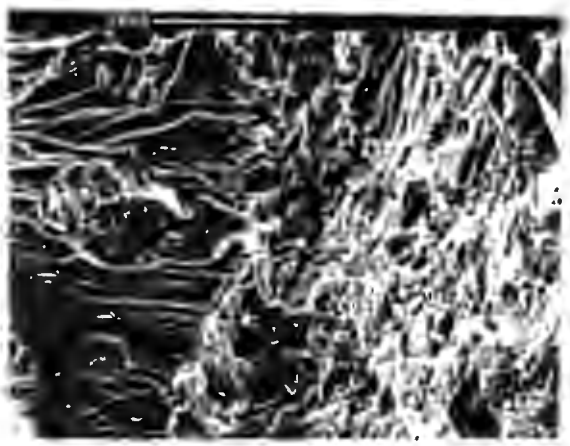

Figure (4.50): Charpy fracture surface appearance of Alloy C after testing at -35 °C.

4.3.3 ALLOY E

In the solution treated condition the room temperature impact resistance of alloy E was very low (5J), indicating a high 40J transition temperature. However, in the 700 °C tempered condition, it was reduced to -61 °C , while heat treating at 800 °C for one hour, which caused a partial austenite reversion, raised the 40J transition temperature to just

above room temperature (Table (4.13)).

When impacted at 88 °C, Alloy E (in the 700 °C tempered condition) exhibits a highly ductile mode of fracture. When tested at -35 °C the majority of the fracture surface has a quasi-brittle appearance, and evidence of intergranular and transgranular cleavage fracture is observed (Fig. (4.51)). Impacting at -72 °C results in an entirely intergranular cleavage fracture mode.

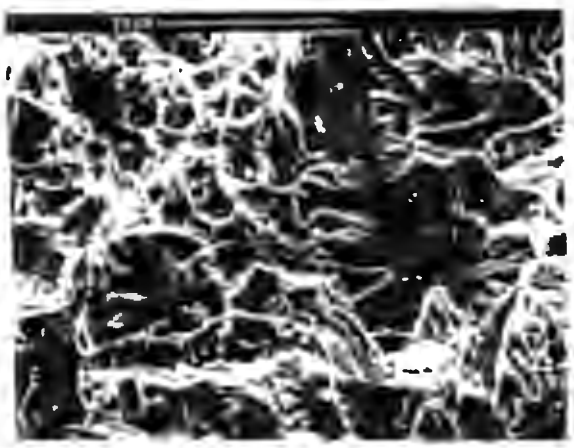

Figure (4.51): Appearance of charpy fracture surfaces of alloy E in the 700 °C tempered condition after impacting at -35 °C.

In the 800 °C heat treated condition, the fracture surface appearance, after impacting at 86 °C, are large inclusion related ductile dimples, surrounded by very fine interlinked networks of ductile dimples (Fig. (4.52a)). However, the specimens fractured at room temperature and 0 °C have quasi-brittle fracture surface appearances, consisting of fine cleavage facets and fine ductile lips. After impacting at -20 and -38 °C the fracture surfaces have an entirely brittle appearance (Fig (4.52b)), although the fine nature and varied orientation of the cleavage facets indicate that the lamellar martensite/ferrite structure does influence crack propagation.

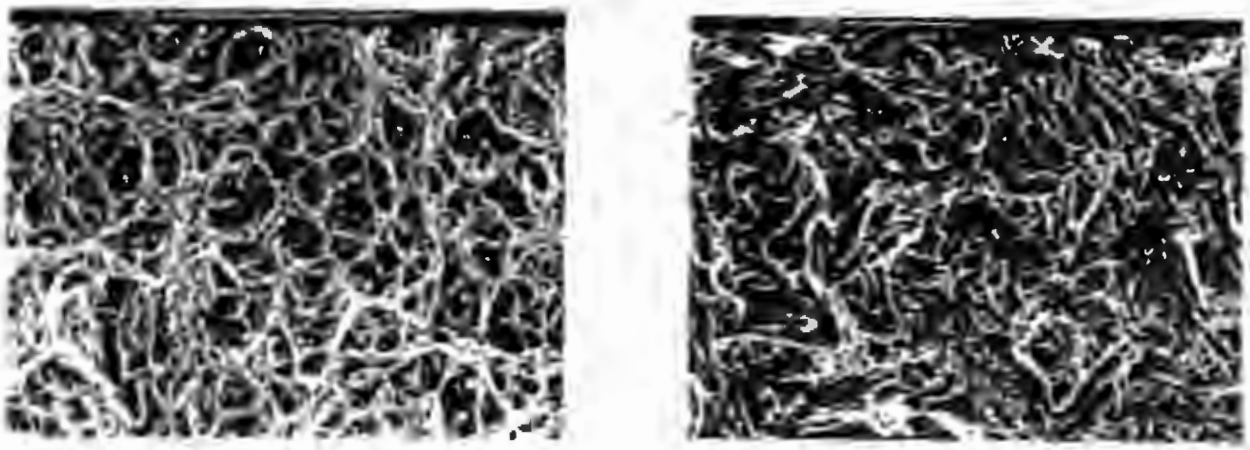

(a) (b)

Figure (4.52): Fracture surface appearance of alloy E (in the 800 °C heat treated condition) after impacting at (1) 86 °C and, (2) -20 °C.

4.4 THERMOMECHANICAL TREATMENT OF ALLOY A, AISI 430 AND AISI 431

4.4.1 INTRODUCTION

A comparison was made between the tensile properties of an experimental dual-phase alloy (Alloy A), and the standard stainless steels AISI 430 and 431, under conditions where the microstructures had been processed to produce fine, equiaxed grain structures by precisely controlled thermomechanical treatments.

4.4.2 MICROSTRUCTURES AND MECHANICAL PROPERTIES

Table (3.3) (page 36) outlines the thermomechanical treatments performed on each of the alloys. The hardness values and average grain size of the alloys, after the various recrystallisation and tempering heat treatments, are shown in Table (4.14).

The microstructure of AISI 430 consists of fine, equiaxed α-ferrite grains, and carbides randomly scattered throughout the ferrite grains (Fig. (4.53a)). A lengthy solution treatment of AISI 431 (at 1030 °C) was necessary in order to dissolve carbide precipitates formed during hot rolling, and thus the grain size is somewhat larger than that of the other

alloys (Table (4.14)). Apart from the presence of a 6 - 8% δ-ferrite, the microstructure in the solution treated condition consists primarily of lath type martensite (Fig. (4.53b)). The microstructure of AISI 431 after tempering at 700 °C for two hours consists of fine lamellar martensite in a ferrite and carbide matrix (Fig. (4.53c)).

ALLOY	HARDNESS [Hv_{30}]	GRAIN SIZE[μm]
AISI 430 (830 W/Q)	163.2	17.5
AISI 431 (1000 A/C)	557	29
" (700 A/C)	293	29
ALLOY A (1000 A/C)	343	F- 7.5 M- 16.5
" (700 A/C)	295	F- 7.5 M- 16.5

Table (4.14): Hardness and grain size values for the rolled alloys after recrystallisation and tempering heat treatments.

The grain sizes of the ferrite and martensite phases of alloy A in the thermomechanically treated condition are little different to that of the starting material (9mm plate). However, the grains of both phases have a more equiaxed appearance, original ferrite bands being broken up to the point of partial or full isolation of individual ferrite grains in the bulk martensite phase. The appearance of the microstructure in the solution treated condition and after intercritical annealing at 700 °C are illustrated in Figures (4.53d) and (4.53e). The hardness values in these heat treated conditions are marginally higher than those of the starting material (9mm plate) in similar heat treated conditions (table (4.7).

The tensile properties of the thermomechanically treated alloys, and their associated stress strain curves, are illustrated in Table (4.15) and Figure (4.54) respectively. The thermomechanical treatment performed on AISI 430 evidently resulted in a fully ferritic structure, with a low tensile strength, high ductility and the presence of a definite yield point, manifested in Luders band formation (Fig (4.54)).

In the solution treated condition, AISI 431 exhibited surprisingly good ductility considering its high tensile strength. After heat treating at 700 °C, the alloy exhibited a combination of attractive yielding characteristics (high initial work hardening rate), moderate tensile strength and good ductility (Fig. (4.54) and Table (4.15)).

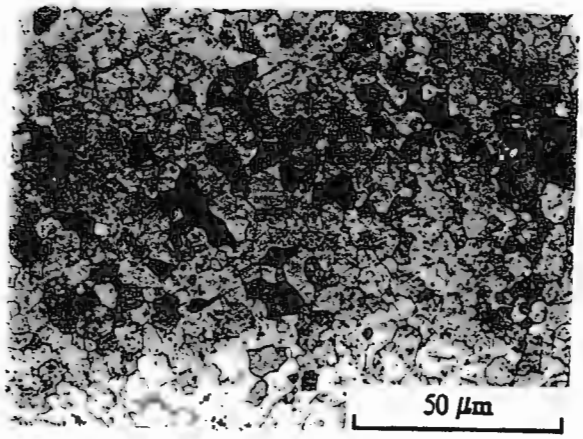

(a)

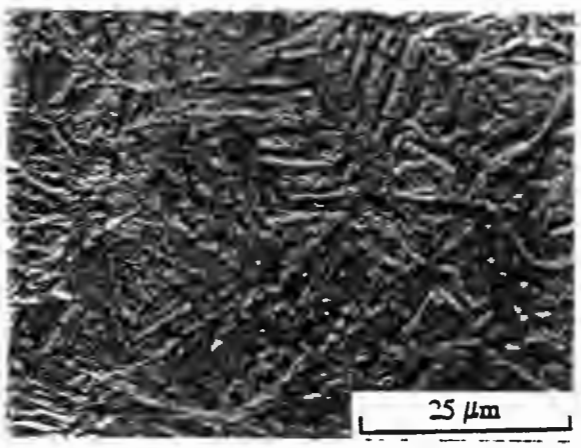

(b)

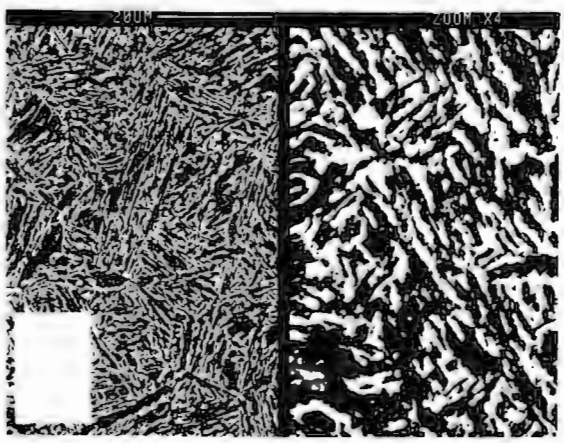

(c)

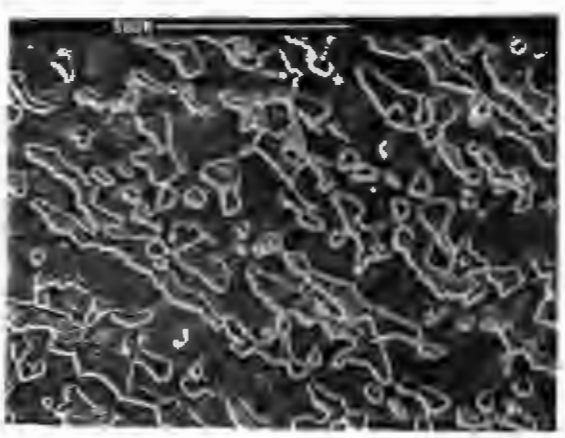

(d)

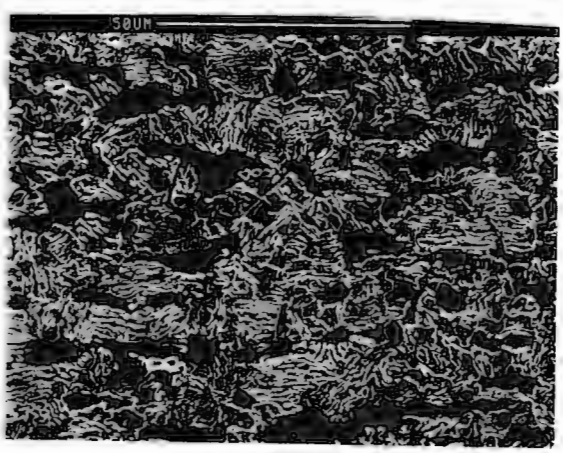

(e)

Figure (4.53) Appearance of the microstructures, after controlled rolling and recrystallisation treatments, of (a) AISI 430, (b) 431 solution treated, (c) 431 700 °C tempered, (d) alloy A solution treated and (e) alloy A tempered at 700 °C.

ALLOY	Heat Treatment	σ_{UTS}	$\sigma_{0.2\%}$	% Elong. [Unif.]	% Elong. [Total]
ALLOY A	S/T	1001	812.0	4.20	14.1
"	700C/2Hrs	821.3	670.1	3.95	13.1
AISI 431	S/T	1917.1	1210.0	4.17	8.2
"	700C/2Hrs	941.1	710.6	7.76	20.5
AISI 430	830C/3Mins	445.2	295.3	16.28	29.7

* SEE TABLE () S/T = SOLUTION TREATED

Table (4.15): Tensile properties of Alloy A, AISI 430 and 431, after specific thermomechanical treatments.

The uniform and total elongation of alloy A in both the solution treated and 700 °C tempered conditions was surprisingly low (Table (4.15)), several percent less than observed during testing of the original plate thickness (8mm plate, Table (4.7)).

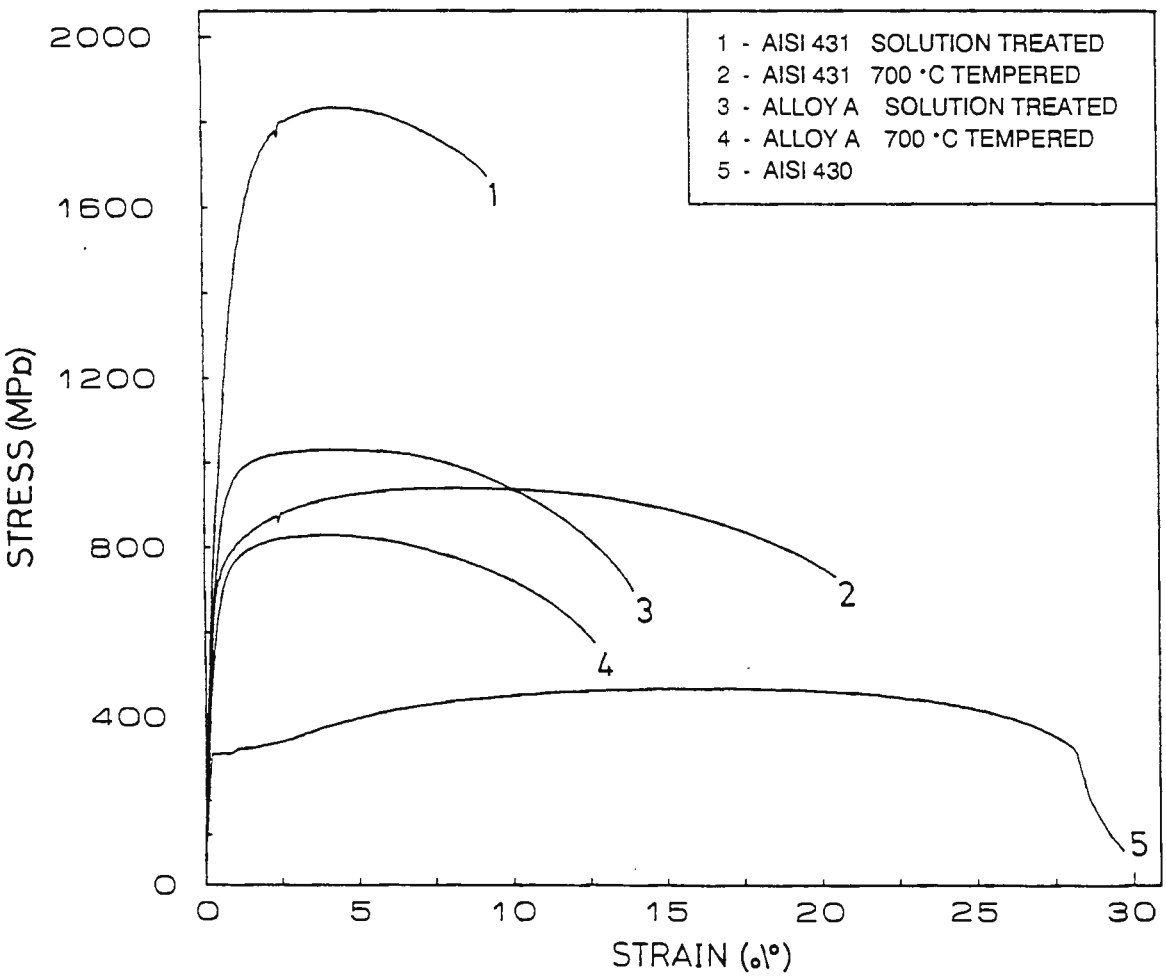

Figure (4.54): Tensile deformation curves for alloys A, AISI 430 and AISI 431 after specific thermomechanical treatments.

4.4.3 DEFORMATION TO FRACTURE OF ALLOY A

The microstructural characteristics of deformation of alloy A from yielding to the point of fracture, in both the solution treated and 700 °C heat treated conditions, were investigated. From sequences of photographs depicting tensile deformation markings on the specimen gauge surfaces, the most prominent and common deformation characteristics and mechanisms of microvoid formation were identified.

4.4.3.1 ALLOY A - SOLUTION TREATED

The main modes of deformation and fracture initiation within alloy A, in the solution treated condition, are schematically illustrated in Fig. (4.55) . The first evidence of surface deformation was observed at approximately 2% strain, as very fine wavy slip lines at approximately 45° to the tensile axis in some ferrite grains. The first visible signs of deformation in the martensite phase were observed shortly after this at approximately 3% strain, as fine ripples in regions of martensite grains (Fig. (4.55a), labelled 1). The localised nature of the deformation suggests it initiates in packets of laths having a favorable orientation for plastic flow with respect to the applied stress.

Macroscopically, the onset of necking in the tensile specimen was visible soon after the termination of uniform elongation (5-7% strain). Increased plastic deformation was observed in the martensite phase, either as ripples across grains or as localized strain concentrations within parts of grains. While in numerous cases the cause of these strain concentrations was not clear, they were often related to narrow martensite sections (Fig. (4.55b), labelled 2). More intense deformation was observed in some ferrite grains (Fig. (4.55a - b)), which occasionally flowed into adjacent martensite grains or built up along ferrite/martensite interfaces. Intense deformation, synonymous with necking, was observed in some ferrite grains in regions of high stress intensity, such as the ferrite regions adjacent to sharp corners in the martensite phase (Fig. (4.55b), labelled 3). However this type of deformation was not very common, and a large portion of the ferrite grains, especially those which were isolated, exhibited little or no surface deformation.

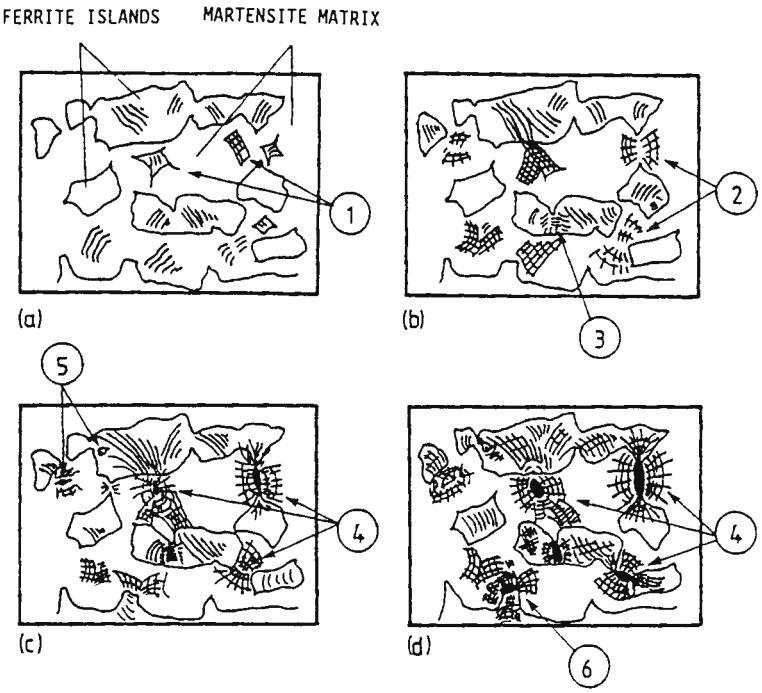

Figure (4.55): Schematic representation of the mechanisms of deformation and fracture initiation in alloy A in the solution treated condition (See text for explanation).

In the region of 7-10% strain, there was a considerable increase in the intensity of deformation in the martensite phase, which was often associated with regions of high stress intensity or high plastic constraint such as narrow martensite sections (Fig. (4.55c), labelled 4) and within large martensite grains. The deformation in these regions can be described as necking due to the localised nature of the deformation. Occasional evidence of fracture within the necked regions was also observed. From approximately 8.5 % strain, evidence was also observed of microvoid formation as a result of inclusion/matrix interfacial decohesion in both of the phases (Figs. (4.55c - d) , labelled 5).

At this level of strain (7-10%) the regions of the martensite phase between the regions of necking in the phase appeared to have experienced comparatively little plastic deformation, and little change was noted in these regions as the strain was increased to the point of fracture.

From approximately 10 % strain to the point of fracture a small amount of evidence of interfacial decohesion between the ferrite and martensite phases was observed (Fig. (4.55d), labelled 6). However, the strain was most often accommodated in the ferrite phase by plastic deformation. Microvoid formation, primarily in the form of fracture within the martensite phase (Fig. (4.55d) labelled 4) and around inclusions, became more frequent as the point of fracture was approached (10-14% strain), and crack propagation between the points of microvoid initiation resulted in the formation of larger voids in a direction perpendicular to the tensile axis, and final fracture. The following sequence of micrographs

shows examples of some of the features of the deformation and fracture initiation in alloy A, in the solution treated condition, that are summarised in Fig. (4.55).

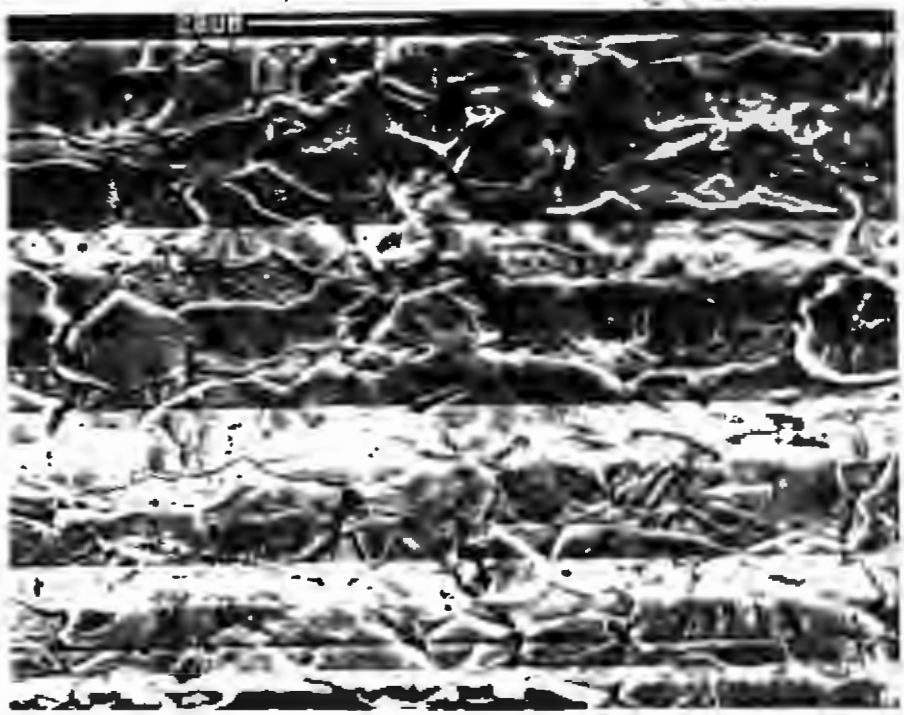

(a)

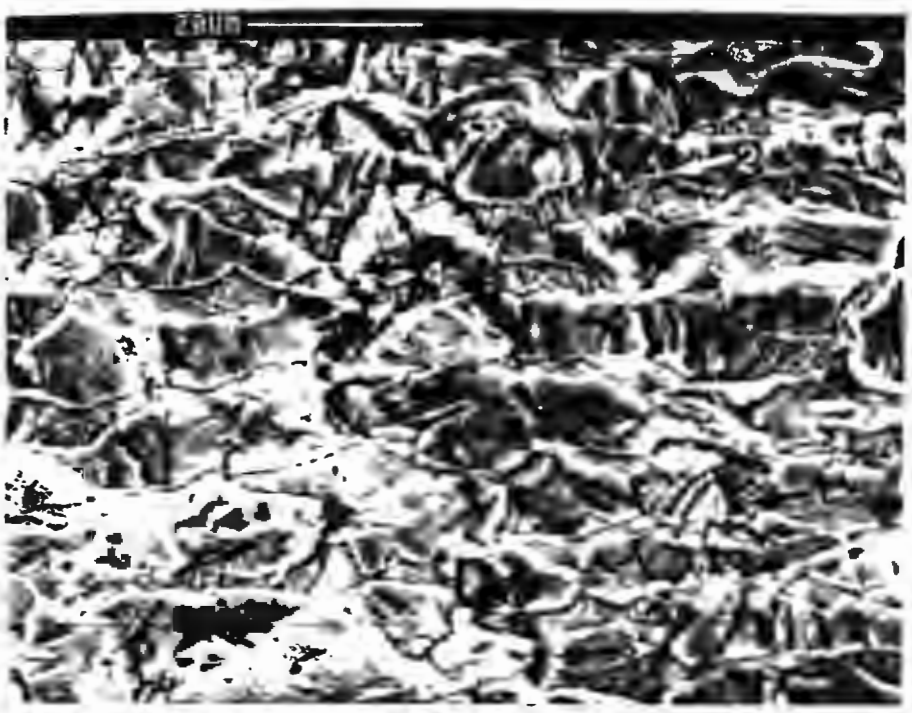

(b)

1- FRACTURE WITHIN THE MARTENSITE PHASE
2- INTERFACIAL DECOHESION BETWEEN THE FERRITE AND MARTENSITE PHASES
3- COMBINATION OF INTERFACIAL DECOHESION AND FRACTURE OF THE MARTENSITE PHASE
4- INCLUSION/MATRIX INTERFACIAL DECOHESION

..... / Fig. (4.56)

(c)

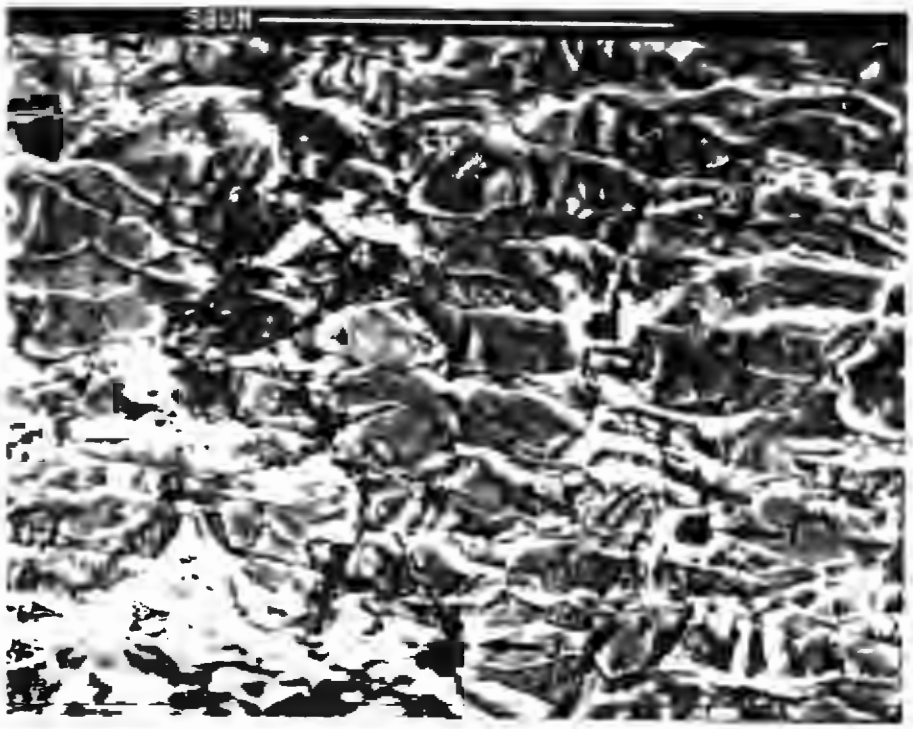

(d)

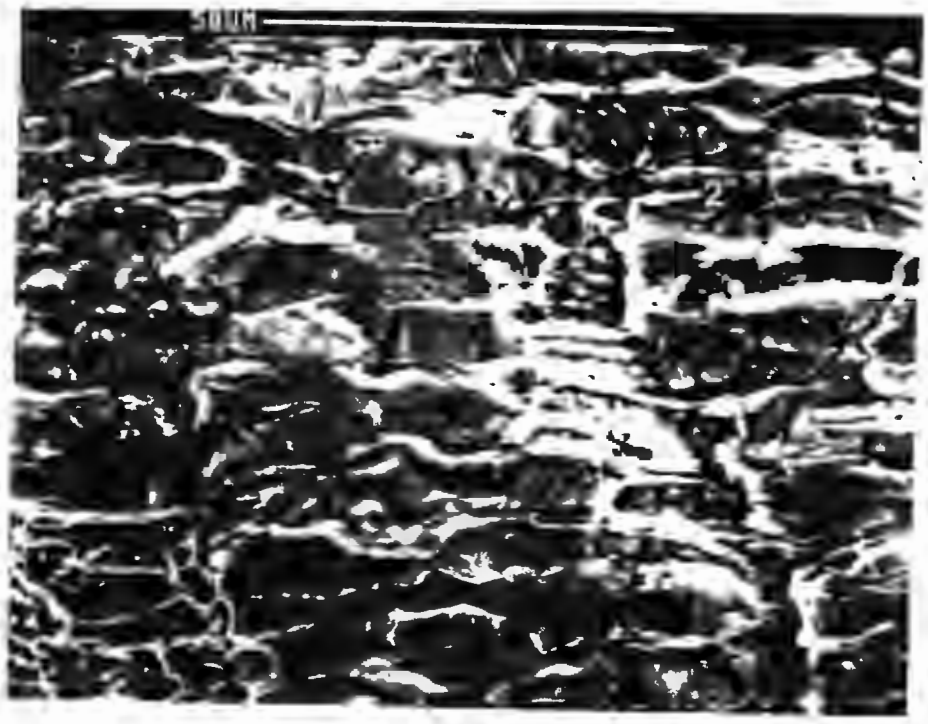

1- FRACTURE WITHIN THE MARTENSITE PHASE
2- INTERFACIAL DECOHESION BETWEEN THE FERRITE AND MARTENSITE PHASES
3- COMBINATION OF INTERFACIAL DECOHESION AND FRACTURE OF THE MARTENSITE PHASE
4- INCLUSION/MATRIX INTERFACIAL DECOHESION

Figure (4.56): Appearance of surface deformation markings on the gauge length of a tensile specimen of alloy A after (a) 7% strain, (b) 8.4% strain, (c) 9.9% strain and (d) fracture.

4.4.3.2 ALLOY A - 700 °C/2 HOURS

The sequence of micrographs in Fig. (4.57) is representative of stages in the process of deformation and fracture initiation in alloy A after heat treating at 700 °C for two hours. Deformation from the elastic limit to the point of maximum uniform elongation was characterised by the onset of slip in the δ-ferrite phase. This was visible as very fine, wavy slip bands in the δ-ferrite phase at 3% strain. Towards the point of maximum uniform elongation (3.5 to 4.5 % strain), the polished and etched surface exhibited a fine 'wavy' nature which suggests there is also deformation within the lamellar composite phase. There was no evidence of plastic deformation of the martensite lamellae in the region of 0 - 4 % strain, which suggests that the wavy appearance of the specimen surface is a consequence of deformation within the soft inter lamellar ferrite.

Once the peak uniform elongation was surpassed and necking was observed, the angle of orientation of the lamellar martensite 'packets' to the tensile axis played an important part in determining the characteristics of deformation to fracture.

In the region of 5 - 8% strain, plastic deformation built up in the δ-ferrite phase, in the form of more intense wavy slip bands. If the orientation of the martensite 'packets' was between 45° and 90° to the tensile axis, deformation was concentrated within the inter lamellar ferrite regions (Figs. (4.57a), (4.57b) and (4.57c), points 1 and 2). A common occurrence observed was parallel slip bands in the δ-ferrite which bridged into the inter-lamellar secondary ferrite (tempered martensite). This possibly results from the orientation of the martensite lamellae being approximately parallel to a principal slip system in the adjacent δ-ferrite phase, which results in deformation extending from the δ-ferrite grains into the inter-lamellar ferrite. In the vicinity of 7 - 10 % strain, evidence was observed which suggests that the constraint applied by the martensite lamellae on deformation within the inter-lamellar ferrite may result in interfacial decohesion between the hard martensite lamellae and the soft inter lamellar ferrite (Figs. (4.57a), (4.57b) and (4.57c), point 1). Evidence was also observed suggesting that this process of inter-lamellar deformation may also lead to fracture of the martensite lamellae, the combination of fracture mechanisms representing a common mode of microvoid initiation (Fig. (4.57b), (4.57c) and (4.57d), points 1 or 2).

When the orientation of the martensite lamellae was between 0° and 45° to the tensile axis, a build-up of stress in the lamellar martensite phase resulted in yielding of the

martensite lamellae. This process was evident after the onset of necking, and progressed rapidly into what appeared to be necking and then fracture of the martensite lamellae. An example is illustrated in Figs. (4.57b - d), point 3). Numerous incidents of fracture of individual martensite ribs was also noted.

Figure (4.57d) illustrates the surface deformation characteristics of the fractured tensile specimen, fracture occurring in the vicinity of the dotted line in Fig. (4.57c). The process leading to final fracture appeared to involve coalescence of the voids formed in the lamellar ferrite/martensite phase.

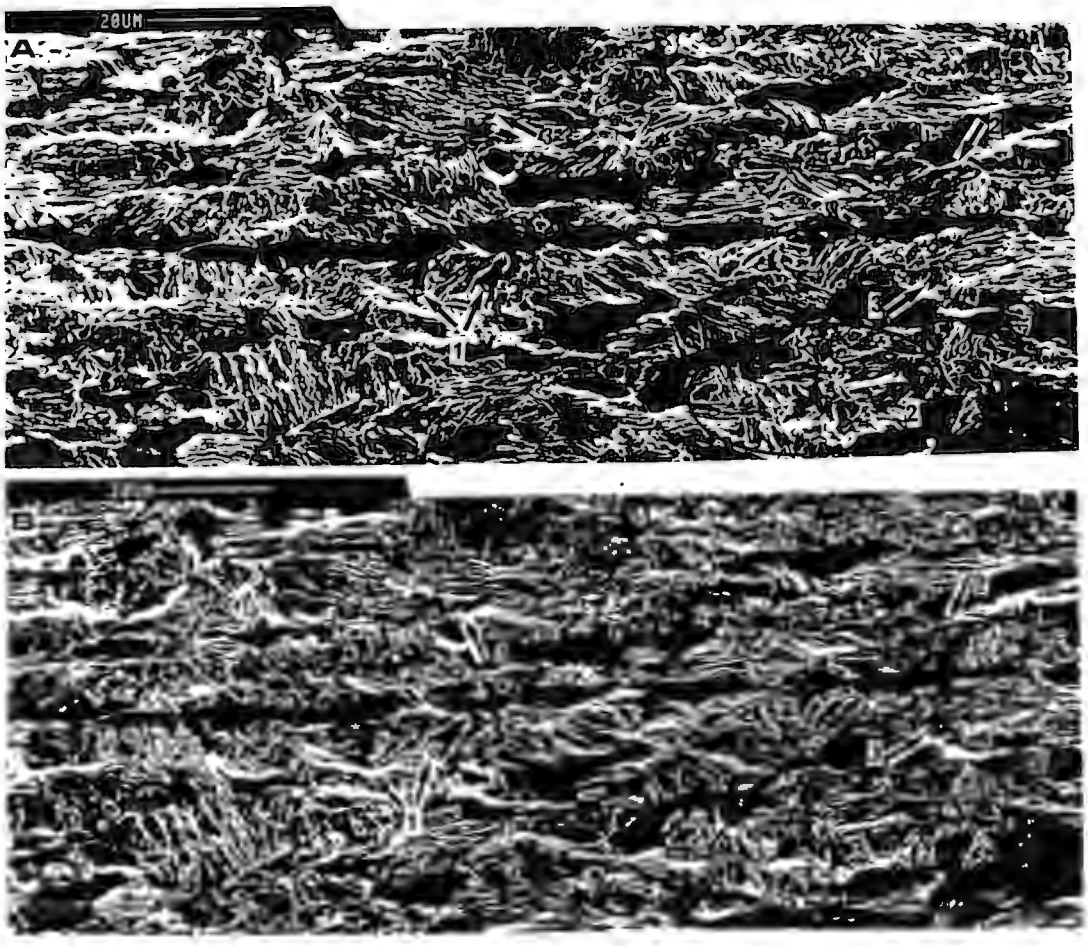

1- VOID FORMATION AS A COMBINATION OF FRACTURE OF THE MARTENSITE RIBS, AND INTERFACIAL DECOHESION THE INTER LAMELLAR FERRITE AND MARTENSITE RIBS.
2- DEFORMATION WITHIN THE LAMELLAR PHASE AS A RESULT OF SLIP IN THE INTER LAMELLAR FERRITE, AND YIELDING AND OCCASIONAL FRACTURE OF TH MARTENSITE RIBS.
3- VOID FORMATION AS A RESULT OF FRACTURE OF THE MARTENSITE 'RIBS'.

..... / Fig. (4.57)

1- VOID FORMATION AS A COMBINATION OF FRACTURE OF THE MARTENSITE RIBS, AND INTERFACIAL DECOHESION THE INTER LAMELLAR FERRITE AND MARTENSITE RIBS.
2- DEFORMATION WITHIN THE LAMELLAR PHASE AS A RESULT OF SLIP IN THE INTER LAMELLAR FERRITE, AND YIELDING AND OCCASIONAL FRACTURE OF TH MARTENSITE RIBS.
3- VOID FORMATION AS A RESULT OF FRACTURE OF THE MARTENSITE 'RIBS'.

Figure (4.57): Various stages in the tensile deformation of Alloy A in the 700 °C tempered condition after (a) 7% strain, (b) 8.5 % strain, (c) 10.3% strain and (d) Fracture.

CHAPTER FIVE

DISCUSSION

5.1 NICKEL ALLOYED STEEL: ALLOY A

The slow rate of diffusion of the substitutional alloying elements (Cr and Ni) is reflected in the small hardness variation that accompanies a one hour heat treatment of alloy A in the temperature range 500 - 900 °C. Thermodynamic constraints on the diffusion of Cr and Ni retard the kinetics of the transformations in the $(\alpha + \delta) + \gamma$ phase field, and this is reflected in the difference of greater than 150 °C between the A_{c1} and A_{c3} temperatures. While the A_{c1} temperature was determined from dilatometry to be 635 °C, the heating rate employed (4 °C/minute) was probably above that required for equilibrium to be reached. This is reflected in the observation of a small amount of fine austenite in the martensite phase after tempering at 600 °C for two hours.

The retarded response to heat treatment at 700 °C, which is within the $(\alpha + \delta) + \gamma$ phase field, revealed the dependence of the transformations occurring on the partitioning of Cr and Ni between the transformation products. The minimum in hardness observed after heat treating for 8 minutes at 700 °C can be associated with a fully tempered microstructure, the microhardness of the martensite phase (352 Hv_{50g}) being considerably lower than that noted after tempering at 600 °C for two hours (396 Hv_{50g}). This reflects the relatively low hardness of the inter-lamellar ferrite in the well defined lamellar composite phase formed after soaking at 700 °C for two hours. The strengthening effect of the lamellar martensite phase is reflected in the increase in hardness as the martensite content increases (10 Hv_{30} between 8 minutes and 1 hour, and 13 Hv_{30} between 1 hour and 2 hours, experimental error ±3 Hv_{30}). While little research has been done on the effect of Ni on the hardness of low carbon martensite, Irvine, Crowe and Pickering[56] noted that increasing the nickel content did marginally increase the strength of martensite in 12% Cr alloys. It is believed that the hardness of the lamellar martensite phase formed after heat treating alloy A at 700 °C is higher than that of the martensite in the solution treated condition (479 Hv_{50g}) as a consequence of the higher nickel content of the lamellar phase,

as reported by Knutsen[13]. Cooling the specimens to -72 °C , subsequent to water quenching from 700 °C (Fig. (4.5)), revealed that there is possibly a small amount of retained austenite in the martensite lamellae, as indicated in the slight increase in hardness. However the increase in hardness was only marginally above the error band for hardness measurements in the water quenched condition (prior to sub zero cooling). The low amount of retained austenite is in agreement with the findings of Grobner and Biss[34] in the analysis of a 16% Cr, 1.5% Mo, 5% Ni ferritic-martensitic alloy. Thus the lamellar composite phases formed after heat treating at 700 °C for two hours consists of two phases with significant differences in hardness and ductility.

5.1.1 MECHANICAL PROPERTIES AND DEFORMATION CHARACTERISTICS

The microhardness of the tempered martensite phase after soaking at 600 °C for two hours (396 Hv_{50g}) was only marginally lower than the overall hardness of the lamellar composite phase formed after soaking at 700 °C for two hours, and this was reflected in the similar tensile strengths of the alloys, since the δ-ferrite remains unchanged during both heat treatments. This provides for an interesting comparison of two microstructures with similar "phase" proportions and strengths, but different microstructural characteristics.

In the 600 °C tempered condition yielding is fairly abrupt (Fig. (5.1)), indicating that deformation in the alloy was close to homogeneous, and that there was not a large difference in the yield strengths of the δ-ferrite and tempered martensite phases. However in the solution treated condition and after soaking at 700 °C for two hours, the onset of yielding occurred at a considerably lower stress than that observed after tempering at 600 °C (Fig. (5.1)), and yielding was continuous as a consequence of the inhomogeneous deformation between the ferrite and martensite phases. The onset of yielding at a comparatively low stress in dual phase steels has been attributed to the introduction of mobile dislocations into the ferrite phase as a result of the martensitic transformation[26,30]. Tanaka et al[85] noted that the yield strength of a low alloy dual phase steel was raised and yield point elongation (Luders extension) was restored after tempering at 170 °C for one hour, which was attributed to the pinning of mobile dislocations by carbon atoms. While tempering a solution treated tensile specimen of alloy A at 150 °C for one hour had no effect on the hardness of the martensite phase (479 Hv_{30}), it is evident that the yield strength was slightly higher than in the solution treated condition and that the work hardening rate in the region of 0 to 0.5% strain was also higher

(Fig. (5.1)). This is a direct consequence of the pinning of mobile dislocations in the ferrite phase by solute carbon atoms, which causes intermittent dislocation activation at sites randomly spread across the gauge length of the specimen as yielding begins, as opposed to the wide spread, and comparatively simultaneous activation of the mobile dislocations present in the solution treated specimen at the onset of yielding.

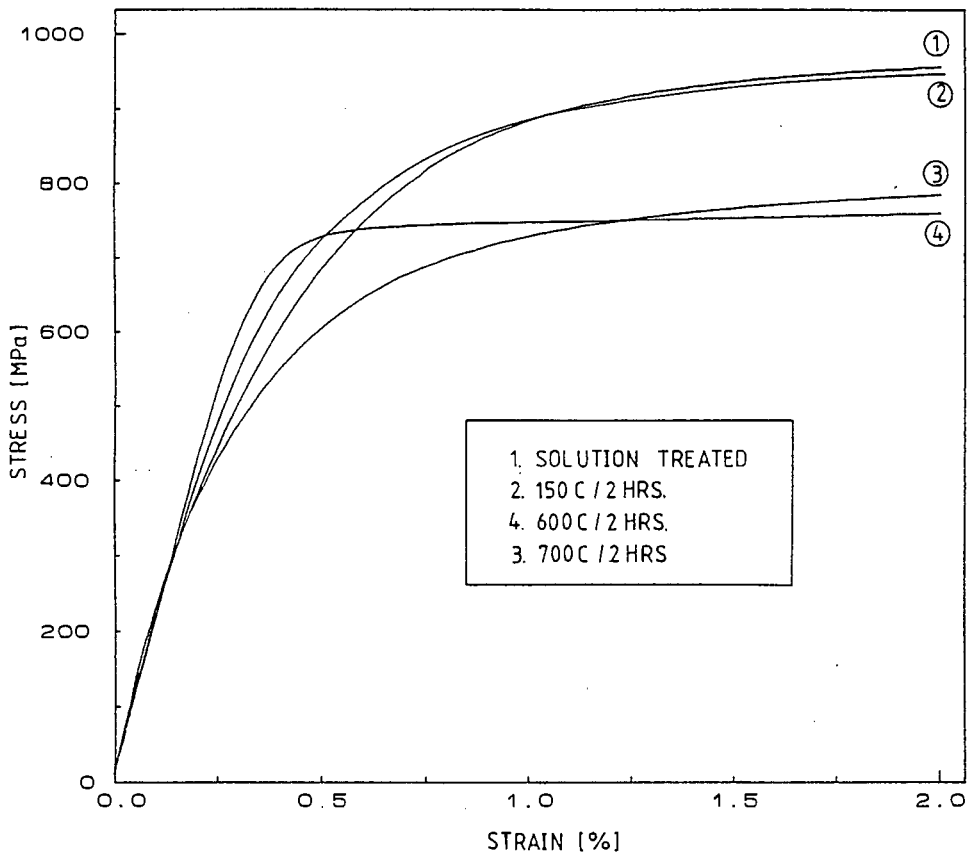

Figure (5.1): Enlargement of a portion of the stress/strain curves of alloy A in Fig. (4.25), illustrating the effect of various heat treatments on the nature of yielding within the alloy.

The strain at which the work hardening rate became equivalent in the solution treated and 150 °C tempered specimens (0.5%) corresponds approximately with the end of the first stage of the three stage deformation found characteristic to low alloy dual phase steels [73,74,75], where deformation in the ferrite phase is constrained by the martensite phase. However, in the early stages of deformation, the higher work hardening rate of AISI 431 (solution treated) and the low work hardening rate of AISI 430 (as received condition) indicate that the continuous yielding characteristics exhibited by dual phase steels can also be attributed to the different work hardening rates of the individual phases.

While the onset of yielding occurred at a similar stress for alloy A in both the solution treated and 700 °C heat treated conditions, the work hardening rate immediately after yielding in the 700 °C heat treated condition was considerably lower than that in the solution treated condition. This can be attributed to the lower martensite content after heat treating at 700 °C , and the high density of mobile dislocation in the inter-lamellar ferrite phase, as noted by Koo and Thomas[26].

The uniform elongation of alloy A in both the solution treated and 700 °C heat treated conditions was low (6%), and the post uniform elongation deformation behavior (the region of necking) in each case was characterized by a rapid drop in stress to the point of fracture (Fig. (4.25)). In view of the improved uniform elongation in the 600 °C tempered condition, it is believed that necking and possibly microvoid initiation begins in the martensite phase in the solution treated condition, or in the lamellar composite phase in the 700 °C heat treated condition, in the proximity of 6% strain.

In the solution treated condition this probably results from the rapid build up of stress in the martensite phase as a result of stress relaxation in the ferrite phase. The ductility of martensite is generally low due to it's highly dislocated morphology, and in view of the high martensite content of alloy A, a low uniform elongation is expected. While it is believed that the lamellar composite phase formed after annealing at 700 °C does have fairly good ductility, the inhomogeneous strain distribution within the composite phase as a result of transfer of the load from the ductile inter-lamellar ferrite to the harder martensite lamellae may result in yielding and possibly fracture within the phase at a low strain (±6% strain). In the 600 °C tempered condition the deformation between the martensite and δ-ferrite phases is more homogeneous, and the tempered martensite phase is more ductile, than in the solution treated or 700 °C heat treated conditions. This accounts for the higher uniform elongation and lower rate at which stress drops after necking in the 600 °C tempered condition.

Fractographic analysis of test specimens of alloy A in the solution treated condition revealed that microvoid initiation (other than around inclusions) occurred in the martensite phase or at ferrite/martensite grain boundaries. Tomota et al[25] noted that as the hardness of the martensite phase of a low alloy steel decreased, the mechanism of microvoid initiation changed from interfacial decohesion to fracture within the martensite phase. Since alloy A in the solution treated condition contains hard, but fairly ductile martensite, one could expect both mechanisms to operate. However inclusions were most

commonly observed in the ferrite phase or at ferrite martensite grain boundaries, and considering the high martensite content of alloy A (71 %), the most common non inclusion related microvoid initiation mechanism would most likely be fracture within the martensite phase.

Fractographic analysis revealed that the high impact resistance of alloy A after soaking at 700 °C for two hours is a consequence of the good crack blunting properties of the lamellar composite phase. The resistance of the lamellar composite phase to crack propagation is a consequence of both the crack blunting ability of the nickel toughened lamellar martensite phase, and the good toughness of the inter-lamellar ferrite (tempered martensite) phase. The latter is supported by the higher toughness of alloy A in the 600 °C tempered condition than in the solution treated condition. As was noted from the analysis of surface deformation markings on the gauge length of alloy A after thermomechanical treatment, fracture is commonly initiated in the lamellar colonies. The passage of cracks thus initiated in the lamellar phase and around inclusions is continually blunted by successive lamellar composite grains. This effect was reflected in the highly deviated nature of cleavage cracks passing through the lamellar composite phase when brittle fractured at -72 °C.

The absence of cleavage cracks in the ferrite phase in any of the heat treated conditions (after mechanical testing at room temperature) suggests that the ferrite phase also has an inherent toughness as a consequence of the low interstitial content. However, in each of the three heat treated conditions the toughness of the δ-ferrite phase is expected to be lower than the martensite phase (or it's transformation products) as a consequence of the sensitivity of the δ-ferrite to a high chromium content[2]. The good impact resistance of alloy A in the 600 °C tempered condition is then mostly a consequence of the high toughness of the tempered martensite phase.

In view of it's low interstitial, high nickel content, the mechanical properties of alloy A, in every sense except ductility, were superior to those of AISI 430 in any of the heat treated conditions in which it was tested. In particular the high impact resistance of alloy A in the solution treated condition, compared to that of AISI 430 in the same condition, suggests that the alloy has sufficient weldability to prevent the need for a post weld heat treatment. While the strength of alloy A is somewhat lower than that of AISI 431 in the solution treated condition, suggesting that thicker sections would be required of the alloy in order to replace 431 in high tensile applications, its impact resistance is also far superior to that exhibited by 431 in any heat treated condition in which it was tested. As a consequence of

its austenitic microstructure, AISI 304 exhibited an impact resistance far superior to that of alloy A, but it's tensile strength, and in particular it's .2% yield strength, is considerably lower. In view of it's higher tensile and yield strengths, although mediocre but sufficient impact resistance, and the savings in cost associated with the lower nickel content alloy A would suit as a substitute for AISI 304 in situations where the environment is not excessively corrosive. Alloy A thus has the potential as a middle of the range 16% chromium stainless steel which may be used as a general substitute for the standard grades previously mentioned. However the cost of such a steel, although lower than AISI 304, would be higher than both AISI 430 and 431 in view of it's higher nickel content, and it is debatable whether the improvement in properties would justify the increase in cost.

5.2 NITROGEN ALLOYED STEELS

5.2.1 ALLOY C

From the comparatively small variation in microhardness of the ferrite phase with tempering temperature, it is apparent that the variation in hardness of the alloy with heat treatment is attributed primarily to the reactions occurring in the martensite phase. This is expected in view of the partitioning of carbon and nitrogen to the austenite during the solution treatment. The transformations occurring during heat treatment between 500 and 900 °C were more or less complete within an hour, which is a consequence of the rapid diffusion of interstitial alloying elements. The constraints on the diffusion of carbon and nitrogen are considerably lower than those experienced by substitutional alloying elements, and thus the inter critical temperature range of alloy C (as determined by dilatometry) is narrow (less than 70 °C). However, there is some doubt as to the exact point of the A_{c3} temperature, since the austenite reversion appears complete by 900 °C (as indicated by hardness measurements and in the dilatometry trace, Fig. (4.7)), but carbon and nitrogen based grain boundary precipitates only dissolve in the temperature range 900 - 1000 °C. This suggests that the austenite reversion is completed in the vicinity of 900 °C, and that further dissolution of precipitates between 900 and 1000 °C results in an increase in the concentration of carbon and nitrogen in the austenite.

While Tizziani et al[45] noted that nitride (Cr_2N) precipitates are clearly visible in the δ-ferrite phase of a type 410 stainless steel (using scanning electron microscopy) after

tempering at 600 °C for one hour, these precipitates were only vaguely visible on polished and etched surfaces of alloy C (using SEM techniques) after prolonged heating (3 hours) at 600 °C. The observation of very fine nitride precipitates (sub micron) in the regions of ferrite grains surrounding ferrite/martensite grain boundaries using TEM analysis of specimens heat treated at 600 °C for one hour implies that the precipitates nucleate in the early stages of heat treatment, before the high dislocation density in this region is affected by the heat treatment, and that the growth of nitrides at 600 °C in 16 % Cr alloys is very slow. Also of interest is the observation of a high concentration of spherical precipitates in the ferrite grains of alloy C after heat treating at 800 °C. Since no precipitates were noted in the δ-ferrite grains of a type 410 stainless steel[45] after heat treating at 820 °C, it is likely that the temperature range for of stability of the nitride precipitates in a 16 % Cr alloy is higher than for a 12% Cr alloy. The fine spherical nature of the precipitates in alloy C suggests that the acicular nitride precipitates observed after tempering at 700 °C, which were determined from TEM analysis to consist of only five or six layers of atoms, are limited in size due to their high surface energy, the surface energy being lowered by forming spherical, incoherent precipitates. Bywater and Dyson[48] determined that nitride precipitates grow in planes which offer the least inter atomic distance mismatch, which also suggests that size of the precipitates is limited.

In view of the high nitrogen content of alloy C, it is believed that the grain boundary precipitates formed at 600 °C, and those within the tempered martensite phase, conform to the $M_{23}(CN)_6$ structure. While Tizziani et al[45] did not note the presence of nitrogen in the precipitates formed on δ-ferrite/martensite grain boundaries after tempering a type 410 stainless steel at 600 °C, the nitrogen content of the alloy was very low. The small effect that heat treating had on the chromium content of the δ-ferrite phase of alloy C may be a consequence of the large amount of chromium nitride precipitates formed in the phase after tempering at 700 °C or above. The actual chromium content of the phase is probably somewhat less than that measured by EDS due to the high chromium content of the grain boundary $M_{23}(CN)_6$ precipitates, as noted by Lee et al[51] after heat treating AISI 430 at 760 °C.

Isothermal heat treatment of alloy C at 700 °C revealed that grain boundary precipitation occurs rapidly (clearly visible after 4 minutes), and that while chromium nitride (Cr_2N) precipitates nucleate on dislocations within the first few minutes at 700 °C, as suggested by the first evidence of these precipitates in the regions adjacent to ferrite/martensite grain boundaries, their growth is somewhat slower than the grain boundary precipitates.

Secondary hardening, observed after two minutes at 700 °C, can be attributed to ultra fine precipitation on dislocations in the martensite phase, and is most probably similar in nature to the phenomenon of 475 °C embrittlement noted in martensitic stainless steels[10,55]. It is unclear whether the secondary hardening in the martensite phase of alloy C is a consequence of Cr_2N or $M_{23}(CN)_6$ precipitation, or an intermediate phase such as Cr_7C_3[56], but it has been reported that Cr_2N precipitation is the cause of secondary hardening in low alloyed, high nitrogen 12% Cr steels[44]. The fairly large drop in hardness in the 10 minute period following secondary hardening is attributed to the growth (Ostwald Ripening) of precipitates in the martensite phase.

5.2.1.1 DILATOMETRIC ANALYSIS: COMPARISON OF ALLOYS A AND C

There are several notable differences between the dilatometry traces of alloys A and C (Figs (4.1) and (4.7)), apart from the differences in their Ac_1 and Ac_3 temperatures. Firstly, the austenite reversion in alloy C is characterized by a much smaller and less defined decrease in the expansion rate than exhibited by Alloy A. This is possibly a consequence of the lower martensite content of alloy C, and the island morphology of the martensite phase. The ferrite matrix surrounding the martensite islands most likely constrains the volume decrease accompanying the austenite reversion. Secondly, in the region of 730 °C (marked in Fig (4.7)) alloy C exhibits an inflection towards a higher expansion rate. While no literature has been found relating to the presence of this inflection point in 17% Cr stainless steels, a similar effect, although somewhat less defined and at a considerably lower temperature, was noted in an Fe-N martensitic steel[86]. The effect was attributed to the transition of α" nitride ($Fe_{16}N_2$, in the tempering reaction $\alpha' \rightarrow \alpha'' + \alpha$) from a state of coherency to a state of incoherency. The inflection at 730 °C in alloy C could thus be attributed to the onset of the transformation of the coherent acicular Cr_2N precipitates (observed at 700 °C) to incoherent spherical precipitates at 800 °C. Since the Cr_2N precipitates grow with a minimum inter atomic mismatch criteria (between the matrix and precipitate), the formation of incoherent globular precipitates would cause an increase in volume.

5.2.1.2 MECHANICAL PROPERTIES AND DEFORMATION CHARACTERISTICS

The decreases in hardness accompanying tempering at 600 and 700 °C accounts for the decrease in 0.2% yield strengths and tensile strengths with increasing tempering

temperature. However the actual yield point, where deviation from elasticity begins, is much lower in the solution treated condition than in either of the tempered conditions, and the yield point becomes more clearly defined as the tempering temperature increases. This is a consequence of the decrease in the difference in hardness between the tempered martensite and δ-ferrite phases after tempering at 600 and 700 °C. The stress at which yielding was first noted in alloy C in the solution treated condition (± 220 Mpa) is considerably lower than the stress at which yielding occurred, in the form of Luders extension, in AISI 430 (295 MPa, after thermomechanical processing, section (4.4)), which supports the theory that mobile dislocations are the cause of the low yield strength of dual phase steels.

Also related to the phase constitution of the alloys was the substantially higher uniform elongation exhibited by alloy C in the solution treated condition than alloy A in the same condition. This is a consequence of the greater ease of plastic flow in the larger ferrite grains of alloy C, which is less constrained by the island nature of the martensite phase than the inter-connected nature of the martensite in Alloy A. It is also related to the lower ductility, and higher hardness of the martensite phase of alloy C as a consequence of the high interstitial content. This is reflected in the small amount of post uniform elongation deformation prior to fracture in alloy C, and in the observation of brittle fracture within the martensite phase as a prominent mode of fracture initiation, along with a small amount of inter granular fracture. These two mechanisms of microvoid initiation have been observed to commonly occur in dual phase steels[80,78,25], but considering the high hardness of the martensite phase, the main mode of fracture initiation by fracture within the martensite phase is contrary to the findings of Tomota et al[25]. This, however, is a possible consequence of the higher martensite content of alloy C than the alloys in their investigation. Cleavage cracks in the ferrite phase of alloy C in the solution treated condition are initiated by fracture within the martensite phase, which provides sharp crack initiation points, and to a lesser extent by interfacial tearing at ferrite/ martensite grain boundaries.

While tempering of alloy C reduced the hardness of the martensite phase, it also decreased the constraint on plastic deformation in both the ferrite and tempered martensite phases. This is illustrated by comparing Figs. (5.2a) and (5.2b). In the solution treated condition (Fig. (5.2a)), while fairly dense slip markings are observed in the ferrite grains where the crystallographic orientation of the ferrite and positioning of the surrounding martensite are favorable, the deformation is generally confined to certain regions within the ferrite grains,

and the slip lines appear more planar and less wavy than those observed in the ferrite grains after tempering at 700 °C (Fig. (5.2b)). This is similar to the observations made by Kunio et al[25] and Shen et al[77] on the effects of increasing the contiguity of the martensite phase on plastic deformation within the ferrite phase, and is in accordance with the observation by Tomota[79] that a more planar slip mode in the ferrite phase of dual phase steels is a consequence of the poor operation of plastic relaxation mechanisms in the ferrite phase as a result of the constraint applied by the martensite phase. However in the region of the fracture surfaces more intense deformation was noted in the ferrite grains than that indicated in Fig. (5.2a). As the stress in the phase increases due to the constraint on plastic relaxation applied by the martensite phase, less favorable slip systems may be activated in the regions where the major slip systems are prevented from operating. Fracture of martensite islands also increases the amount of deformation observed in ferrite grains.

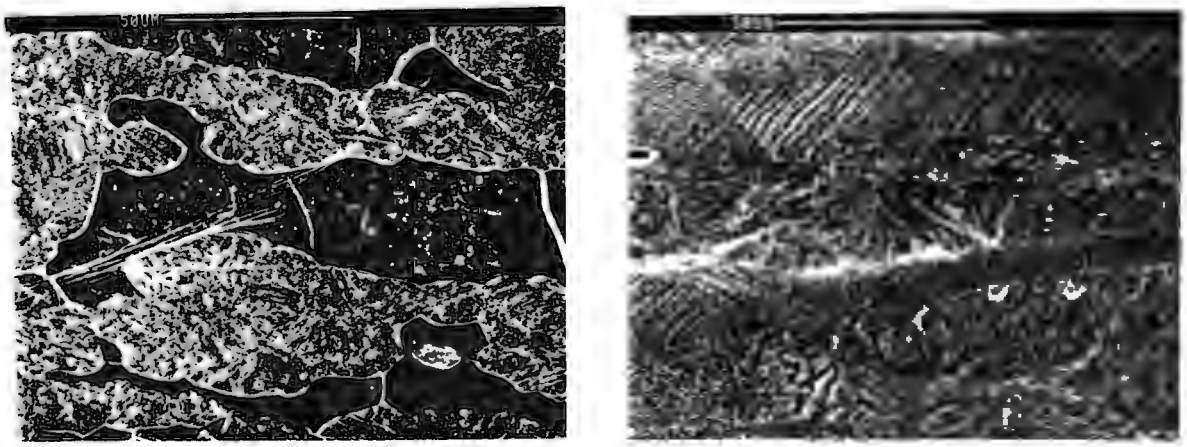

(a) (b)

Figure (5.2): The appearance of slip markings in the ferrite phase of Alloy C on the gauge lengths of tensile specimens in (a) the solution treated condition (6% strain), and (b) after tempering at 700 °C for two hours (11% strain).

The ductility and impact resistance of alloy C was improved by tempering at 600 and 700 °C, although the alloy exhibited a high susceptibility to intergranular rupture. This occurred primarily between the δ-ferrite and tempered martensite phases, and is a consequence of carbonitride $M_{23}(CN)_6$ precipitation[65,66]. These precipitates, combined with the marked directionality of the micro structure due to rolling, accounts for the high susceptibility of the alloy to lateral cracking after tempering. While the effect of the nitride precipitates on the toughness of the alloy was inconclusive, due to the fine nature of the precipitates, the presence of regions of ultra fine microvoid formations on impact fracture surfaces suggest that the acicular nitride precipitates may have an adverse effect on the toughness of the alloy, as noted by Grubb and Wright[65] in a 26% Cr ferritic

stainless steel. However the ferrite phase of alloy C probably has a low inherent toughness as a consequence of the high chromium content[2], and this is reflected in the numerous instances observed of blunting of sub surface cracks propagating through the ferrite phase by tempered martensite grains. The high toughness of the tempered martensite phase stems from its fine sub-cell microstructure. The lower toughness observed in the 600 °C tempered condition than in the 700 °C tempered condition is a consequence of the marginally higher susceptibility to inter granular fracture in the 600 #C, and of the finer nature of precipitates in the ferrite and martensite phases which provide more resistance to dislocation motion.

The combination of tensile strength and toughness exhibited by alloy C in both the 600 and 700 °C tempered conditions is superior to that of AISI 430 in any heat treated condition it was tested. This is a consequence of the nitrogen alloyed dual phase microstructure of alloy C. However the dual phase microstructure does not reduce the sensitivity of the alloy to the detrimental effects of interstitial alloying elements in solution, as is reflected in the poor impact resistance in the solution treated condition. Thus the superior properties that are achieved by tempering the nitrogen alloyed steel would be destroyed by welding. The impact resistance of alloy C in the 600 and 700 °C tempered conditions is similar to, if marginally better than, that exhibited by AISI 431 in each of the heat treated conditions in which it was tested. In particular, alloy C in the 600 °C tempered condition provides an attractive alternative to AISI 431 in the as received condition in view of it's lower nickel content, similar tensile strength and superior impact resistance. However, AISI 431 is most commonly used in the hardened (and stress relieved) condition for high tensile applications where impact resistance is of secondary importance. While alloy C has a significantly lower hardenability than AISI 431 as a consequence of it's lower nickel and interstitial content, it also has a higher susceptibility to cleavage fracture than AISI 431, as is reflected in the appearance of their respective tensile fracture surfaces in the solution treated condition. When the above factors are taken into consideration, it appears that although nitrogen alloyed dual phase steels can provide mechanical properties comparable to, and in some cases superior to, standard stainless steels of a similar grade (ie AISI 431 and 430), the low weldability of alloy C reduces the credibility of the alloy as a commercially viable competitor to the well established standard grades.

5.2.2 ALLOY D

The (C + N) level in Alloy D is approximately 60 % of that contained in alloy C, and this manifests itself in a significantly lower martensite content and a larger ferrite grain size for alloy D. While the response of alloy D to heat treatment is very similar to that of alloy C, the extent of grain boundary precipitation in alloy D after tempering at 600 °C for one or three hours, and the extent of Cr_2N precipitation within the δ-ferrite phase after tempering at 700 °C, is lower than that observed in alloy C after the same heat treatments. The lower grain boundary precipitation is possibly a consequence of the significantly lower carbon content of alloy D (.032 wt.%) than alloy C (0.05 wt.%), and is supported by the observation of considerably more advanced grain boundary precipitation in AISI 430 after tempering at 600 °C than that observed in either alloy C or alloy D due to the higher carbon content (0.065 wt%) and low nitrogen content in AISI 430 . The rate of precipitation of carbide precipitates ($M_{23}C_6$) at 600 °C is thus believed to be higher than that of nitrogen rich precipitates ($M_{23}(CN)_6$), which is in accordance with the findings of Tizziani et al[45] in 12% Cr stainless steels. More generally, carbon rich ($M_{23}C_6$) precipitates appear to form at a lower temperature than precipitates rich in nitrogen, and this is supported by the observation of spherical precipitates in the δ-ferrite phase of AISI 430 after tempering at 700 °C, while similar precipitates are evident in alloy C only after tempering at 800 °C.

Analysis of Fe-Cr-N phase diagrams reveals that the nitrogen content of the ferrite and martensite phases of 16 wt% Cr stainless steels is unaffected by variations in the total nitrogen content dissolved in the alloy. However, lowering the chromium content of the δ-ferrite phase lowers the solubility of nitrogen[46]. In view of the 1 wt.% difference in the chromium contents, as determined by EDS analysis, of the δ-ferrite phase in alloys C and D (in the solution treated conditions), the lower observed nitride concentration in the ferrite in alloy D than in alloy C after tempering at 700 °C may be a consequence of the initially lower amount of nitrogen dissolved in the phase.

The dilatometry trace for alloy D was very similar to that of alloy C, exhibiting the same inflection towards a higher expansion rate at approximately 740 °C, and a similarly small decrease in expansion rate representing the onset of austenite formation, which is a consequence of the low martensite content of the alloy. It is interesting that the inter-critical temperature range of alloy D is comparable to that of alloy C. Since the formation of austenite is most likely controlled by the dissolution of precipitates, this is expected since

the tempered martensite in both alloys C and D contain precipitates of similar composition.

5.2.2.1 MECHANICAL PROPERTIES AND DEFORMATION CHARACTERISTICS

In the solution treated condition, the stress at which yielding begins in alloy D (100 MPa, Fig. (5.3)) is substantially lower than that observed in alloy C (approximately 240 MPa). This is a consequence of the finer island type martensite and lower martensite content of the alloy D. As the martensite content decreases, the load bearing capacity of the phase decreases, and the portion of the load carried by the ferrite phase is higher. This results in the motion of dislocations, which are introduced into the ferrite phase as a consequence of the martensitic transformation, at a lower stress. As was characteristic to alloy C, tempering of alloy D at 600 °C and 700 °C results in more abrupt yielding than in the solution treated condition (Fig. (5.3)). This is a consequence of the more homogeneous deformation within the alloy as the difference in hardness between the tempered martensite and ferrite phases decreases. However, as was also noted in alloy C, the alloy did not exhibit yield point elongation in either the 600 or 700 °C tempered condition. This suggests that even though the alloy contains only 38 % tempered martensite in the 700 °C tempered condition, this quantity is above the critical amount, and the hardness difference between this phase and the δ-ferrite phase is still above the critical difference, required to prevent yield point elongation (Luders extension)[70].

In the solution treated condition the post-yielding tensile deformation characteristics of alloy D were similar to those exhibited by alloy C, although at a somewhat lower stress. While deformation in the δ-ferrite phase appeared less constrained than in alloy C, as indicated in more intense surface deformation markings in the vicinity of the fracture surface and its marginally higher total elongation, the mechanisms of deformation and fracture initiation in both the alloys are comparable. Fracture appears to be initiated by fracture within the martensite phase and by interfacial tearing, and this leads to cleavage fracture of the surrounding ferrite, which is notch sensitive due to the interstitial alloying elements trapped in solution[29,32].

While the good impact resistance of both alloys C and D in the 700 °C tempered condition can be attributed to the high resistance of the tempered martensite phases to cracks propagating through the δ-ferrite phase, the substantially higher impact resistance, in the

700 °C tempered condition, of alloy D compared to alloy C can be attributed to two microstructural differences. Firstly, the lower nitrogen content of alloy D results in a lower density of nitride precipitates in the ferrite phase, and thus a lower susceptibility to the adverse affects of nitride precipitation. This is reflected in the more feathery appearance of fractured impact specimens of alloy D, and the relative absence of the fine ductile dimple features observed on fractured impact specimens of alloy C, which are possibly associated with the high density of Cr_2N precipitates in the δ-ferrite phase of alloy C. Also related to the interstitial content is the higher carbon content of alloy C, which, in view of the comparatively low impact resistance of AISI 430 in the 700 °C tempered condition, appears to have a more adverse affect on impact resistance than nitrogen.

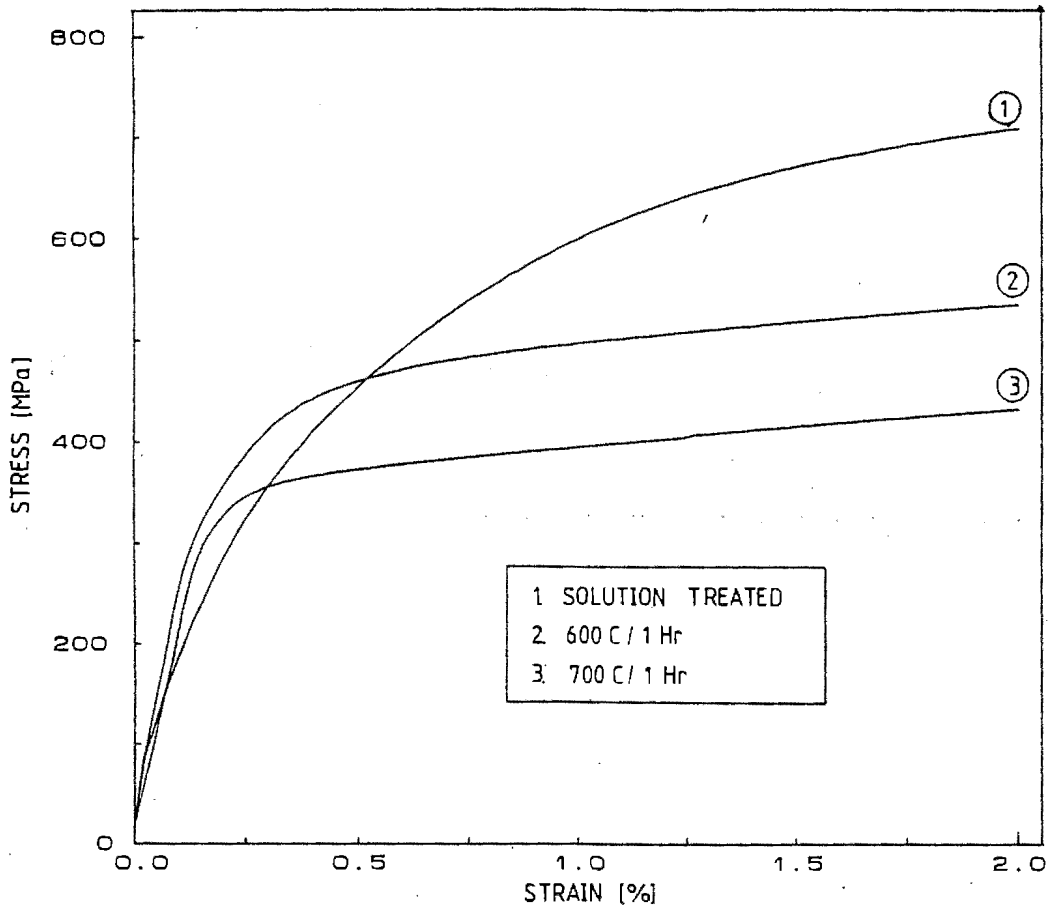

Figure (5.3): Enlargement of a portion of the stress strain curve of alloy D in Fig. (4.34), indicating the effect of heat treatment on the yield characteristics of the alloy.

Secondly, the smaller δ-ferrite/martensite grain boundary surface area (per martensite island) associated with the finer martensite grains in alloy D, and the narrow, elongated nature of these grains in the direction of rolling (perpendicular to the test direction),

results in interfacial decohesion being a less significant mode of crack propagation than in alloy C. This was evident from the analysis of cross sections of fractured charpy specimens. Comparison of the appearance of fractured tensile specimens of AISI 430 and alloy D in the 600 °C tempered condition revealed that a high carbon content causes a higher susceptibility to intergranular fracture than a high nitrogen content. The higher carbon content of alloy C than alloy D may thus contribute to the higher susceptibility of alloy C to intergranular fracture, and thus the lower impact resistance, in the 700 °C tempered condition, of alloy C than alloy D. Thus the higher interstitial content of alloy C is more detramental to the impact resistance than the larger δ-ferrite grain size of alloy D. However, as is common to dual phase steels[13,66], impact specimens of alloy D did exhibit a marked susceptibility to lateral cracking.

While the differences in toughness and ductility between AISI 430 and alloy D have been so far attributed to the more detrimental effects of carbon rich grain boundary precipitates than nitrogen rich grain boundary precipitates, the higher toughness of alloy D in both the 600 and 700 °C tempered conditions may also be attributed to the banded nature of the martensite phase. AISI 430 was received as a softened, primarily single phase material, and the dual phase ferrite/martensite structure was obtained by heating in the dual phase temperature range. The martensite appeared as somewhat equiaxed grains, although arranged in bands in the direction of rolling. These equiaxed grains, as opposed to the elongated grains of alloy D, provide less resistance to cracks propagating in a direction perpendicular to the tensile axis.

In the 700 °C tempered condition alloy D has a toughness which is far superior to that of either AISI 430 or 431 in any of the heat treated conditions in which they were tested. However the alloy suffers from a poor impact resistance in the solution treated condition, as was noted for alloy C. The low weldability of the alloy associated with this poor impact resistance, and the comparatively low tensile strengths of alloy D in the 700 °C tempered condition (which is comparable to that of AISI 430), somewhat mask the attractive impact resistance exhibited by the alloy. While alloy D provides an attractive alternative to AISI 430, which similarly suffers from a low weldability, it would not suit for the high tensile applications in which AISI 431 is commonly used. Thus if alloy D is to be judged entirely by it's impact resistance in the 700 °C tempered condition, there appears to be potential for it's development, but the poor weldability and low tensile strength would limit the scope of it's applications.

5.2.3 ALLOY E

Although alloy E has the highest martensite content of the four experimental alloys, the composition of the alloy can be considered a compromise between that of alloy A and that of alloy C. While containing 1 wt.% nickel in solution, the alloy exhibits a large variation in hardness with heat treatment between 500 and 900 °C, which is a consequence of the high nitrogen content. However, in the 600 and 700 °C tempered conditions, grain boundary and interlath precipitation is somewhat finer than that observed in alloy C. This is a consequence of the lower carbon content of alloy E (0.026 wt.%) than alloy C, and the slower rate at which nitrogen rich precipitates ($M_{23}(CN)_6$) are formed than carbon rich precipitates ($M_{23}C_6$) during tempering at 600 and 700 °C, as was noted in the comparison of alloy C and AISI 430.

The austenite reversion in alloy E manifests itself as two clearly definable inflection points on the dilatometry trace (Fig. (4.20)), as opposed to the considerably less obvious inflection point exhibited by alloys C and D. As was noted in the comparison of the dilatometry traces of alloys A and C, this is a consequence of the higher martensite content of alloy E, and the inter-connected nature of the martensite phase in alloy E as opposed to the island type martensite morphology in alloys C and D. The inter-critical temperature range of alloy E is intermediate between that of alloy C and alloy A, and this is a consequence of the composition of alloy E being intermediate between that of alloys A and C. However the onset of the austenite reversion (A_{c1} temp.) in alloy E is more clearly defined than in alloy A, and this is a consequence of the higher temperature at which the transformation begins in alloy E, and the more rapid rate of diffusion of nitrogen compared to nickel between the newly forming austenite and tempered martensite phases. A slower heating rate would produce a more clearly defined A_{c1} temperature in alloy A.

5.2.3.1 MECHANICAL PROPERTIES AND DEFORMATION CHARACTERISTICS

In the solution treated condition, the significantly lower ferrite content of alloy E, and the isolated nature of the fine ferrite grains, results in the onset of yielding (deviation from elasticity) at a higher stress during tensile testing (±400 MPa, Fig. (5.5)) than that observed in alloys C or D. The alloy behaves as a fundamentally single phase martensitic alloy, and this is reflected in its low uniform elongation (3.5 %) and very high work hardening rate in the first 0.5% deformation, similar to that exhibited by AISI 431 in the solution treated condition. It is interesting to note from Fig. (5.4) that tempering at 600 to 700 °C

successively increased the Youngs Modulus over that observed in the solution treated condition. While the increase is rather small, as is expected from the small change in the lattice constant in the BCT to BCC transformation, the effect is reproducible and has been acknowledged to occur in steels[87], although its effect on the elastic properties of steels is regarded as negligible. However slight the change in modulus may be, it suggests that the different elastic behavior of martensite and ferrite results in partitioning of stresses between the two phases during elastic loading of dual phase steels. More precisely, the higher Youngs modulus of the ferrite phase results in partitioning of stress to that phase. This, in conjunction with the mobile dislocation theory[26,30,77], would then further justify the low elastic limits exhibited by alloys C and D.

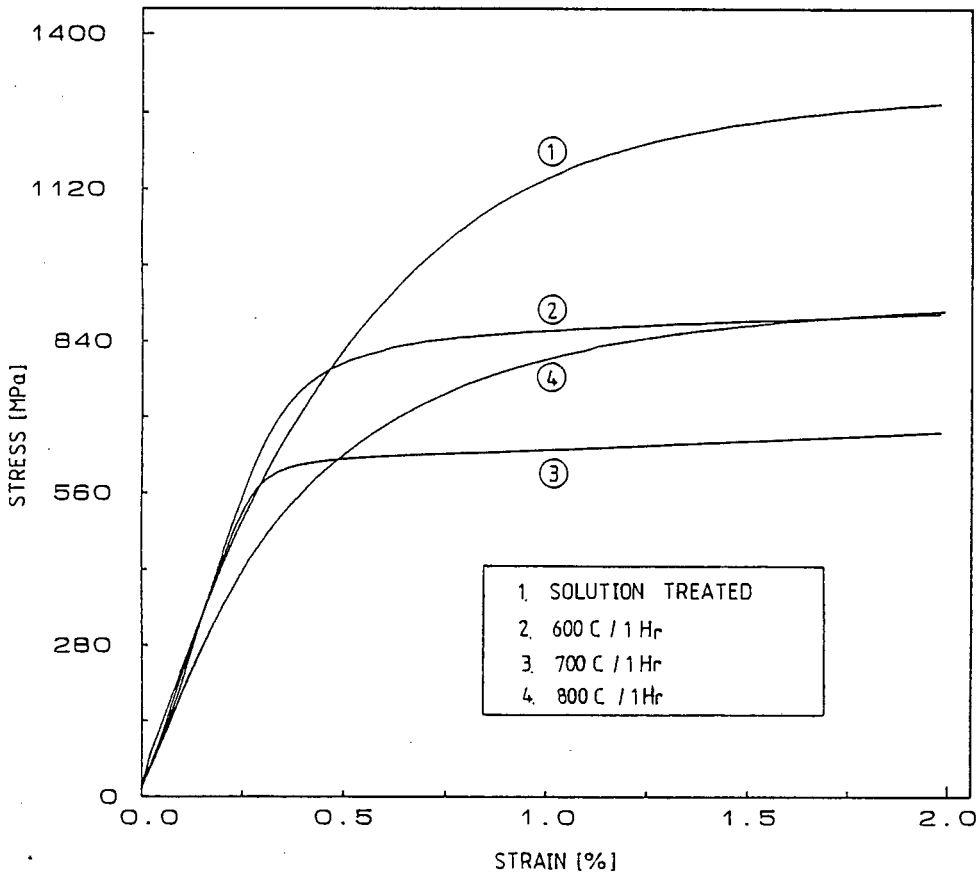

Figure (5.4): Enlargement of a portion of the stress strain diagram for alloy E (Fig. (4.39)), indicating the effect of heat treatment on the nature of yielding in the alloy.

Comparing the impact resistance of alloys C, D and E in the 700 °C tempered conditions reveals that there is not a simple relationship between the toughness of tempered dual phase steels and the volume fraction of tempered martensite. The higher impact resistance of alloy E than alloy C in the 700 °C tempered conditions is related to the higher δ-ferrite content of alloy C, which has a lower toughness than the tempered martensite phase and

which also results in a higher δ-ferrite/martensite grain boundary surface area, these regions being common sites for microvoid initiation. A similar observation was made in the comparison of alloys C and D, where D has a low martensite content and therefore a low δ-ferrite/tempered martensite grain boundary surface area. It appears that the toughness of 16 % Cr dual phase stainless steels in the 700 °C tempered conditions is affected by the amount of δ-ferrite/tempered martensite grain boundary surface area. In alloys with a low ferrite/martensite grain boundary surface area, such as alloys D and E, decohesion at inclusion-matrix interfaces is the most common mode of microvoid formation.

The advantages of a lamellar dual phase structure, as described by Koo and Thomas[26] for a low alloy dual phase steel, are apparent in the combination of a low yield strength (Fig. (5.4)), intermediate tensile strength and high uniform and total elongation (Fig. (4.39)) exhibited by alloy E after intercritical annealing at 800 °C. This is a consequence of the presence of hard, strong martensite of low ductility in a soft, ductile ferrite matrix. While this allows for significant composite strengthening[81], deformation occurs with greater ease in the lamellar composite phase than in an entirely martensitic structure, which results in a higher ductility. However, while the formation of the lamellar composite phase in alloy A results in the highest recorded impact resistance for the alloy (85 J), the formation of the lamellar structure in alloy E causes a decrease in impact resistance below that observed in the 700 °C tempered condition. In alloy A, the high impact resistance is attributed to the crack blunting effect of the lamellar composite phase which contains 'tough', nickel containing martensite. However, the lamellar martensite component of the composite phase in alloy E has a lower toughness than that in alloy A as a consequence of its lower nickel and higher interstitial content. This results in brittle fracture of the martensite lamellae during impact testing, which has an adverse effect on the toughness of the alloy. However, the lamellar composite phase is essentially a fine grained, dual phase structure, which in itself improves the toughness, and this is reflected in the relatively acceptable level of impact resistance exhibited by alloy E after heat treating at 800 °C (37 J). The improvement in toughness of alloy E after inter-critical annealing at 800 °C over that noted in the 600 °C tempered condition can be attributed to two differences in the modes of fracture. Firstly, alloy E exhibits a marked susceptibility to intergranular fracture in the 600 °C tempered condition. This effect was also noted by Landon et al[49] in a type 422 stainless steel, and was attributed to the detrimental effects of carbide precipitation. This observation is supported by the extremely high susceptibility of AISI 431 in the 600 °C tempered condition to intergranular fracture (far more so than that observed in alloy E), which had a detrimental effect on the impact resistance of the alloy. Secondly, the

continual change in direction (and energy) of cracks propagating through the lamellar composite phase formed after heat treating at 800 °C dissipates a significant amount of energy.

The marked directionality of fine ductile dimples on tensile fracture surfaces, and particularly on the shear lips of impact fracture surfaces, of alloy E after inter critical annealing at 800 °C suggests that fracture is initiated in the lamellar colonies by fracture of the martensite phase. This observation is based on similarities in the appearance of fracture surfaces of alloy E and the pearlite colonies of a ferrite/pearlite steel, as investigated by Cuddy and Bassim[82], and also suggests that fracture initiation in lamellar colonies with a favourable orientation (parallel to the tensile axis) occurs by a similar mechanism (a combination of tensile and shear loading) to that noted for fracture within the pearlite colonies of the ferrite/pearlite alloy (Fig. (2.15)).

The finer scale of the lamellar martensite formed in AISI 431 after inter critical annealing at 700 °C for two hours, than that observed in alloy A after inter-critical annealing at 700 °C and in alloy E after inter-critical annealing at 800 °C, is believed to be a consequence of the closer proximity of the heat treating temperature (700 °C) to its A_{c1} temperature. The substantial improvement in toughness of the AISI 431 in this condition, above that exhibited by alloy E in the 800 °C heat treated condition, is a consequence of both the higher nickel content of the AISI 431 and the finer nature of the lamellar martensite phase. The latter explanation is supported by the observation that the ductility of ferrite/pearlite steels is increased as the pearlite structure is refined[88]. The toughness of AISI 431 in the 700 °C heat treated condition can be regarded as the peak toughness for the alloy, since increasing the heat treating temperature would result in further dissolution of carbide precipitates, and decreasing the heat treating temperature would increase the susceptibility of the alloy to intergranular (cleavage) cracking. In view of the significantly higher impact resistance of alloy E in the 700 °C tempered condition than AISI 431 in the same heat treated condition, it is evident once again that nitrogen is less detrimental to the toughness of 16% Cr alloys than carbon.

Of the high nitrogen experimental alloys, alloy E in the 700 °C tempered condition provides the most attractive combination of tensile strength and toughness. This can be attributed primarily to the superior resistance to crack propagation afforded by the predominantly tempered martensite microstructure, which has the benefit of an intermediate nickel content (which, as noted in alloy A, is beneficial to the toughness of

tempered martensite), and of the strengthening provided by the dispersion of nitrogen based precipitates. In this heat treated condition, alloy E also has a far superior combination of tensile strength and toughness to that exhibited by AISI 430 in any heat treated condition it was tested. While the tensile strength is generally somewhat lower than that of AISI 431, the impact resistance of alloy E in the 700 °C tempered condition is considerably higher than that exhibited by AISI 431 in any heat treated condition in which it was tested. In the 800 °C intercritically annealed condition, alloy E provides a combination of tensile strength and impact resistance on a par with that of AISI 431 in the as received and 700 °C heat treated conditions. However, the hardenability of alloy E is somewhat less than that of AISI 431, and while the impact resistance of the alloy in the solution treated condition is marginally better than that exhibited by the alloys C and D, as a consequence of it's higher nickel content, alloy E would also have a poor weldability. It thus appears that the properties of alloy E can be manipulated, by varying the heat treating temperature, to match and surpass the tensile and impact properties exhibited by both AISI 430 and 431. In view of its lower nickel content than AISI 431, alloy E would also provide a more cost effective alternative. However, as has been noted in the analysis of alloys C and D, the low weldability of E somewhat reduces the viability of such an alloy as a marketable product in competition with the commonly encountered standard alloys of a similar grade.

5.3 STANDARD STAINLESS STEELS: AISI 304, 430 AND 431

While various aspects of the microstructures and mechanical properties of AISI 430 and 431 have been mentioned in the discussion of the nitrogen alloyed steels, a number of additional observations are worthy of mention.

In the as received condition (hot rolled and annealed), AISI 430 had a large grain size (up to 180 μm in length) and thus the impact resistance of the alloy was low (30 J). The improvement in toughness after tempering at 700 °C (which was preceded by a solution treatment at 1000 °C) can be attributed to two factors. Firstly, the presence of tempered martensite in the microstructure provides an effective resistance to cracks propagating through the ferrite grains (as noted in alloys C and D), and secondly the nucleation and growth of austenite from ferrite grain boundaries during the solution treatment effectively reduces the ferrite grain size. As was noted by Harase and Shimisu[72], although using a slightly different heat treating schedule, this heat treatment prevents Luders extension,

which is common to single phase ferritic steels, and it may also improve the cold formability of the alloy.

From the comparison of tensile and impact fracture surfaces of AISI 431 in the 600 °C tempered condition, it is evident that the deleterious effects of carbide precipitation in this heat treated condition are only evident at high strain rates. While the fractured tensile specimens had thick shear lips surrounding the fracture surfaces, which consisted of fine ductile dimple formations, the impact specimens exhibited no lateral contraction and shear lip formation, and the mode of fracture was almost entirely intergranular cleavage cracking. A similar, although less obvious effect was noted for alloy 81 in the 600 °C tempered condition. It is possible that during impact testing the fine distribution of precipitates within the tempered martensite phase impede the motion of dislocations (which have an inherent sensitivity to strain rate as a consequence of the BCC structure), and thus the lowest energy path for the propagating cracks is along precipitate laden prior austenite grain boundaries.

The higher impact resistance measured for the laboratory solution treated AISI 304 specimens, than in the as received condition, is probably due to this heat treatment being more effective regarding dissolution of precipitates compared to what might have been carried out in the original production process.

5.4 DUCTILE TO BRITTLE TRANSITION BEHAVIOR

In view of the low impact resistance of alloys C and E in the solution treated condition, the impact transition temperature was not measured, but it has been noted that in 16 wt.% Cr alloys which contain in excess of .03%(C+N) in solution the impact transition temperature is approximately 150 °C[32]. The deleterious effect of interstitial alloying elements in solution in the martensite phase is also illustrated by alloy E in the 800 °C heat treated condition, where the 40 Joule transition temperature is significantly higher (just above room temperature) than that observed in the 700 °C tempered condition, as a consequence of the partitioning of nitrogen into the growing austenite phase while heat treating at 800 °C. However, as is pointed out in the discussion of alloy E, a measure of impact resistance is provided by the lamellar martensite/secondary ferrite composite phase, and this is reflected in the fine, uneven nature of cleavage facets on the brittle fracture surfaces (observed after testing at room temperature and below) and in the impact resistance of 32

Joules at 0 °C. Thus while alloy E in the 700 °C tempered condition has good impact resistance at low temperatures and a moderate tensile strength, moderate room temperature toughness and a higher tensile strength is produced by heat treating at 800 °C.

In contrast to the high nitrogen steels, alloy A exhibits a transition temperature well below room temperature (-25 °C) in the solution treated condition. The improvement in the impact transition temperature after heat treating at 700 °C is attributed to the good crack blunting properties of the lamellar composite phase, and in particular to the high toughness of the soft inter-lamellar ferrite. An advantage of alloy E over alloy A is that a similarly low impact transition temperature (±-60 °C) can by achieved in alloy E with a shorter heat treating time (1 hour at 700 °C as opposed to two hours), and with less precise temperature control. This is a consequence of the wider sub-critical temperature range of alloy E, which allows a higher tempering temperature and thus a more rapid, and more complete transformation of the martensite phase into a tough subcell structure. However one must keep in mind that the weldability of alloy A would be superior to that of alloy E, as is reflected in the difference in their respective impact resistance in the solution treated condition.

The lower transition temperature of alloy E than alloy C, in the 700 °C tempered conditions, is a consequence of the difference in the phase constitutions of the two alloys. While the island type martensite of alloy C reduces the room temperature toughness as a consequence of the susceptibility to intergranular fracture (along δ-ferrite/ martensite boundaries), the higher δ-ferrite content raises the impact transition temperature as a consequence of its susceptibility to cleavage fracture. This was reflected in the increased evidence of cleavage fracture as the test temperature was lowered. It is however unclear whether the higher nickel content of alloy E (1 wt.%) than alloy C (.5 wt.%) has any influence on the toughness or transition temperature, since the 40 J transition temperature of alloy E in the 700 °C tempered condition is similar to that of alloy A after the same heat treatment, even though alloy A has a higher nickel content than alloy E and a low interstitial content.

While the nitrogen alloyed steels, AISI 430 and AISI 431 exhibited low room temperature toughness in the solution treated conditions, indicating poor weldability, it appears that the nitrogen alloyed steels in the 700 °C tempered condition are more suited to low temperature applications than the two standard alloys in the as received condition, both of which had a room temperature impact resistance of approximately 40 Joules. This is a

consequence of three factors; the grain refining effect associated with dual phase microstructures, the high toughness associated with the tempered martensite, and the superior toughness associated with tempered martensite containing a high nitrogen, low carbon content than vice versa. However, alloy A is superior to both the nitrogen alloyed steels and the standard alloys in terms of its low 40 Joule transition temperatures in the solution treated and 700 °C tempered conditions.

5.5 THERMOMECHANICALLY TREATED ALLOYS

The intention of the thermomechanical treatments performed on AISI 430 and 431 was to produce fine grained microstructures which are truly representative of the ferritic and martensitic grades of stainless steel. This was achieved with 430, although the lengthy heat treatment at 1040 °C required to dissolve the carbide precipitates formed during hot rolling of AISI 431 resulted in a significantly larger grain size.

The tensile deformation curves of AISI 431 and 430 clearly reflected the low ductility and high strength associated with martensitic steels, and the high ductility, low strength and yield point elongation associated with a fully ferritic microstructure. In the 700 °C tempered condition, the fine lamellar dual phase structure of AISI 431 provided a compromise of the properties (tensile strength and ductility) associated with a single phase ferritic and a single phase martensitic microstructure.

The small difference in grain size of either the ferrite or martensite phases of alloy A before and after the laboratory rolling procedure is a consequence of the lengthy anneal required at 1000 °C to achieve full recrystallisation of the microstructure in view of the rather slow diffusion of Cr and Ni which partition between the δ-ferrite and martensite phases[13]. However both the ferrite and martensite phases had a more equiaxed structure than that observed prior to the laboratory rolling procedure, and the ferrite grains were partially of fully isolated from one another as opposed to the elongated bands observed before the thermomechanical treatment. In effect the contiguity of the martensite phase was increased. As was noted by Kunio et al[24], an increase in contiguity of the martensite phase increases the constraint on deformation in the δ-ferrite phase, and reduces the extent of deformation bridging between adjacent ferrite grains. Observation of surface deformation markings revealed that this was the cause of the low ductility exhibited by

alloy A. While slip initiated in δ-ferrite grains of alloy A, in both the solution treated and 700 °C heat treated conditions, the onset of deformation in the martensite or lamellar composite phase occurred at a low strain, and was shortly followed by necking in those regions. This can be attributed to the high volume fraction and contiguity of the martensite phase (or lamellar composite phase), which constrains the δ-ferrite phase from deforming and thus the martensite phase is forced to deform. Comparison of the tensile deformation curves of AISI 430 and 431 (after the thermomechanical treatments) reveals that martensite has a much higher work hardening rate in the early stages of deformation (0,5 - 3% strain) and a considerably lower ductility than ferrite. The ductility of the martensite phase (or lamellar composite phase) in alloy A is thus exceeded and the fracture strain of the phase is reached in the early stages of deformation, which leads to microvoid formation and eventual fracture.

The equiaxed nature of the martensite grains in the solution treated condition can increase stress concentrations in that phase. This is reflected in the observation of relatively little plastic deformation of the martensite phase in the regions bridging sites of necking microvoid formation. The higher ductility exhibited by the alloy prior to the laboratory rolling schedule is thus a consequence of the less constrained deformation in the elongated ferrite grains and the lower susceptibility of the elongated martensite grains to stress concentrations. While the process of tensile deformation and fracture in the 700 °C heat treated condition is generally the same as that in the solution treated condition, the details are more complex in view of the lamellar structure formed in the original martensite phase. The mechanism of fracture initiation within the lamellar composite phase is dependent on the orientation of the martensite lamellae with respect to the tensile axis. When approximately parallel to the tensile axis, fracture of the martensite lamellae occurs under combined tensile and shear loading, as described by Cuddy and Bassim[82] for the fracture of pearlitic steels. If the ribs are more randomly orientated or approximately 90° to the tensile axis, fracture is initiated by a combination of interfacial tearing between the martensite lamellae and the inter lamellar ferrite, and fracture of the martensite lamellae. However this description is somewhat simplified, and the ductility of the lamellar composite grains is influenced by a number of factors, including the orientation of the slip systems in the inter lamellar ferrite with respect to both the tensile axis and the orientation of the lamellar martensite ribs, as noted by Su, Sun and Yang[36] for the fracture of a low alloy, lamellar type dual phase steel.

It is evident from this analysis that the particular δ-ferrite content of alloy A is somewhat

detrimental to its ductility. Analysis of the nitrogen alloyed steels revealed that an unconnected, island type martensite morphology results in improved ductility. Thus the ductility of alloy A would be increased by decreasing the martensite content. However, the toughness of low interstitial, ferritic-martensitic stainless steels is improved by increasing the martensite content, as was noted by Hayden and Floreen[7] and Wright and Wood[6].

CHAPTER SIX

SUMMARY AND CONCLUSIONS

6.1 SUMMARY

Alloy A had an impact resistance in excess of 60J and a tensile strength in excess of 800 MPa in all the heat treated conditions in which it was tested. This is a consequence of the high nickel, low interstitial content which produces a fine grained high volume fraction martensite structure after solution treating at 1000 °C. However, in both the solution treated and 700 °C tempered conditions, the alloy suffered from a low uniform elongation, which was emphasized after the alloy had been thermomechanically treated. This has been shown to be a consequence of the high martensite content and the inter-connected morphology of the martensite in alloy A, which in restricting the amount of strain in the ferrite phase, is forced to deform, and necking and microvoid formation occur within the martensite phase at a low strain in view of its low ductility. Analysis of the modes of deformation and fracture initiation in alloys C and D in the solution treated conditions revealed that greater uniform elongation is obtained due to the less constrained deformation in the ferrite matrix which surrounds the elongated martensite islands, but that fracture still initiates in the martensite phase. However, the detrimental effect of interstitial alloying elements in solution in 16 wt.% Cr alloys is reflected in the poor impact resistance of alloys C, D, and E in the solution treated condition, which even in view of the grain refining effect associated with dual phase microstructures, is no improvement on that exhibited by AISI 430 and 431 in the solution treated condition. Moderate to good impact resistance can be achieved by heat treating the nitrogen alloyed steels at 700 °C for one hour, but substantial losses in strength are incurred as a consequence of the removal of nitrogen from solution. The relationship between volume fraction of tempered martensite and impact resistance is not simple, as reflected in the higher impact resistance of alloys D and E than alloy C in the 700 °C tempered conditions. This effect has been related to the susceptibility to intergranular fracture at δ-ferrite/martensite interfaces, where the larger surface area of this interface per martensite island in alloy C provides a lower resistance to crack propagation. Nevertheless, the presence of a high concentration of nitride

precipitates in the ferrite phase of alloy C in the 700 °C tempered condition may also reduce its toughness. The effects of nitrogen as an alloying element in 16 wt.% Cr alloys (in the 600 and 700 °C tempered conditions) has been shown to be less detrimental to the toughness than carbon as a consequence of the slower rate at which nitrogen-rich grain boundary precipitates form compared to the rate of formation of carbon-rich grain boundary precipitates. This is manifested by the lower susceptibility of the nitrogen alloyed steels to intergranular fracture and is reflected in the superior impact properties of the nitrogen alloyed steels over those of the standard stainless steels after tempering at 600 and 700 °C.

Analysis of the deformation characteristics of the experimental dual phase steels revealed that continuous yielding is a consequence of the presence of mobile dislocations at martensite/ferrite interfaces and the different work hardening rates of the ferrite and martensite phases. While continuous yielding is suppressed by reducing the hardness difference between the martensite and ferrite phases (through tempering), yield point elongation (Luders extension) was not observed in any of the experimental alloys after tempering as a consequence of the hardness difference between the tempered martensite and ferrite phases being above a critical value. The formation of a lamellar composite phase during intercritical annealing of alloys A and E resulted in continuous yielding of the alloys, although for each alloy the work hardening rate in the first 0.5 % strain was lower than that in the solution treated condition as a consequence of the lower martensite content. The high impact resistance achieved in alloy A as a consequence of the lamellar composite phase is attributed to the good crack blunting properties of both the soft inter-lamellar ferrite and the nickel toughened martensite. However, the presence of nitrogen in solution in the martensite lamellae adversely affected the toughness of alloy E, although the toughness was still comparable to that of AISI 430 in the as received condition, while its tensile strength was almost double that of AISI 430 in the as received condition. Although a low ductile to brittle transition temperature is achieved by tempering the nitrogen alloyed steels (particularly alloy E), the impact transition temperature of the nitrogen alloyed steels is raised well above room temperature by the redissolution of precipitates, which indicates that the nitrogen alloyed steels are not as readily weldable as the low interstitial nickel alloyed steel, which has a transition temperature well below room temperature after a solution treatment.

Of the high nitrogen steels, alloy E has the most favourable composition in terms of the combination of ductility, toughness and tensile strength that can be achieved in the alloy

through various heat treatments. The properties of the alloy are superior to those of AISI 430, and in many respects to those of AISI 431. However, alloy A has a combination of tensile strength and toughness which is more attractive than any of the experimental or commercial alloys tested, except for AISI 304, which, in view of its austenitic structure has outstanding impact resistance.

6.2 CONCLUSIONS

(1) The level of toughness and tensile strength that can be achieved in a low interstitial, nickel alloyed 16 wt.% chromium stainless steel containing 71 % martensite, in the solution treated (hardened) condition and after heat treating at 600 and 700 °C, suggests that the alloy has superior weldability to both AISI 430 and 431, and is an attractive alternative to these alloys.

(2) Nitrogen in solution in 16 wt.% chromium stainless steels is detrimental to the impact resistance, and no benefit is gained from the dual phase microstructure. A high impact resistance can be achieved in high nitrogen dual phase stainless steels by tempering at 700 °C, but significant losses in strength are incurred.

(3) Dual phase ferritic martensitic stainless steels in the solution treated (hardened) condition have a low yield strength, and exhibit continuous yielding characteristics as a consequence of both the high density of mobile dislocations in the regions of ferrite grains adjacent to ferrite/martensite grain boundaries, and the different work hardening characteristics of the ferrite and martensite phases. Decreasing the hardness difference between the ferrite and martensite phases decreases the constraint on deformation in the ferrite phase, and yielding becomes more homogeneous.

(4) In the hardened condition, the ductility of dual phase stainless steels which have an inter-connected type martensite morphology is lower than those which have an island type martensite morphology, and is a consequence of the concentration of strain in the martensite phase in the inter-connected type martensite morphology.

(5) Fracture of dual phase ferritic martensitic stainless steels in the hardened condition is initiated primarily by fracture within the martensite phase, while a secondary mechanism in operation is interfacial tearing at ferrite/martensite grain boundaries. Fracture is brittle in high nitrogen stainless steels and ductile in a nickel alloyed steel with a low interstitial content.

(6) In tempered, high nitrogen dual phase steels, the main mode of fracture initiation is interfacial decohesion at ferrite/martensite grain boundaries as a consequence of precipitation in those regions.

(7) The level of impact resistance achieved in high nitrogen stainless steels tempered at 700 °C is a consequence of the high toughness of the tempered martensite phase which consists of fine, dislocation free sub-cells. Minimising the ferrite content is beneficial to both the strength and the toughness.

(8) A combination of high strength and good ductility can be achieved in dual phase steels with lamellar ferrite/martensite microstructures. The impact resistance is sensitive to the interstitial content in solution in the lamellar martensite phase, although the essentially fine grained structure of the lamellar composite phase contributes to the toughness of the alloys.

(9) In the tempered condition, nitrogen is less detrimental to the toughness of 16 wt% chromium stainless steels than carbon.

(10) A nitrogen alloyed steel containing 11 % δ-ferrite exhibits a combination of tensile strength and toughness in the 700 °C tempered and intercritically annealed conditions which makes it a potential substitute for AISI 430 or AISI 431, but it exhibits no improvement in weldability over that of the two standard stainless steels.

REFERENCES

(1) SEDRICKS A.J., : "Corrosion of Stainless Steels"; John Wiley and Sons (Pub.), New York, p 1,2

(2) Colombier L., Hochmann J. (1967) :"Stainless and Heat Resisting Steels"; Edward Arnold (Pub.), Great Britain, pp 7-65.

(3) A.S.M METALS HANDBOOK: 'Metallography, Structures and Phase Diagrams'; Metals Park, Ohio 44073, 8th edition, v8, p 291.

(4) PICKERING F.B. (1979) in : " Micon '78: Optimising of Processing, Properties and Service Performance Through Microstructural Control"; Proc. of Conf., Abrams H, Maniar G N, Nail D A, Soloman H D (Eds.), ASTM - STP 672, pp 263 - 296.

(5) PECKNER D., BERNSTEIN I.M. (1977): "Handbook of Stainless Steels"; Mc Graw Hill, New York, p 4,60

(6) WRIGHT R.N., WOOD J.R., (1977): "Fe-Cr-Mn Duplex Ferritic Martensitic Stainless Steels"; Met. Trans.A, v8A , pp 2007 - 2011.

(7) HAYDEN H.W., FLOREEN S.F., (1970): "Influence of Martensite and Ferrite on the Properties of Two Phase Steels Having a Microduplex Structure"; Metal. Trans.A, v1A, pp 1955 - 1959.

(8) CHUANG Y.Y., CHANG Y.A. (1987): "A Thermodynamic Analysis and Calculation of the Fe-Cr-Ni Phase Diagram"; Met. Trans. A, v18A, pp 733-745.

(9) ASM METALS HANDBOOK (8th EDITION): "Metallography, Structures and Phase Diagrams"; Metals Park, Ohio,44073, v8, pp 424-426.

(10) PICKERING F.B. (1984): "Physical Metallurgical Development of Stainless Steels"; in "Stainless Steels '84", Proc. of Conf., Goteborg, The Inst. Met., London. pp 2-28.

(11) CHADWICK G.A. (1972): "Metallography of Phase Transformations"; Butterworths (Pub), London, pp 92-93.

(12) BROWN E.L., WHIPPLE T.A., KRAUSS G. (1982) in: "Duplex Austenitic-Ferritic Stainless Steels"; Proc. of Conf.,St Louis, USA, pp 665-691; ASM Metals Park, Ohio, 1983.

(13) KNUTSEN R.D. (1989): "A Microstructural Examination of Duplex Ferrite-Martensite Corrosion Resistant Steels"; PhD Thesis, University Of Cape Town.

(14) HONEYCOMBE R.W.K. (1981): "Steels- Microstructures and Properties"; Edward Arnold (Pub), London, pp 188-191, 211-233.

(15) STEIGERWALD R.F., (1977): 'The Effects of Metallic Second Phases in Stainless Steels'; Corrosion, v 3 , n9, pp 338-343.

(16) Le FEVRE J., TRICOT R., GUEUSSIER A., CASTRO R. (1974): "Properties of a New Family of Stainless Steels Without Nickel"; Met. Trans. A, v5A, pp 2277-2285.

(17) BROOKS C.R., (1979) : "Heat Treatment of Ferrous Alloys"; Hemisphere ,N.Y., McGraw Hill , pp 191-197.

(18) SPEICH G.R. (1981) : "Physical Metallurgy of Dual Phase Steels"; in "Fundamentals of Dual Phase Steels", Proc. of Conf., R.A. Kot and B.L. Bramfitt (Eds.), Chicago, Illinois, AIME, pp 3-46.

(19) HAYAMI S., FURUKAWA, T (1975) in : "Microalloying '75"; Proc. of Conf., Vanitec, London, pp 78-87.

(20) RASHID M.S., (1976): "A Unique High Strength Sheet Steel With Superior Formability"; SAE Preprint 760206.

(21) KOO J.Y., YOUNG J.M., THOMAS G, (1980): "On The Law Of Mixtures in Dual-Phase Steels"; Met. Trans., v11, p52.

(22) HONEYCOMBE R.W.K., (1984): "The Plastic Deformation of Metals"; Edward Arnold (Pub.), London, p253.

(23) UGGOWITZER P., STUWE H.P., (1982): "Tensile Fracture Of a Dual-Phase Steel"; Mat. Sci. Eng., v55, pp 181-189.

(24) KUNIO T., SHIMIDZU M., YAMADA K., (1975): "An Effect of Second Phase Morphology on the Tensile Fracture Characteristics Of Carbon Steels"; Eng. Frac. Mech., v7, pp 411-417.

(25) TOMOTA Y., YOSHINO H, KUROKI K, (1977): "Effect of Ductility of the Second Phase on Ductile Fracture"; Scripta. Met., v11, pp 853-856.

(26) KOO J.Y., THOMAS G., (1977): "Design of Duplex Fe/X/0.1C Steels for Improved Mechanical Properties"; Met. Trans. A, v8A, pp 525-528.

(27) CHEN H., CHENG G., (1989): "Effect of Martensite on The Tensile Strength of Dual Phase Steels"; J. Mat. Sci., v24, pp 1991-1994.

(28)SPEICH G.R., MILLER R.L., (1981) : "Mechanical Properties of Ferrite Martensite Steels"; in "Structure and Properties of Dual-Phase Steels", Proc. of Conf., R.A. Kot and J.W. Morris (Eds.), AIME, New York, pp 145-182.

(29) BINDER W.O., SPENDELOW H.R., (1951); Trans. ASM, v43, pp 759-777

(30) BALLIGER N.K., GLADMAN T, (1981): "Work Hardening of Dual-Phase Steels"; Met. Sci., pp 95-108.

(31) CHANG P., PREBAN A.G., (1985): " The Effect of Ferrite grain Size and Martensite Volume Fraction on The Tensile Properties Of Dual Phase Steels"; Acta. Met., v33, n5, pp 897-903.

(32) ABO H., NAKAZAWA T., (1977) : "Role of Carbon and Nitrogen on the Toughness and Intergranular Corrosion of ferritic stainless Steels"; in "Stainless steel '77", Proc. of Conf., London, Climax Molybdenum Co., pp 35 - 37.

(33) BALL A., HOFFMAN J.P. (1981): "The Microstructure and Properties of a Steel Containing 12% Cr Designated 3Cr12 (Cromweld)"; Metals Tech., v8, pp 329-338.

(34) GROBNER P.J., BISS V., (1984): 'Microstructural Strength Relationships in a Hardenable Stainless Steel With 16% Cr, 1.5% Mo, and 5% Ni'; Met. Trans., 15A , pp 1379 - 1387.

(35) RAMESH R., KIM N.J., THOMAS G, (1990): "Improvement in the Toughness of Fe-Cr-Mn-C Steels by Thermal-Mechanical Treatments"; Met. Trans. A, v21A, pp 683-695.

(36) SU M., SUN S.M., YANG D.Z., (1987): "An In Situ Observation Of Tensile Fracture in a Lamellar Dual Phase structure"; Scripta. Met., v21 , pp 801-804.

(37) YANG D., SUN X., LEI T, (1983): "Effect of Intercritical Quenching on the Microstructure and Tensile Properties of Steels 15 and 15Mn2Nb"; J. of Mat. Sci., v18, pp 2727-2731.

(38) STREICHER M.A., (1973): "The Role of Carbon, Nitrogen, and Heat Treatment in the Dissolution of Fe-Cr Alloys in Acids"; Corrosion; v29 , n9, pp 337-362.

(39) DEMO J.J., (1982): "Structure, Constitution and General Characteristics of Ferritic Stainless steels"; in "Source Book of Ferritic Stainless Steels", Lula R.A. (Ed.), Philadelphia, ASTM, p4.

(40) HERTZMAN S., JARL M., (1987): "A Thermodynamic Analysis of the Fe-Cr-N System"; Met. Trans.; 18A , pp 1745 - 1752.

(41) CASTRO R., TRICOT R., (1979): "Study of the Isothermal Transformations in 17% Cr Stainless steels, Part 1"; in "Metallurgical Evolution of Stainless Steels", Pickering F.B. (Ed.), ASM Metals Park, Ohio 44073, and Metals Society, London, pp 230-239.

(42) CASTRO R., TRICOT R. (1979) : "Study of the Isothermal Transformations in 17% Cr Stainless Steels, Part 2: Influence of Carbon and Nitrogen"; in "Metallurgical Evolution of Stainless Steels", Pickering F.B. (Ed.), ASM Metals Park, Ohio 44073, and Met. Soc., London, pp 245-253.

(43) BROWN R.S. (1979): "A Short Course in Stainless Steel Welding"; Materials Engineering, v90, n5, p 34-39.

(44) PICKERING F.B., (1976): "Physical Metallurgical of Stainless Steel development"; Int. Met. Rev., pp 227-268.

(45) TIZIANI A., GIORDANO L., FEDRIZZI L.,MOLINARI A.,MARCHETTI F., (1986): "Nitrides Transformation in AISI Type 410 S.S. Treated at Different Temperatures and Their Characterisation by Auger Spectroscopy"; J. of Mat. Sci. Lett.; v5 , pp 573 - 576.

(46) HERTZMAN S., (1987): "An Experimental and Thermodynamic Study of the Fe-Cr-C-N System at 1273 K"; Met. Trans.A, v18A, p1753.

(47) KUO K.H., JIA C.L., (1985): "Crystallography of M23C6 and M6C Precipitates in a Low Alloy Steel"; Acta Met., v33, n6, pp 991-996.

(48) BYWATER K.A., DYSON D.J., (1975): "The Precipitation of Cr2N in 17% Cr Steels"; Met. Sci., v9, pp 155-162.

(49) LANDON P.R., CALIGIURI R.D., DELECTSKY P.S., (1983): "The Influence of M23CN6 Compound on the Mechanical Properties of Tp 422 Stainless Steel"; Met. Trans.A, v14A , p1395.

(50) A.S.M METALS HANFBOOK, (1971): 'Metallography, Structures and Phase Diagrams'; Metals Park, Ohio 44073, 8th ed., v8, pp 422 - 424.

(51) LEE J.B., SMITH J.F., GEIGER A.L., KAH D.H., (1985): "An Analytical Electron Microscope Examination of Sensitised AISI 430 S.S."; Corrosion, v41 ,n 2, pp 76 - 80.

(52) DEVINE T.M., (1988): "Kinetics of Sensitization and Desensitization of Duplex Stainless Steels", Acta. Met., v36, pp 1491-1501.

(53) VITEK J.M., KLUEH R.L., (1983): "Precipitation Reactions During the Heat Treatment of Ferritic Steels"; Met. Trans.A, v24A , p1047.

(54) BRIANT C.L., MULFORD R.A., HALL E.L., (1982): "Sensitization of Austenitic Stainless Steels:(1) Controlled Purity"; Corrosion Nace, v38, n9, pp 468-477.

(55) COURTNALL M., PICKERING F.B., (1976): "The Effect of Alloying on 485 °C Embrittlement"; Met. Sci., v10, pp 273-276.

(56) IRVINE K.J., CROWE D.J., PICKERING F.B.: "The Physical Metallurgy of 12% Cr Steels"; Metallurgical Evolution Of Stainless Steels,(As in Ref. 10), p43.-62

(57) IRVINE K.J., PICKERING F.B. (1979): "High Strength 12% Cr Steels"; in "Metallurgical Evolution Of Stainless Steels", Pickering F.B. (Ed), A.S.M, Metals Park, Ohio 44073, and Metals Society, London, pp 63-77.

(58) AITA C.R., LAD R.J., PURDES A.J., (1979): "Age Hardening of Martensitic Stainless With Niobium and Copper Additions"; Scripta Met., v13 , pp 771 - 775.

(59) BRANDIS H, HEIMANN W., (1984): "Nitrogen Bearing High Strength Austenitic Stainless Steels"; in "Stainless Steels '84", Proc of Conf. p 97.

(60) KNUTSEN R.D., BALL A., HEWITT J., HOFFMAN J.P., HUTCHINGS R., (1987): "Review of the Physical Metallurgy, Properties and Applications of a Dual Phase Martensitic Stainless steel designated 3CR12"; in "Stainless Steels '87", Proc. of Conf. at Univ. of York, Inst. of Metals , p512-520.

(61) ASM METALS HANDBOOK (9th EDITION): "Properties and Selection: Stainless Steels, Tool Materials and Special Purpose Metals"; Metals Park, Ohio 44073, p29.

(62) "Effect of Composition on the Ductility and Toughness of Ferritic Stainless Steels"; in "Metallurgical Evolution Of Stainless Steels", Pickering F.B. (Ed.); ASM Metals Park, Ohio 44073, and Inst. of Met., London, p260-274.

(63) SWALIN R.A., (1972): "Thermodynamics of Solids"; 2nd edition, Wiley, New York, p

(64) ODETTE G.R., LUCAS G.E., MAITI R., SHECKHERD J.W., (1984): "Micromechanical Mechanisms of Cleavage Fracture in Martensitsc Stainless Steels"; Journal Of Nucleur Materials, v 122 & 123 , pp 442 - 447.

(65) GRUBB J.F., WRIGHT R.N., (1979): "The Role of C and N in the Brittle fracture of Fe-26Cr"; Met. Trans. A, v10A, 1247-1255.

(66) DeARDO A.J., (1977): "An Investigation of the Mechanisms of Splitting that Occur in Tensile Specimens of High Strength Low Alloy Steels"; Met. Trans. A, v8A, pp 473-486.

(67) SPEIDEL M.O., (1987): "High Nitrogen Stainless Steels: Austenitic, Duplex and Martensitic"; in "Stainless Steels '87", Proc. of Conf. at Univ. of York, Inst. of Metals, pp 247 - 252.

(68) WAHLBERG G., DUNLOP G.L., (1987): "Nitrogen Strengthening of Duplex Stainless Steels"; in "Stainless Steels '87", Proc. of Conf., York, Inst. of Met., p291

(69) TRUMAN J.E.; COLEMAN M.J., PITT K.R., (1977): "Note on the Influence of Nitrogen on the Resistance to Pitting of Stainless Steels"; Br. Corr. Journal ,v12 , n4, pp 236 -238.

(70) GRUSHKO B, WEISS B.Z., (1989): "Yield Behaviour of a Dual-Phase Steel"; Scripta. Met., v23, pp865-870.

(71) MOYER J.M., ANSELL G.S., (1975): "The Volume Expansion Accompanying the Martensitic Transformation in Fe-C Alloys"; Met. Trans A, 6A, pp 1785-1791.

(72) HARASE J, SHIMISU RY, (1987): "Effest of Second Phase on the Yield Point of SUS 430 Stainless Sheet"; Trans ISIJ, v27, p B-213.

(73) GERBASE J., EMBURY J.D., HOBBS R.M., (1981): "The Mechanical Behaviour of Some Dual-Phase Steels- With Emphasis on Initial Work Hardening Rate"; in "Structure and Properties of Dual Phase Steels", Proc. of Conf., R.A. Kot and J.W. Morris (Eds.), AIME, New York, pp 118-144.

(74) RIGSBEE J.M., VANDER-AREND P.J., (1979): "Laboratory Studies of Microstructure and Microstructure-Property Relations in Dual-Pase Steels"; in "Formable HSLA and Dual Phase Steels", Proc. of Conf., R.A. Kot and J.W. Morris (Eds.), AIME, New York, pp56-58.

(75) MATLOCK D.K., KRAUSS G., RAMOS L.F., HUPPI G.S., (1981): "A Correlation of Processing Variables With Deformation Behaviour of Dual-Phase Steels"; in "Structure and Properties of Dual-Phase Steels", Proc of Conf., R.A. Kot and J.W. Morris (Eds.), AIME, New York, pp 62-90.

(76) KORZEKWA D.A., MATLOCK D.K., KRAUSS G. (1984): "Dislocation Structure as a Function of Strain in Dual-Phase Steels"; Met. Trans. A, v15A, pp 1221-1229.

(77) SHEN H.P., LEI T.C., LIU J.Z., (1986): "Microscopic Deformation Behavior of Martensitic-Ferritic Dual Phase Steels"; Mat. Sci. Tech., v2, pp28-33.

(78) SZEWCZYK A.F., GURLAND J., (1982): "A Study of The Deformation to Fracture of a Dual-Phase Steel"; Met. Trans A, v13A, pp 1821-1826.

(79) TOMOTA Y., (1987): "Effect of Morphology and Strength of Martensite on the Cyclic Deformation Behaviour in Dual-Phase Steels"; Mat. Sci. Tech., v3, p415

(80) RAY R.K., (1984): "Tensile Fracture of a Dual Phase Steel"; Scripta. Met., v18 , pp 1205 - 1209.

(81) KELLY A., DAVIES G.J., (1965); Met. Rev., v10, p1.

(82) CUDDY J.K., BASSIM M.N., (1990): "Ductile Fracture Mechanisms in AISI 4340"; Mat. Sci. Eng., vA125, pp 43-48.

(83) "THE MAKING SHAPING AND TREATING OF STAINLESS STEELS", 9th Edition, United States Steel Corp., Pillsburgh, (1971) p. 1168.

(84) HAOQUAN W., SPEAR W.S., POLONIS D.H., (1987): " Influence of Annealing and Aging Treatments on the Embrittlement of Type 446 Stainless Steel"; J. of Mat. Eng., v9, pp 51-56.

(85) TANAKA T., NISHIDA M., HASHIGUCHI K., KATO T. (1979): "Formation and Properties of Ferrite Plus martensite Dual-Phase STruuctures"; in "Structures and Properties of Dual Phase Steels", as in ref. 73, pp 221 - 241.

(86) CHENG L., (1990): "Phase transformations in Iron Base interstitial Martensites"; PhD Thesis, Delft University of Technology, The Netherlands, pp 129 - 151.

(87) SMITH M.C., (1956) : "Principles of physical Metallurgy"; Constable and Co. Ltd. (Pub), London, p188 -190.

(88) DALLAR M., BERNSTEIN I.M., THOMPSON D.W., (1988); Acta Met. , v 36, p311.